STUDY OF EQUILIBRIUM CRITICAL PHENOMENA IN FLUID ARGON

Thesis by

Shyue Yuan Wu

In Partial Fulfillment of the Requirements

For the Degree of

Doctor of Philosophy

California Institute of Technology

Pasadena, California

1972

(Submitted December 7, 1971)

the past is gone ; the future ...

yet to be pursued.

ACKNOWLEDGMENT

Most of all, I wish to express my sincere appreciation to my research advisor, Professor C. J. Pings, for his invaluable guidance, encouragement, and support throughout the course of this work. Also, I am especially grateful for his understanding, patience, and concern.

I am deeply indebted to H. H. Reamer for his extensive contributions which included equipment modification, data collecting, and review of the experimental section of the thesis. Thanks to G. A. Griffith for constructing part of the equipment.

The major work of Proposition I was done under the supervision of Professor B. H. Sage. I wish to thank Dr. A. F. Collings for his helpful technical suggestion on this section and for his reviewing the thesis.

In the preparation of the thesis, the frequent assistances in various ways from M. A. Piliavin is deeply appreciated. Thanks to R. A. Stratton and J. F. Gray for typing the text and preparing the figures respectively.

During my graduate studies I have received financial support from the California Institute of Technology in the forms of Graduate Teaching and Research Assistantships and a summer fellowship from the ARCS Foundation. I am also indebted to the Air Force Office of Scientific Research and to the Shell Companies Foundation for financial support. These supports are hereby gratefully acknowledged.

My education is primarily a result of the constant care, encouragement, and sacrifice of my parents. To them, I will be eternally grateful. I would like also to thank my brother and sisters for their interest and affection.

ABSTRACT

The refractive index of fluid argon was measured by using the method of angle of minimum deviation for $\lambda_{Na} = 5893\text{Å}$. The measurements were carried out along the coexistence curve and along fourteen single phase isotherms from 150.7° to 163°K at pressures from 40 to 90 atmospheres.

The Lorentz-Lorenz relation was used to relate the refractive index data to the densities and subsequently to find the isothermal compressibilities along the singla phase isotherms. Following the law of rectilinear diameter and the simple power laws for critical exponents, the values of the critical temperature and exponents for argon were found to be $T_c = 150.725^{\circ} \pm 0.010^{\circ}\text{K}$, $\beta = 0.3574 \pm 0.0027$, and $\gamma = 1.170 \pm 0.013$. Also values of $n_c = 1.08611$ and $P_c = 47.983$ atm were determined. These values agree well with others reported for argon. Comparison of the values of β and γ with those predicted by the classical theory and the three-dimensional lattice gas model suggests that the latter gives a better description of the critical behavior of fluid argon.

Analysis of the reduced chemical potential differences, computed from the refractive index data along the singla phase isotherms, has been made by using the scaled equation of state first proposed by Widom. Reasonable values of T_c and γ were obtained when the value of β determined above was used.

TABLE OF CONTENTS

LIST OF FIGURES

Appendices - Figures

LIST OF TABLES

I. INTRODUCTION

In recent years there have been many theoretical and experimental investigations of the thermodynamic anomalies of a fluid near its gas-liquid critical point. In the present study, measurements of the refractive index of fluid argon were carried out in the vicinity of critical point. Experimental data were analyzed to determine the critical exponents β and γ, which characterize the thermodynamic anomalies. Comparison is made with theoretical studies.

1. Lorentz-Lorenz Relation

The refractive index n can be related to the density ρ through the Lorentz-Lorenz relation

$$\frac{n^2-1}{n^2+2}\frac{1}{\rho} = \frac{4\pi}{3}\frac{N_o}{M}\alpha_m \qquad (1)$$

where α_m is the molecular polarizability, M the molecular weight, and N_o Avogadro's number. As was formulated by the classical method of Lorentz[1], Equation (1) is rigorously valid for a cubic lattice of nonpolar spherical molecules assuming constant polarizability and neglecting fluctuations in local field. Expanded theories[2,3,4] based on statistical mechanical analysis have taken into account the effect of statistical fluctuation in the induced dipole moment and the effect of the variation of polarizability due to molecular interaction, and have produced density-dependent and temperature-dependent correction terms to Equation (1). Experimental evidences[5,6,7] showed that for many nonpolar fluids the density and temperature dependences of

the Lorentz-Lorenz function, $LL = (n^2 - 1)/(n^2 + 2)\rho$, are very small and no more than a few percent. For argon, recent analysis[8] of extensive refractive index measurements indicated that there is no more than a 1.5% variation from a LL value of 4.19 cm^3/mole throughout the three states of matter and with a temperature range of 20°K to 300°K. Hence there is probably little error introduced in relating the refractive index to the density by Equation (1) without correction terms.

In analyses of asymptotic behavior of a fluid near its gas-liquid critical point, the possibility that Lorentz-Lorenz function might become anomalous should be taken into consideration. Teague[8] has measured the refractive index of argon on the gas-liquid coexistence curve over the temperature range from about 30°K to within 0.01°K below the critical temperature. The measurements were combined with the density data reported by Levelt[9] to compute the Lorentz-Lorenz function, which appears to show a divergence near the critical density. However, there is good reason to believe that this is the result of a discrepancy of $\pm$0.017°K between the temperature scales used in the two different laboratories generating the density and the refractive index data. A theoretical study on the validity of Equation (1) near the critical point has been made by Larsen *et al*[10]. They pointed out that the small imaginary part of the refractive index undergoes an anomaly at the critical point, as is evidenced by the phenomenon of critical opalescence. The homogeneity of the medium assumed in deriving Equation (1) is not present near the critical

point where density fluctuations are significant. However, according to their estimate, for argon the effect of density fluctuations on the real part of the refractive index is less than one part in 10^4 near the critical point.

Henceforth, for practical purposes, we can use Equation (1) to relate the refractive index of argon to its density. It is noted that near the critical point there has not been a precise experimental confirmation of the validity of Equation (1). Furthermore, using Equation (1), it is possible to express the isothermal compressibility, defined as $K_T = -\frac{1}{V}(\frac{\partial V}{\partial P})_T = \frac{1}{\rho}(\frac{\partial \rho}{\partial P})_T$, explicitly in terms of refractive index and its pressure derivative as follows:

$$K_T = \frac{6n}{(n^2 - 1)(n^2 + 2)} (\frac{\partial n}{\partial P})_T \qquad (2)$$

2. Critical Anomalies

For many years, the classical equation of state of van der Waals has been used to describe the equilibrium behavior of fluid systems. Following this equation, three principal predictions concerning the anomalous behavior near the gas-liquid critical point are:

(i) that the difference between liquid and gas densities on the coexistence curve follows a square-root law,

$$\rho_L - \rho_G = B(T_c - T)^{1/2} \quad , \quad (T \to T_c^-) \tag{3}$$

(ii) that the isothermal compressibility shows a divergence as a simple pole along the critical isochore

$$K_T = \Gamma/(T - T_c) \quad , \quad (\rho = \rho_c, \; T \to T_c^+) \tag{4}$$

(iii) that the specific heat at constant volume along the critical isochore shows a discontinuity but not a divergence at the critical point

$$C_v(T) = C_c^{\pm} - D^{\pm}|T - T_c| \quad ,$$

$$(T \gtrless T_c \quad \text{with} \quad C_c^- - C_c^+ = \Delta C > 0) \tag{5}$$

where the constants B, Γ, C_c, and D can be expressed in terms of the van der Waals parameters. Fisher[11] has indicated that these predictions follow from all other empirical equations of state of classical type, e.g., Berthelot, Beattie-Bridgeman, etc., and in fact are a direct consequence of the implicit or explicit assumption that the free

energy and the pressure can be expanded in a Taylor series in density and temperature at the critical point.

However, it has been long recognized that these classical predictions are in conflict with the observed critical anomalies of real fluids. Experimental evidence has shown that the density difference on the coexistence curve varies approximately as the cube root of the temperature difference $(T_c - T)$ [12-14], and that the specific heat at constant volume shows a weak divergence near the critical point[15-18]. In order to describe the critical anomalies of real fluids, it is generally assumed that the various properties of the fluid near the critical point diverge according to simple power laws, which using Fisher's notation[19] may be expressed as

$$f(z) \approx z^{\lambda} \qquad \text{as} \quad z \to 0+ \tag{6}$$

More precisely this means that

$$\lim_{z \to 0^+} \left\{\frac{\ln f(z)}{\ln z}\right\} = \lambda \tag{7}$$

and λ is called the critical exponent. It is realized that $f(z) = Fz^{\lambda}$ is asymptotically valid approaching the critical point. Accordingly, the critical anomalies of a fluid similar to the three classical predictions, Equations (3)-(5), are described as follows:

(i) density difference on the coexistence curve

$$|\rho - \rho_c| = B'(T_c - T)^{\beta} \quad , \quad (T \to T_c^-) \tag{8}$$

(ii) isothermal compressibility

(a) on the critical isochore above critical temperature

$$K_T = \Gamma(T - T_c)^{-\gamma} \quad , \qquad (\rho = \rho_c,\ T \to T_c^+) \tag{9}$$

(b) along the coexistence curve in the one-phase region

$$\rho^2 K_T = \Gamma'(T - T_c)^{-\gamma'} \quad , \qquad (T \to T_c^-) \tag{10}$$

(iii) Specific heat at constant volume

(a) on the critical isochore above critical temperature

$$C_v = (A^+/\alpha)(T - T_c)^{-\alpha} \quad , \qquad (\rho = \rho_c,\ T \to T_c^+) \tag{11}$$

(b) along the coexistence curve in the one-phase region

$$C_v = (A^-/\alpha')(T - T_c)^{-\alpha'} \quad , \qquad (T \to T_c^-) \tag{12}$$

These critical exponents are not completely independent. Rushbrooke[20] showed that thermodynamic considerations impose the following inequality on the exponents

$$\alpha' + 2\beta + \gamma' \geq 2 \tag{13}$$

An analogous inequality

$$\alpha' + \beta(1 + \delta) \geq 2 \tag{14}$$

has been derived by Griffiths[21] and Rushbrooke[22], where δ is the exponent denoting the pressure behavior along the critical isotherm. These inequalities become exact equalities for a fluid obeying a classical equation of state.

All classical equations of state are based on a model of a fluid in which attractive forces between the molecules have a very long range. In fact, the range of attraction in a real fluid is not very long and each molecule is strongly influenced by at best a few shells of neighboring molecules. As Fisher[11] pointed out, the critical behavior of a fluid may also be studied theoretically from a model based on extremely short-range interaction. The most thoroughly examined theory of the critical behavior is the simple lattice gas model. In this, each molecule occupies a site of a lattice to the exclusion of other molecules and interacts, attractively, only with nearest-neighbor molecules. The lattice gas model is translated[23] from the magnetic Ising model for which the numerical results have been obtained through a power-series expansion method[24,25] for most two-dimensional and three-dimensional lattice structures. Rigorous solution for the plane square lattice gas along its critical isochore has been obtained by Onsager[26]. The critical anomalies predicted by the lattice gas model depend on its dimensionality. The critical exponents found for two-dimensional models[24,26-29] are $\beta = \frac{1}{8}$, $\gamma = \gamma' = 1\frac{3}{4}$, and $\alpha = \alpha' = 0_{\log}$ (i.e., the specific heat diverges logarithmically), and they satisfy the equality in Equation (13) precisely. The exponents found for three-dimensional models[30-34] are $\beta = 0.313 \begin{smallmatrix}+0.003\\-0.006\end{smallmatrix}$, $\gamma = \gamma' = 1.250 \pm 0.003$, $\alpha = 0.125 \pm 0.015$, and $\alpha' = 0_{\log}$ or $0.066 \begin{smallmatrix}+0.160\\-0.040\end{smallmatrix}$. They verify Equation (13) only within the numerical uncertainty. It should be noted that because the repulsive core of the interaction between molecules is represented merely by exclusion of a single lattice site, the lattice gas models have a

built-in symmetry with respect to the critical density

$$\frac{1}{2}(\rho_L + \rho_G) = \rho_c \tag{15}$$

Thus, Equation (8) is equivalent to

$$\rho_L - \rho_G = B(T_c - T)^{\beta} \tag{16}$$

where $B = 2B'$.

Previously, Guggenheim[14] had shown that Equation (16) with $\beta = 1/3$ described the observed coexistence curve data of a wide range of simple fluids quite well. An analysis of the coexistence curve data of xenon[35] by Fisher[11] showed that $\beta = 0.345 \pm 0.015$. Recently, Sengers et al[36] indicated that one can use Equation (8) for both the liquid and gas branches of the coexistence curve:

$$\rho_L - \rho_C = B_L'(T_c - T)^{\beta_L} \tag{17}$$

$$\rho_C - \rho_G = B_G'(T_c - T)^{\beta_G} \tag{18}$$

These two equations correspond to the general coexistence curve equation with the leading term only,

$$\rho^{\pm} = \rho_c[1 + B_1^{\pm}(T_c - T)^{\beta_1^{\pm}} + B_2^{\pm}(T_c - T)^{\beta_2^{\pm}} + \cdots] \tag{19}$$

where "+" refers to the liquid and "-" to the gas. This equation was first postulated by Van Laar[37] from classical theory and has been recently developed by Green et al[38] from a generalization of the parametric representation for thermodynamic scaling. In fitting Equations (17) and (18) to the experimental data[39] of CO_2, N_2O, and

$CClF_3$, Sengers et al[36] demonstrated that certain symmetry features established by Van Laar for the classical case seemed to be present in real fluids as well, namely $B_L' = B_G' = B'$ and $\beta_L = \beta_G = \beta$ (i.e., $B_1^+ = -B_1^-$ and $\beta_1^+ = \beta_1^-$). Since the law of rectilinear diameter

$$\frac{1}{2}(\rho_L + \rho_G) = \overline{\rho} = \rho_c[1 + a(T_c - T)] \tag{20}$$

is quite well obeyed by the experimental data, it is very likely that $B_2^+ = B_2^-$, $\beta_2^+ = \beta_2^- = 1$, and there is a near-cancellation of this higher-order term on forming the difference $\rho^+ - \rho^-$ (or $\rho_L - \rho_G$). Thus, the asymptotic expression Equation (16) can be fitted over a larger range of $(T_c - T)$ than can Equation (17) or Equation (18). The values of exponent β obtained from the fit to Equation (16) are 0.3475 ± 0.0006 for CO_2, 0.3482 ± 0.0007 for N_2O, and 0.354 ± 0.007 for $CClF_3$. In earlier work on argon[9], Sengers[40] found that the liquid and gas densities on the coexistence curve could be fitted together to the following equation

$$|\rho - \rho_c[1 + a(T_c - T)]| = B(T_c - T)^{\beta} \tag{21}$$

with the exponent $\beta = 0.3621 \pm 0.0004$. Using the Lorentz-Lorenz relation, Teague[8] has related the refractive index data of argon on the coexistence curve to its densities which were analyzed by including higher order terms in Equation (16) and varying the value of T_c over a slight range. It was found that, at the minimum standard deviation of the fit, the coefficients of the higher order terms no longer make a significant contribution to the fit and the exponent β has a value of

0.3643 ± 0.0066 .

There are relatively very few experimental studies of the isothermal compressibility K_T of fluid near the critical point. An analysis of the maximum isothermal compressibility of xenon above T_c by Fisher[11], based on the PVT measurements by Habgood and Schneider[41], indicated that the critical exponent $\gamma > 1.1$ and, rather uncertainly, $\gamma \simeq 1.2 - 1.3$. Since the maximum of K_T on an isotherm differs from the value of K_T at $\rho = \rho_c$ on the same isotherm, the exponent determined from this analysis is not the same as that from Equation (9). Recently, from their PVT measurements of argon in the critical region, Grigor and Steele[42] have shown that the analysis of K_T on the critical isochore ($\rho_c = 0.530$ gm/cm^3) above T_c gave the value of the exponent, $\gamma = 1.24 \pm 0.04$, and those of K_T in the one phase region below T_c at the condensation and the boiling points gave $\gamma'_{gas} = 1.24 \pm 0.04$ and $\gamma'_{liquid} = 1.22 \pm 0.04$, respectively.

Extensive measurements of specific heat at constant volume for argon and oxygen along the critical isochore have been made by Voronel et al[15-18]. They found that the specific heat could be fitted quite well by a logarithmic singularity of the form

$$C_v(T) = -A^{\pm} \ln|1 - T/T_c| + C^{\pm} , \qquad (T \gtrless T_c) \tag{22}$$

This is the same as Equation (11) with $\alpha = 0$, or Equation (12) with $\alpha' = 0$. Edwards et al[43] have measured the specific heat of xenon along the critical isochore and analyzed their data using Equation (11).

A value for the exponent α of about 0.08 was obtained.

Thus, experimental evidence suggests strongly that the critical anomalies of real fluid are nonclassical in nature and analogous to those predicted by the lattice gas models.

A different approach to the analysis of critical anomalies using all available data in the critical region instead of data along a preferred curve (coexistence curve, critical isochore), has been recently developed. Widom[44] first suggested that all known critical anomalies of real fluids can be properly incorporated by a scaled equation of state which has a certain homogeneity or scaling property which holds asymptotically as the critical point is approached. Later, Griffiths[45] showed that this scaled equation of state is exactly equivalent to those proposed for the magnetic Ising model[46-48]. This has the form

$$\Delta\mu = \Delta\rho|\Delta\rho|^{\delta-1} h(x) \tag{23}$$

where $\Delta\mu = [\mu(\rho,T) - \mu(\rho_c T)]/(P_c/\rho_c)$ is the reduced chemical potential difference along isotherms. $h(x)$ is a function of the scaled variable $x = \Delta T/|\Delta\rho|^{1/\beta}$ only, which ranges from the value $-x_o$ on the coexistence curve to $+\infty$ on the critical isochore. (Here $\Delta T = (T - T_c)/T_c$ and $\Delta\rho = (\rho - \rho_c)/\rho_c$ are in reduced units.) The main hypotheses underlying this equation of state are that (i) the chemical potential $\mu(\rho,T)$ is analytic in the vicinity of critical point throughout the entire one-phase region with possible exclusion of the phase boundary, and (ii) the chemical potential difference $\Delta\mu$ is antisymmetric with respect to ρ_c. These imply that $\mu(\rho_c,T)$ is

analytic at all temperatures and $\Delta\mu$ is analytic everywhere, except perhaps on the phase boundary. As was shown by Griffith, these hypotheses lead to some general conditions which must hold for the function h(x), for Equation (23) to be thermodynamically acceptable and to yield the critical anomalies consistent with those described by Equations (8)-(12) for real fluids. Subsequently, the critical exponent for a given property is found to be the same above T_c as below, and the inequalities of Equations (13) and (14) are fulfilled as equalities, that is,

$$\gamma = \gamma' = \beta(\delta - 1) \tag{24}$$

$$\alpha = \alpha' = 2 - \beta(\delta + 1) \tag{25}$$

Recently, Vicentini-Missoni et al[49,50] showed that Equation (23) can successfully describe the observed critical anomalies of a number of fluids and ferromagnets, if proper choices are made for T_c, β, and δ. They proposed a closed form for the function h(x)

$$h(x) = E_1\left(\frac{x+x_o}{x_o}\right)\left[1 + E_2\left(\frac{x+x_o}{x_o}\right)^{2\beta}\right]^{(\gamma-1)/2\beta} \tag{26}$$

where E_1 and E_2 are adjustable constants. This functional form of n(x) satisfies most conditions imposed on it except for the higher order terms in the series expansion of h(x) for large x. They found that Equation (23) with the proposed form for h(x), Equation (26), gave good fits to the experimental data in the critical region of CO_2 [13], Xe [41], and He^4 [51] in a density range of about $\pm$30 percent from critical, and the determined values of critical exponents varied only

slightly from substance to substance. Two kinds of fit were made; one[49] in which β and x_o were assumed to be independently known from an analysis of the phase boundary (Equation (16)), determining the rest of the four parameters by linear least-squares method; and the other[50] simultaneously determining all six parameters by non-linear least-squares method. In general, there were no significant differences in the parameters determined by the two methods. The critical exponents are found to be: $\beta = 0.350$, $\gamma = 1.26$ for Xe; $\beta = 0.355$, $\gamma = 1.24$ for He^4; and $\beta = 0.352$, $\gamma = 1.22$ for CO_2.

II. APPARATUS

The method of angle of minimum deviation has been used to measure the refractive index of fluid argon near critical state for $\lambda_{Na} = 5893$ Å. The measurements were made by introducing the sample of argon in a prism-shaped cell on the table of a spectrometer. A sodium lamp was used as the light source and the angle of minimum deviation, the temperature, and the pressure were measured. The refractive indices were obtained by the following relation[52]:

$$n = \sin \frac{1}{2}(A+D) \,/\, \sin \frac{1}{2} A \tag{27}$$

where A is the apex angle between the prism faces of the cell.

The apparatus has been described previously[6,8,53]. Several modifications and refinements have been made to improve the accuracy of measurements and the stability of control systems, which grow in importance near the critical state of the fluid studied.

1. Optics

The set-up of the optical system involving the cell, cryostat, and spectrometer, shown in Figure 1, is the same as described by Teague[54]. The general procedure for the adjustments of spectrometer given by Houston[52] was followed. In order to check and adjust the position of the cell after it has been enclosed in the cryostat, a new small mirror was mounted on one of the outside edges of the cell. Details of this operation are described in Appendix A.

The apex angle of the cell, A , was determined at room temperature both by the direct reflection method and by calibration with water. Details of this determination and experimental results are also given in Appendix A. The final value of A used to calculate the refractive index for all measurements is 44° 16.14' $\pm$ 0.31' , which is less than the value 44° 18.57' determined by Teague[8] for the same cell.

An improved procedure to use the spectrometer for measuring angles with better accuracy was established and discussed in Appendix B. The experimental uncertainty in determining the angle of minimum deviation, D absolute, was estimated to be $\pm$0.09 minutes of arc.

Since the cell was seated inside the cryostat which was evacuated to a vacuum lower than 10^{-4} mm Hg during the measurement, the refractive index measured was the true refractive index and not relative to air. However, two small errors could occur. The first could be caused by the possibly imperfect parallelism of both faces of all the windows, and the other by the two outermost cryostat windows being

not exactly parallel to each other and forming a small angle prism between the air outside and the vacuum inside. These errors are reduced significantly, if not completely, by taking the instrument zero reading of the spectrometer for the evacuated cell seated inside the cryostat with the same alignment of all windows as for the filled cell.

2. Temperature

The temperature measurement and control systems were much the same as described by Abbiss[6] and Teague[54].

A copper-constantan thermocouple attached to the inner shield was used to measure and control the shield temperature which was set 2 to 3 degrees below the temperature at which the cell was to be controlled. For the range of temperature studied, 145 to 163°K, it was found that the liquid nitrogen jacket used as the uniform heat sink needed only to be kept filled to a depth much less than 1" as stated before[54], and a controlled current of 0.1 ampere was sufficient for the 12.5 ohms shield heater to maintain a stable shield temperature.

A miniature platinum resistance thermometer, No. 4 in the series discussed by Knobler[55] and Honeywell[56], was used to measure and control the temperature of the cell. It has an ice point (273.15°K) resistance of 100.04718 ohms and has been calibrated[55] against an NBS certified strain free platinum resistance thermometer over the range of 75 to 300°K with an accuracy of ± 0.005°K. The miniature thermometer was embedded in a groove at the back edge of the cell and held in place by Wood's metal. An aluminum foil radiation shield was placed over the thermometer to eliminate the radiation loss from the ends that extended past the edge of the cell.

For the early runs of isotherms higher than 151°K, the conventional measuring method[54] using two potentiometers was employed. The current through the thermometer was determined from the potential drop across a 10 ohm reference standard resistor by a Leeds and

Northrup K-6 potentiometer. The potential drop across the thermometer corresponding to the desired resistance was set on a second Leeds and Northrup Wenner potentiometer. The difference in potentials between the thermometer and the Wenner was fed to the DC amplifier-controller system which supplied the necessary current, 0.005 to 0.010 amperes, to the cell heater and controlled the cell temperature within $\pm 0.001^{\circ}K$.

The refractive index of the fluid near critical isotherm changes very rapidly with temperature. In order to have the cell temperature stable within $\pm 0.001^{\circ}K$, it is necessary that both the potentiometers and the thermometer power supplies be sufficiently stable between standardizations and measurements. However, in practice, the complete cycle of standardizations and measurements cannot keep up with the normal small drift of the batteries used for power supplies of the circuits.

An improved measuring method was established and is shown in Figure 2. It was similar to that described by Daneman and Mergner[57] and only required that the ratio of the currents, not each one individually, in the potentiometer and thermometer circuits be stable. Since the control circuit must be constantly connected for stable temperature control, to avoid short circuit, modification was made by adding a 300 mfd oil-filled capacitor in which both poles were switched alternately to the standard resistor leads of the thermometer circuit and the standard cell terminals of Wenner potentiometer. A reference standard resistor, STD Ω_1, of 1000.04 ohms (at $25^{\circ}C$) was used in place of the original 10 ohms one.

At the beginning of each run, the thermometer circuit current was set within 0.3% of 0.001 amperes, the current used in the calibration of thermometer. The current used in the Wenner potentiometer was standardized by balancing the potential drop across its standard cell terminals, set at 1.01926 volts, with the one across the STD Ω_1 in the thermometer circuit through the use of the capacitor. A Leeds and Northrup 2284C High Sensitivity Galvanometer was used as the null detector in capacitor circuit. During the optical measurements the change of current in the thermometer circuit was compensated for by restandardizing the potentiometer current in the same fashion as before. This restored the ratio of the currents in two circuits and kept the ratio $R_t/\text{STD } \Omega_1$ equal to $R_w/\text{STD } \Omega_2$ which stayed constant with fixed dial settings on the potentiometer and equal to $E_w/1.01926$ for the specified standard potentiometer current.

Although the thermometer calibration[55] is considered accurate to $\pm 0.005^{\circ}K$, additional uncertainty was introduced by the comparison of the two potentiometers as required in the old conventional measuring method. A total absolute uncertainty of $\pm 0.015^{\circ}K$ is claimed for the temperature measured. For the improved method, since only one potentiometer was used and the uncertainty introduced by restoring the ratio of currents in two circuits was small, the temperature measurement is considered to be accurate within $\pm 0.010^{\circ}K$.

To prevent the possible freezing of the sample fluid in the inlet line, a current of 0.01 amperes was constantly supplied to the inlet heater placed on the inlet line above the inner shield chamber. The sample inlet line inside the shield chamber was coiled above the

cell to minimize heat conduction along the line to the cell. In addition, a new 10 ohm electrical heater was wound around the middle section of the coiled line and supplied by a constant current of 0.01 amperes to compensate the radiation and convection heat loss from the line to the shield. Two copper-constantan thermocouples, one placed at the midsection of the coiled line and the other just above the cell, were used to monitor the temperature. All the wires from inside the inner shield chamber were coiled above the cell and anchored to the top of the shield chamber to minimize the heat flow along the wires. Lucite plugs in an Edwards fitting were used to bring the wires out of the vacuum chamber.

The external control circuits for both the shield and the cell temperature control consisted of the same type commercial Leeds and Northrup components: #9835B DC amplifier, Speedomax G recorder, Series 60 C.A.T. control unit, and a self-saturating reactor power package. Under most operating conditions, only proportional control was used. In order to limit the control current through the shield and the cell heaters and operate the control unit power package in the linear response range, external power dissipation resistors were added to the control circuits. The power supplies for the inlet and the coiled line heaters were commercial 6-volt dry batteries connected with a decade resistor box for current adjustment.

3. Pressure

For the first three runs, Run III, IV and V, the pressure of the sample fluid in the cell was measured with a Texas Instruments Model 141 precision pressure gauge connected directly to the sample line. The gauge containing a stainless steel Bourdon tube with a maximum pressure range of 5000 psi had been calibrated between 240 to 1500 psi with a Hart balance dead weight tester. The details of the calibration and the experimental data are given in Appendix C. The overall limits of accuracy placed on the pressure measurement by the gauge were ± 0.3 psi.

As the temperature of the sample fluid approaches the critical isotherm, higher sensitivity and precision on the pressure measurement and control are required for maintaining a stable thermodynamical state of the sample fluid in the cell. The pressure was then measured directly with the Hart balance dead weight tester, as shown in the schematic diagram of Figure 3.

A model P3D differential pressure transducer made by Pace Engineering Company, North Hollywood and containing a magnetic stainless steel diaphragm of ± 0.1 psi range was used as a null detector between the oil pressure measured by the Hart balance and the sample gas pressure. The pressure transducer operates on the variable reluctance principle. Pressure difference across the diaphragm resulted in proportional deflection and consequent change in the inductance ratio between two pickoff coils embedded in the cases on either side of the diaphragm. A model CD10 miniature carrier-demodulator made by Pace Engineering Company was used to pick up the inductance ratio change and

convert it to a DC output displayed on a microampere meter. The zero of the whole null detecting system was established by venting both sides of transducer to the atmosphere. The sensitivity of the system was tested with a known water head pressure on gas side and adjusted to be 0.015 psi per division on the microampere meter. The reproducibility of the null position effected by the hysteresis of the diaphragm and the instability of the demodulator was found to be 0.03 psi by alternately overpressuring 50 psi on either side of diaphragm and then venting both sides to the atmosphere.

The principle of operation of the Hart balance dead weight tester is based on the use of a differential piston loaded by known weights to produce an oil pressure which can be calculated from the constants of the instrument. The piston is placed in a very closely fitted cylinder to form the pressure chamber which is connected to a pressure bench by a steel capillary inlet. In order to eliminate the vertical friction between the piston and the wall of the cylinder, the piston must be kept rotating. The original rotating mechanism consists of an electric motor and a belt and pulley system which drives a claw connected to the axle coupled to the top end of the cylinder. To eliminate the possible small vertical forces associated with the drive linkage, the rotating mechanism must be disengaged for each final pressure reading. Modification has been made by replacing the original mechanism with a small motor and belt system which drives the claw directly at a lower rotating speed of 30 to 40 rpm. No pressure difference between engaging and disengaging the new rotating

mechanism can be sensed by the transducer null detecting system. Therefore a precise oil pressure can be maintained constantly without interruption by disengaging the rotating mechanism.

For this study, a piston with a calibrated effective area of 0.31096 $\pm$ 0.00002 square inches at 20°C was used in the balance. The weights had been calibrated and converted into the mass figures which represented true masses minus the mass of the displaced air volumes. The calibrations were done for a standard piston height in the measuring cylinder and a fixed static head of oil acting upon the underside of the lower end of the weight axle. In calculating the oil pressure, deviations from the above have been taken into account and a correction factor for local gravity has been applied.

The absolute pressure on the sample fluid at the center of the cell was obtained from the sum of (1) oil pressure measured on the balance, (2) hydrostatic oil head from the piston inlet to the diaphragm, (3) gas head from the diaphragm to the cell, and, finally, (4) the barometric pressure measured with a Princo Fortin barometer. The final pressures were then reported in atmospheres.

The reproducibility of the pressure measurement is that of the Hart balance, 1 in 20,000, except for a few measurements below 600 psig in which the reproducibility is limited to that of the null detecting system, $\pm$ 0.03 psi. The absolute accuracy of the pressure measurement is that of the Hart balance, 1 in 10,000.

Since the argon sample cylinder used only gave a pressure of 650 psia at 70°F, the sample was first condensed in a cold trap at liquid nitrogen temperature and then warmed to room temperature to

higher pressure indicated by the Bourdon gauge as shown in Figure 3. Next, the sample was added to the system through a needle valve E and the approximate pressure was read on the Texas Instrument pressure gauge. Simultaneously the oil pressure was increased with valve A closed using valve C (away from closed position) as a volume-displacement intensifier. Great care was taken to prevent overpressure on either side of the diaphragm in the transducer by increasing the pressure on both sides very slowly and keeping them nearly equal as indicated by the microampere meter close to the null position. After the desired sample pressure was reached, valve E was closed. The pressure balance with the weights corresponding to the same pressure was pressurized by the oil injector. The Heise gauge was employed to monitor the approximate oil pressure during the loading. Valve A was then opened and fine adjustment of the oil pressure was made with the small weights on the pressure balance. During the optical measurement the pressure balance with the fixed weights remained connected to the oil line and provided a constant pressure against which the sample pressure was balanced. Since a portion of sample inlet line is exposed to the room temperature which may have small fluctuations, small variation of sample pressure may occur. Valve D on the sample inlet line was used (away from the closed position) as a small volume-displacement plunger and manually adjusted to control the sample pressure in balance with the constant oil pressure.

To prevent possible accidental overpressure in the cell, a bursting disc of type G made by Hoke Manufacturing Company was connected to the sample inlet line for safety purposes. The pressure at which the disc will blow out is 1800 psig.

4. Sample

The argon sample used in this study was "research grade" argon obtained from the Linde Division of Union Carbide Corporation, which supplied a batch analysis for the sample showing less than 20 ppm impurities.

To insure the integrity of the sample in the cell, the sample inlet lines were checked initially for leakage with a model MS-8 leak detector made by Vacuum-Electronic Engineering Company, New York. Within the sensitivity of the detector, 1-2 ppm, there was no detectable leakage found in the lines. At the beginning of each experimental run the sample lines were evacuated with a vacuum pump and then purged by alternately filling to above atmospheric pressure with the sample and evacuating. After purging, the lines were evacuated to a vacuum of 1×10^{-3} mm Hg and then closed to the vacuum pump to check any leakage which might have developed due to high pressurization in the lines from the previous run. If the pressure in the closed lines did not rise to more than 4 or 5×10^{-3} mm Hg in one minute, it was considered that the poorer vacuum was a result of reaching a static pressure within the lines and that no significant leakage had developed. The sample lines were immediately filled to above atmospheric pressure so that the contamination would be unlikely if small undetectable leaks had developed. For the same purpose, the lines were also maintained under a pressure above the atmosphere after each run.

Several attempts were made to analyze the argon sample with a mass spectrometer. The samples were collected from the inlet lines

into a glass bulb which had been evacuated and purged with the sample. The analysis of the sample showed about 0.1% or 1000 ppm impurities, mostly air. This may be attributed to the residual air absorbed on the glass of the sample bulb or to contamination by the mass spectrometer.

III. EXPERIMENTAL PROCEDURE AND DATA

The inner and outer chambers of the cryostat were evacuated to below 10^{-3} mm Hg continuously. After the cryostat had been cooled down by liquid nitrogen, the level of which was appropriately controlled, the shield heater was used with the L & N control unit to maintain the inner shield at 2 to 3 degrees below the temperature of the state to be studied. The cell temperature as measured by the platinum resistance thermometer was then controlled to the corresponding set potential of the Wenner potentiometer. The instrument zero reading on the spectrometer was recorded for the evacuated cell.

1. Single Phase Isotherms

The argon sample was admitted to the cell, while the pressure was measured approximately by the T.I. pressure gauge. Due to the compression of the sample in the cell, the temperature would first increase. After the temperature was restored automatically by the control system, the sample pressure decreased. To reach the desired sample pressure, several fillings were needed. With the temperature under control, the sample pressure was found to vary slightly due to the portion of inlet line exposed to the room temperature. Valve D (shown in Figure 3) was manually adjusted to control the sample pressure in balance with the constant oil pressure which was measured with the Hart balance dead weight tester. The angle of minimum deviation was then measured in a time interval of 10 to 15 minutes, while both the cell temperature and the sample pressure were held constant and the refracted light image was sharp and distinct.

On each isotherm, 8 to 12 data points were measured in the manner described above. It is desirable to have the measurements of the angle of minimum deviation evenly spaced, however, this is not readily achieved experimentally. The pressure was increased in such a way that the angle measurements were also increased by approximately 10 to 20 minutes of arc. For the isotherms of higher temperature, the compressibility of the sample fluid was small and the angle of minimum deviation did not vary significantly over the pressure range. Therefore, larger steps in pressure were necessary. As the compressibility became larger for the isotherms near the critical temperature, small increments in pressure were taken to have the same interval of the angle of minimum deviation.

Fourteen isotherms between 163.004°K and 150.701°K were studied. The experimental data are reported in Table I. As mentioned in Section II, the cell temperatures in Run III to Run XX were measured by the conventional method using two potentiometers and the sample pressures in Run III to Run V were measured with the T.I. pressure gauge. The improved temperature and pressure measuring methods were used in the later runs.

Only one run was made for each isotherm at 163.004°, 160.003°, 156.998°, and 153.923°K . For all other isotherms, at least two runs were made at the same temperature. Effort was made to have the first data point of each run measured at the same pressure and similarly for the last data point. In smoothing the data on each isotherm, the experimental data of different runs were plotted on a large-scale

graph and a flexible spline was used to draw a single smooth curve through the data points. In general, the data of separate runs of the same isotherm were consistent with one another. Run VII at 152.018°K and Run XXXI at 152.999°K are two exceptions. In plotting the data of these runs, they fall into a separate curve from those of other runs at the same temperature. This discrepancy is attributed to possible errors in the temperature and pressure measurements. The data of these runs are excluded in the final results. For similar reasons, a few data points of various runs for the isotherm at 151.002°K are also excluded. They are indicated by * in Table I. Data points indicated by † in Table I are consistent with others of the same isotherm, however, they are excluded in the final results for smoothness in the later analysis by cubic spline fit of the data (see Section IV.2).

The effect of small temperature differences on the data of angle of minimum deviation became more prominent in approaching the critical temperature. For each of the isotherms at 150.899°K, 150.799°K, and 150.751°K, in plotting the data of separate runs of the same isotherm, distinct curves can be drawn and shown to differ, in terms of temperature, by an amount equivalent to approximately 0.006°K. This may be attributed to the reproducibility of the temperature measurement. The final analysis of these data will be discussed later in Section IV.2. Since the compressibility near the critical density on these isotherms was very large, slight change on the sample pressure due to small fluctuations of oil pressure on the Hart balance and the barometric pressure caused a very large variation on the measurement

of angle of minimum deviation. The states for the middle data points on these isotherms were less stable than the others. The refractive light images, although still distinct, showed slight broadening. Larger experimental uncertainties on the angle measurements were observed for these data points.

The data of Run XXIX at 150.701^{o}K were single phase at lower and higher pressures, but coexisting gas and liquid phases were observed at one pressure. This indicates that the critical temperature is above this temperature, 150.701^{o}K, and below 150.751^{o}K, the temperature of the last completely single phase isotherm.

2. Coexisting Gas-Liquid States

The cell was filled with argon sample fluid until the gas-liquid interface appeared at the center. The vapor pressure data of argon reported by Levelt[9] were used to check approximately the sample pressure in the cell as indicated by the T.I. pressure gauge. Over a period of one or two hours when the cell temperature was controlled constant to $\pm 0.001^{\circ}K$, the relative amounts of gas and liquid phases in the cell changed as they approached thermal equilibrium. Small adjustments on the total amount of the sample in the cell were then made so that the gas-liquid interface reappeared at the center of the cell. The measurements of the angles of minimum deviation for both phases were recorded in an interval of one hour while the following criteria of equilibrium and homogeneity for the sample in the cell were held: (1) the cell temperature was held constant within $\pm 0.001^{\circ}K$, (2) the relative amounts of the two phases did not change (i.e., the interface stayed at the center of cell), (3) the light images refracted from the two phases were both sharp and distinct. The vapor pressure of the sample was then measured with the Hart balance dead weight tester. Measurements in this manner were carried out from $148.51^{\circ}K$ to $150.72^{\circ}K$ in five experimental runs and recorded in Table II. At the beginning of Run 1, several readings of instrument zero V_o, as well as V_1 and V_2 (see Appendix B) were taken on the spectrometer and the averages of the readings were fixed and used throughout the subsequent runs. Relative errors in the measured angles of minimum deviation D were estimated from the uncertainty in the readings V (see Appendix B).

At 148.513°K, which is about two degrees below the critical temperature, the temperature stability and the equilibrium conditions of the sample fluid in the cell were obtained without much difficulty. The measurements at this temperature were repeated as the first data point of each run to check the consistency in the reproducibilities of the temperature, pressure, and optical measurements and the integrity of the sample fluid in the cell. From the data recorded, no systematic errors could be noted.

As the critical temperature is approached, small fluctuations in temperature can cause large changes of phase of the fluid in the cell and can decrease the stability of the system. In order to achieve the same stability in control as before, the temperature difference between the cell and the shield was decreased. This decreased the heat loss from the cell to the shield and caused the cell to respond more slowly and stably. At the same time the current in the coiled line heater was increased to prevent the condensation of the sample fluid along the coiled inlet line inside the inner shield.

Near the critical state of the sample fluid, the refracted light images seen in the viewing telescope of the spectrometer became broad and indistinct, and the measurements of angle of minimum deviation had larger uncertainties. It is felt that this was due to density gradients in the cell, which would be caused by even a very small fluctuation of temperature. For the measurements at 150.658°K and 150.675°K in Run 4 , the refracted light images showed slight broadening but were still quite distinct along the edges. For the measurement at 150.711°K, although a clear interface between the two

coexisting phase could still be seen at the center of the cell, the light images were much broader and less distinct.

Run 5 of the coexisting gas-liquid states and Run XXIX of the single phase isotherm at 150.701^{o}K were both part of a continuous operation. In Run 5, the first data point of coexisting gas-liquid state gave the value of angle of minimum deviation for the gas phase only, since there was very little liquid present in the cell. For the next data point, great care was taken with true equilibrium conditions in the cell. The angle measurements for both phases were recorded over a period of half an hour while the gas-liquid interface stayed at the center of the cell. Next, the cell temperature was increased to 150.720^{o}K. Great difficulty was encountered in maintaining stable conditions in the cell. Very broad and indistinct light images were observed in the viewing telescope. The two images would alternately increase or decrease in brightness (sometimes simultaneously) and there were also instances when there were no visible images. This phenomenon is very close to what occurs in the critical opalescence. The final angle measurements were recorded over a short period of 10 minutes when both images were bright and the relative amounts of two phases in the cell did not change appreciably. Larger experimental uncertainties were observed for these measurements. Under the same conditions and several hours later, the same measurements at this temperature, 150.720^{o}K, were repeated to check their reproducibility. Then, the cell temperature was decreased to 150.701^{o}K. The angle measurements for the coexisting phases were made after the

equilibrium was reached. The reproducibility of the measurements at 150.701°K was better than that at 150.720°K.

3. Comparison of Data

For coexisting gas-liquid states above 150°K, the data of angles of minimum deviation versus temperature, recorded in Table II, are plotted and shown in Figure 4. For the purpose of comparison, the data in the same region measured by Teague[54] are also plotted in Figure 4. The experimental uncertainties in the temperature measurements are shown by error bands for the representative points. The uncertainties in the angles are too small to be represented on the plotting scale used. In terms of temperature differences, the data from the present study are in general 0.02°K higher than those obtained by Teague[54] for the corresponding angle of minimum deviation. If the temperature error bands are taken into account for both sets of data, they agree within the uncertainty limit. It is felt that the data from the present study are more accurate, since the temperature and angle measuring methods have been improved (see Section II.3 and Appendix B).

For single phase fluid states, the data of Run III at 163.004°K, listed in Table I, are plotted in Figure 5 and compared with the data at 163.156°K reported by Teague[54]. The experimental error bands of the angles of minimum deviation and the pressures are too small to be represented on the plotting scale used. A smooth curve is fitted through the data points of Run III at 163.004°K. In terms of the temperature difference, the correspondence between the two sets of data is relatively good.

IV. RESULTS AND ANALYSES

1. Refractive Index

The values of refractive indices were computed by using Equation (27),

$$n = \frac{\sin \frac{1}{2}(A+D)}{\sin \frac{1}{2} A} \tag{27}$$

where D is the measured angle of minimum deviation recorded in Tables I and II, and A is the apex angle between the prism faces of the cell. The value of A used was $44^{\circ}16.14' \pm 0.31'$, which was determined by calibration with water (see Appendix A). This value differs from that reported by Teague[8], $44^{\circ}18.57' \pm 0.41'$, for the same cell. It is felt that this new value of A is more accurate, since the methods of measuring the angle and the temperature have been improved. This discrepancy in the value of A produces deviations in the refractive index ranging from a minimum of 0.0000232 at $D = 72.28'$ to 0.001121 at $D = 348.92'$.

From the experimental uncertainties in angle A, $\pm 0.31'$, and in angle D, $\pm 0.09'$, the errors in refractive index n can be calculated from the equation,

$$\sigma_n = \frac{\sin \frac{1}{2} D}{2 \sin^2 \frac{1}{2} A} \sigma_A + \frac{\cos \frac{1}{2}(A+D)}{2 \sin \frac{1}{2} A} \sigma_D \tag{28}$$

The error ranges from a minimum of 0.0000354 at $D = 72.28'$ to 0.0000475 at $D = 348.92'$.

The computed values of refractive indices for the coexisting gas-liquid states are tabulated in Table III, and plotted versus temperature in Figure 6. At the state 148.513°K, the refractive indices shown are the averages of the measurements made during different runs. The refractive indices tabulated for the state 150.701°K and 150.720°K are averages of the repeated measurements made during Run 5. The errors in refractive indices for each state, as calculated from Equation (28), are also tabulated in Table III.

The computed values of refractive indices for single-phase states along each isotherm are listed in Table IV. Figure 7 shows the results of refractive indices versus pressures for isotherms from 163.004°K to 152.018°K. Figure 8 shows the similar results for isotherms from 151.509°K to 150.701°K. For those isotherms with multiple runs, as mentioned in Section III, effort was made to have the first data point of each run of the same isotherm measured at the same pressure. The average of the results of these measurements is listed as the first entry of the isotherm shown in Table IV. The succeeding entries are shown in the order of increasing pressure by combining the results of separate runs. (The data points indicated by * in Table I are excluded.) The last entry of the isotherm is obtained in a manner similar to the first one. For isotherms at 150.899°K, 150.799°K, and 150.751°K, the results of separate runs are listed separately as Set I, II, and III of each isotherm.

2. Isothermal Compressibility

Based on Equation (2), the isothermal compressibility K_T can be computed from the refractive index n and its pressure derivative $(\partial n/\partial P)_T$. Since the experimentally measured quantity is the angle of minimum deviation D , it is advisable to calculate $(\partial n/\partial P)_T$ from the following relation

$$(\frac{\partial n}{\partial P})_T = \frac{\cos \frac{A+D}{2}}{2 \sin \frac{1}{2} A} (\frac{\partial D}{\partial P})_T \tag{29}$$

where $(\partial D/\partial P)_T$ can be estimated directly from the experimental data. Using Equations (2), (27), and (29), K_T may be expressed as follows:

$$K_T = F(A,D) (\frac{\partial D}{\partial P})_T \tag{30}$$

where

$$F(A,D) = \frac{3(1 - \cos A) \sin(A+D)}{[\cos A - \cos(A+D)][3 - \cos(A+D) - 2 \cos A]}$$

The method used for estimating the derivative $(\partial D/\partial P)_T$ is known as cubic spline fit[58] which is the numerical analogue of the "draftsman's" spline with the personal bias eliminated. The method consists of joining the data points by sections of cubics, requiring that the slopes and curvature be continuous at the junction points. The details of the algorithm are discussed in Appendix D. As a result of relaxing the overall requirement of analyticity, the quality of derivatives obtained from this method is superior to that from polynomial interpolation.

The decision was made to fit the experimental data in the form of pressure versus angle D. This facilitates the direct interpolation of $(\partial D/\partial P)_T$ and K_T from the value of D_c. This will be discussed in some detail in Section IV.6. For the smoothness of the fit, points indicated by † in Table I were not included in the fit and thereby not listed in Table IV. The effect of errors in the experimental data on the smoothness of the fit becomes more prominent when the critical temperature is approached. For the isotherm at 150.899°K, separate fits for the three sets of data give comparable results. For the isotherm at 150.799°K, the derivatives of the middle points obtained from the fit of data set I are negative and physically insignificant. Similar results are obtained from the fits for the two sets of data at 150.751°K. However, by including an additional point interpolated from a graph of angle D versus pressure, the fit of set II at 150.751°K yields reasonable derivatives and isothermal compressibilities for all data points.

The estimated value of $(\partial D/\partial P)_T$ and the values of K_T subsequently computed from Equation (30) are listed in Table IV. Figures 9 and 10 show the isothermal compressibilities along the isotherms 152-163°K and 150.75 - 151.5°K, respectively. For each of the isotherms at 150.899°K, 150.799°K, and 150.751°K, only data set II are shown in Figure 10 and used in the later analyses. No isothermal compressibility was computed along the isotherm at 150.701°K, since there will be no analysis of isothermal compressibility below the critical temperature.

The errors in $(\partial D/\partial P)$ obtained above cannot be ascertained easily. Comparisons have been made of these values of $(\partial D/\partial P)_T$ and

those estimated visually from a graph of angle D versus pressure. In general, they differ by about 5-10% as is shown in Table V for selected isotherms. The error in $(\partial D/\partial P)_T$ is considered to be $\pm 5\%$ of the value of $(\partial D/\partial P)_T$. The error in K_T is estimated to be $\sigma_{K_T} = \pm 0.05\ K_T$, and is due mostly to the error in $(\partial D/\partial P)_T$ since $F(A,D)$ in Equation (30) can be established with a relatively high accuracy.

3. Data Weighting and Least Squares Fit Technique

To analyze the experimental data describing the critical anomalies, it is necessary to assign proper weights to the data to allow for the increasing experimental errors as the critical state is approached. Moreover, since analyses were made by fitting the data to the equations in terms of differences, e.g., $T - T_c$, etc., with the same experimental errors in the measured quantities ρ (or n) and T, the data points closer to the critical state will have larger errors in the differences $\rho - \rho_c$ and $T - T_c$, and corresponding lower weights in the fit.

There are three independent sources of experimental error: those in the refractive index, the temperature, and the pressure measurements. As indicated in Section IV.1, the error in refractive index σ_n is calculated from the experimental uncertainties in angle A and in angle D using Equation (28). The temperature error σ_T from one isotherm to another is the precision of the temperature measurement, $\pm$ 0.010°K. The pressure error σ_P is 1 in 10,000, or $\pm$ 0.01% P.

In using Lorentz-Lorenz relation Equation (1) to relate the refractive index to the density, it is convenient to define a grouping $\phi = (n^2-1)/(n^2+2)$. The error in ϕ due to the error in n is given by the following expression

$$\sigma_\phi = \frac{6n}{(n^2+2)^2} \sigma_n \qquad (31)$$

In the fits performed in the succeeding sections, various functions of the measured quantities are used. Variances of measured quantities are

obtained as the squares of the respective experimental errors, and are combined to give the final variance of the function used in the fit. The weight attributed to the function in the fit is the inverse of the final variance. In general, the equations to be fitted, e.g., Equations (8), (9), and (23), etc., are transformed into the logarithmic forms to facilitate the use of linear least-squares fit method. Care is taken in assigning the proper weights to the new functions in the logarithmic form.

The linear least-squares fit technique developed by Williamson[59] is used in the analyses throughout this study. In this method, not only the error in the dependent variable, but also the error in the independent variable is taken into account in the fitting. The latter is often overlooked and sometimes[36,49,50] assumed to contribute as a part of the former according to the form of the fitted equation. A few analyses were made using the nonlinear least-squares fit technique developed by Marquardt[60] and the method of linear regression analysis[61], in neither of which weight assignment was carried out.

4. Rectilinear Diameter Analysis

As discussed in Section 1.1, for practical purposes the Lorentz-Lorenz relation can be used to relate the refractive index to the density. Thus, the law of rectilinear diameter (Equation (19)) can be rewritten into the following form:

$$(\phi_L + \phi_G) / 2 = \phi_c[1 + a(T_c - T)] \tag{32}$$

or written as

$$\overline{\phi} = \phi_o - dT \tag{33}$$

where $\phi_L = [(n^2 - 1)/(n^2 + 2)]_{Liquid}$ and $\phi_G[(n^2 - 1)/(n^2 + 2)]_{Gas}$ were computed from the experimental values of n_L and n_G, respectively. The weight attributed to $(\phi_L + \phi_G)/2$ or $\overline{\phi}$ was found to be $4/(\sigma^2_{\phi_L} + \sigma^2_{\phi_G})$, where σ_{ϕ_L} and σ_{ϕ_G} were calculated from Equation (31). The results of the fit to Equation (33) are presented in Table V and in Figure 11. The estimated error in $\overline{\phi}$ for each point is also shown in Figure 11. The error in T, $\sigma_T = 0.01^{\circ}K$, is smaller than the plotting symbol on the graph and is not shown. The fitted line fits essentially all the data points within their experimental errors. The value of ϕ at the critical point ϕ_c may be obtained by extrapolating this line to the best value of T_c to be determined in the next section.

A curve diameter expressed by the following equation

$$(\rho_L + \rho_G)/2 = \rho_c + d_{cd}(T_c - T)^{1-\alpha'} \tag{34}$$

has been recently found by Widom and Rowlinson[62] in a certain continuum model which has an underlying symmetry closely analogous to

that of the lattice gas. It is noted that this diameter has a singularity comparable with that in the specific heat $C_v(T)$ (Equation (12)). Using Equation (1), it follows from Equation (34) that

$$(\phi_L + \phi_G)/2 = \phi_c + d_{cd}(T_c - T)^{1-\alpha'} \tag{35}$$

The same experimental data used above were fitted to Equation (35) with a variety of values of α'. The standard deviation of the fit passes through a minimum at $\alpha' = -0.09$, as shown in Figure 12. Although Sengers et al[36] indicated that slightly negative values of α' are favored in the similar analysis using the data of CO_2, N_2O, and $CClF_3$, the value of α' from the present study is contrary to the general finding[15-18,43], $0 \leq \alpha' < 0.1$ from the specific heat analyses.

5. Determination of Exponent β on the Coexistence Curve

Using the Lorentz-Lorenz relation, equation (16) can be expressed in the following form

$$\phi_L - \phi_G = B_\phi (T_c - T)^\beta \tag{36}$$

or

$$\ln(\phi_L - \phi_G) = \ln B_\phi + \beta \ln(T_c - T) \tag{37}$$

The experimental data of ϕ_L and ϕ_G listed in Table VI were used to fit to Equation (37). The weights assigned to the functions $\ln(\phi_L - \phi_G)$ and $\ln(T_c - T)$ were $(\phi_L - \phi_G)^2/(\sigma^2_{\phi_L} + \sigma^2_{\phi_G})$ and $(T_c - T)^2/\sigma^2_T$, respectively. Linear least squares fits of Equation (37) were carried out for a sequence of assumed values of T_c. The best fit is obtained when the standard deviation of the data from the fitted equation reaches a minimum. The final results of the best fit are shown in Table VII and Figure 13. The deviations of the experimental values of $\ln(\phi_L - \phi_G)$ from the calculated values are shown in Figure 14. In these figures, the estimated errors of the data points are shown by error bands. Where the error bands are not shown explicitly, they are smaller than the plotting symbols used.

In a similar manner, the same experimental data of ϕ_L and ϕ_G were used separately to fit the following equations

$$\ln(\phi_L - \phi_C) = \ln B'_{\phi_L} + \beta_L \ln(T_c - T) \tag{38}$$

$$\ln(\phi_C - \phi_G) = \ln B'_{\phi_G} + \beta_G \ln(T_c - T) \tag{39}$$

which were transformed from Equations (17) and (18). Here the values

of ϕ_c for various assumed values of T_c used in the fits were computed from the fitted line of rectilinear diameter, i.e., Equation (33). The weights assigned to $\ln(\phi_L - \phi_C)$ and $\ln(\phi_C - \phi_G)$ were $(\phi_L - \phi_C)^2/\sigma^2_{\phi_L}$ and $(\phi_C - \phi_G)^2/\sigma^2_{\phi_G}$, respectively. The coefficients obtained from the best fits to Equations (38) and (39) are presented in Table VIII. They do not agree with those obtained from the fit to Equation (37), which are included in Table VIII. Comparison of the values of β shows that $\beta_L > \beta > \beta_G$. Using the same value of T_c, 150.725°K, as determined from the fit to Equation (37), the coefficients obtained for the fits to Equations (38) and (39) are also presented in Table VIII. The discrepancy of the values of β reduces slightly.

The above results seem to indicate that the higher order terms in the general coexistence curve equation (Equation (8)) and the correction terms in the Lorentz-Lorenz relation (Equation (1)) might be significant. Since the available method for resolving the significance of the higher order terms is that of linear regression analysis which is not suitable for use with an equation such as Equation (8), Teague[8] has expanded Equation (37) into the following form:

$$\ln(\phi_L - \phi_G) = \ln B + \beta \ln(T_c - T) + A_1(T_c - T) + A_2(T_c - T)^2 \qquad (40)$$

Based on the same data for ϕ_L and ϕ_G used above, the results of the fit to Equation (40) for various assumed values of T_c are listed in Table IX. It is found that the standard deviation of the data from the fitted equation passes through a minimum at $T_c = 150.725$°K, where

simultaneously the standard error of β reaches its minimum and the coefficients of higher order terms no longer contribute to the fit at 95% confidence level. This finding confirms that obtained by Teague[8]. Similarly, Equations (38) and (39) can be expanded into the following forms:

$$\ln(\phi_L - \phi_C) = \ln B'_{\phi_L} + \beta_L \ln(T_c - T) + A_{1L}(T_c - T) + A_{2L}(T_c - T)^2 \quad (41)$$

$$\ln(\phi_C - \phi_G) = \ln B'_{\phi_G} + \beta_G \ln(T_c - T) + A_{1G}(T_c - T) + A_{2G}(T_c - T)^2 \quad (42)$$

With the same finding as above, the best fits to Equation (41) and Equation (42) yield the same values of T_c , 150.725°K . Also, the values of β obtained agree with that from Equation (40) within numerical uncertainty, as shown in Table VIII. Since no data weighting can be employed in the present linear regression analysis, the results of the fits to Equations (40)-(42) are considered less reliable than those from the fits to Equations (37)-(39) with proper data weighting. It is felt that the relation $\beta_L = \beta_G = \beta$ cannot be proved definitely from the experimental data of this study.

The best values of T_c and β are those obtained from the fit to Equation (37); namely, $T_c = 150.725^{\circ}K$ and $\beta = 0.3574 \pm 0.0027$. The value of β agrees with that reported by Teague[8], 0.3643 ± 0.0066, within numerical uncertainty. Since the accuracy of the temperature measurement is 0.010°K, the absolute value of T_c determined should be taken as $150.725^{\circ}K \pm 0.010^{\circ}K$, which is higher than that obtained by Teague[8], $150.704^{\circ}K \pm 0.015^{\circ}K$. This may be attributed to the fact that

in this study the temperatures were measured by an improved method and, in general, were 0.02^{o}K higher than those measured by Teague for the same state (see Section III.3).

6. Determination of Exponent γ on the Critical Isochore

The critical isochore is established by the value of $\phi = (n^2 - 1)/(n^2 + 2)$ at the critical point ϕ_c using the Lorentz-Lorenz relation (Equation (1)). ϕ_c can be computed from the fitted line of rectilinear diameter (Equation (33)). Based on the best value of T_c, 150.725°K, as determined in the last section, ϕ_c was found to be 0.0564984, which yielded the values $n_c = 1.08611_{45}$ and $D_c = 242.626$ minutes of arc. Values of $(\partial D/\partial P)_T$ at $D = D_c$ on each isotherm were interpolated from the same spline fit of pressure versus angle D as performed in Section IV.2. Subsequently, the values of isothermal compressibility K_T were computed using Equation (30) and were fitted to Equation (9) in the following logarithmic form

$$\ln K_T = \ln \Gamma - \gamma \ln(T - T_c) \tag{43}$$

The weights assigned to the functions $\ln K_T$ and $\ln(T - T_c)$ were $K_T^2/(0.05\ K_T)^2$ and $(T - T_c)^2/\sigma_T^2$, respectively. The results of the least-squares fit are presented in Table X and Figure 15. The value of γ determined was 1.170 ± 0.013. The fitted line passes through most of the data points within their experimental uncertainties (except for the one nearest to the critical temperature) which are too small to show on the scale of the figure.

For a similar reason as was discussed in the last section, Equation (43) was modified to include higher order terms

$$\ln K_T = \ln \Gamma - \gamma \ln(T - T_c) + A_{1K_T}(T - T_c) + A_{2K_T}(T - T_c)^2 \tag{44}$$

Using linear regression analysis (unweighted data), the same set of K_T data used above was fitted to Equation (44). It was found that the higher order terms had no significant contributions to the fit at 95% confidence level. Essentially then, the result is the same as having performed a fit to Equation (43) with unweighted data. The value of γ obtained from this fit was 1.214 ± 0.028 . The fitted line is also shown in Figure 15. Clearly, the previous fit to Equation (43) with weighted data is better and the significance of the weighting of data cannot be ignored.

Since the value of T_c of $150.725^{\circ}K$, as determined in the last section, is reliable to $\pm 0.010^{\circ}K$, the effect of variation of T_c as a parameter on the fit to Equation (43) was examined. Least-squares fit (weighted data) to Equation (43) were carried out for a sequence of assumed values of T_c in the same manner as above for $T_c = 150.725^{\circ}K$. The results are shown in Table XI. The standard deviation of the fit, σ_{fit}, reaches a minimum at $T_c = 150.731^{\circ}K$, where the value of γ is found to be 1.161 ± 0.013 which agrees well with that for $T_c = 150.725^{\circ}K$ within numerical uncertainty. The result of the fit at $T_c = 150.731^{\circ}K$ is shown in Figure 16.

7. Maximum Isothermal Compressibility

Using the scaled equation of state, Equation (23), Widom[44] showed that the locus of the inflection points in the pressure-density isotherms, i.e., $(\partial^2 P/\partial^2 \rho)_T = 0$, was confined entirely to the region $\rho \leq \rho_c$. As the critical point is approached, this locus in a temperature-pressure plane is found to approach the curve

$$\rho - \rho_c = -b(T - T_c)^{2\beta} \tag{45}$$

Later, Sengers[40] indicated that the locus of the maximum compressibility on each isotherm, i.e., $(\partial K_T/\partial \rho)_T = 0$, behaved similarly. It follows that the compressibilities along each of these loci have the same exponent γ as the compressibility along the critical isochore as the critical point is approached.

From the same spline fit of pressure versus angle D as performed on each isotherm in Section IV.2, the interpolated values of $(\partial D/\partial P)_T$ and K_T at equal intervals of $\Delta D = 2'$ were computed. The angle D_m at which K_T is a maximum was found by using the 5-point formula developed by Salzer[63] for finding the argument for which a function has a given derivative, and letting the derivative $(\partial K_T/\partial D)_T = 0$. Subsequently, the values of n, ϕ, $(\partial D/\partial P)_T$, and K_T were obtained at this angle D_m and are presented in Table XII. For comparison, the values of the maximum of K_T estimated visually from large graphs of Figures 9 and 10 and the relative percentage difference from those obtained above numerically are also listed in Table XII.

In Figure 17, the temperature and the function along this locus of maximum compressibility are plotted. The large scattering of the data points is probably due to the inaccuracy inherent in locating the maximum. However, it is clear that these points cannot be accounted for by a smooth extension of the straight line characterizing the rectilinear diameter of coexistence curve, which was determined in Section IV.4. The dashed curve in Figure 17, which fits the data points reasonably well, was obtained from the least-squares fit to the equation

$$\phi - \phi_c = -b_\phi (T - T_c)^{2\beta} \tag{46}$$

with $T_c = 150.725^{\circ}K$ and $\beta = 0.3574$. It should be noted that the curve has infinite slope at the critical point.

The maximum compressibilities obtained by the above numerical method were fitted to Equation (43) in the same way as the compressibilities on the critical isochore discussed in the last section. The result of the least-squares fits (weighted data) are listed in Table XIII. For $T_c = 150.725^{\circ}K$, the exponent γ was found to be 1.149 ± 0.012. However, the standard deviation of the fit reaches the minimum at $T_c = 150.738^{\circ}K$ where $\gamma = 1.131 \pm 0.013$. These values of T_c and γ do not agree with those obtained from the analysis of the compressibility on the critical isochore. It is felt that this may be attributed to the inaccuracy inherent in the determination of maximum compressibility.

8. The Scaled Equation of State[44]

A. Evaluation of the Chemical Potential Difference $\Delta\mu$

Using the Lorentz-Lorenz relation (Equation (1)) and the thermodynamic relation

$$\mu(\rho,T) - \mu(\rho_c,T) = \int_{P(\rho_c,T)}^{P(\rho,T)} \frac{1}{\rho}\, dP \tag{47}$$

the reduced chemical potential difference along an isotherm can be evaluated by the following equation:

$$\Delta\mu = \frac{\phi_c}{P_c} \int_{P(\phi_c,T)}^{P(\phi,T)} \frac{1}{\phi}\, dP \tag{48}$$

where

$$\Delta\mu = [\mu(\rho,T) - \mu(\rho_c,T)] \,/\, (P_c/\rho_c)$$

and

$$\phi = (n^2-1) \,/\, (n^2+2)$$

To avoid the errors which may occur due to inverse interpolation, the integral in Equation (48) is calculated by using the following relationship:

$$\int_{P(\phi_c)}^{P(\phi)} \frac{1}{\phi}\, dP = \left(\frac{P(\phi)}{-\phi} - \frac{P(\phi_c)}{\phi_c}\right) - \int_{\phi_c}^{\phi} P\, d\left(\frac{1}{\phi}\right) \tag{49}$$

The values of ϕ on each isotherm were calculated from the refractive index data presented in Table IV. A cubic spline fit of pressure

versus $(\frac{1}{\phi})$ was then performed. Thus, the integral $\int P\, d(\frac{1}{\phi})$ can be evaluated analytically for each interval between two adjacent data points (see Appendix D, Equation (D-11)). The value of ϕ_c used in Equations (48)-(49) was 0.0564984, as determined earlier from the rectilinear diameter analysis based on $T_c = 150.725^{\circ}K$. The value of P_c used in Equation (48) was 47.983 atm, obtained from the extrapolation of the vapor pressure data listed in Table III to $T_c = 150.725^{\circ}K$.

The values of $\Delta\mu$ obtained in this way on each isotherm and the corresponding reduced density $\Delta\phi = (\phi - \phi_c)/\phi_c$ are listed in Table XIV and shown in Figures 18 and 19. It can be seen that the antisymmetry of $\Delta\mu$ below and above ϕ_c assumed by the scaled equation of state is well satisfied within the range of data shown in these figures. Data points listed in Table XIV with $\Delta\mu < -0.45$ or $\Delta\phi < -0.19$ are not shown in Figure 18. The antisymmetry of these points cannot be tested for lack of corresponding data above ϕ_c. However, antisymmetry is assumed for these points because of the good agreement obtained in the cases where such a test could be made.

B. Analyses of the $\Delta\mu, \Delta\phi$ Data

In Equation (23), the reduced density $\Delta\rho$ can be replaced by $\Delta\phi$ through the Lorentz-Lorenz relation and the exponent δ is related to β and γ by Equation (24). Thus, Equation (23) can be rewritten as

$$\Delta\mu = \Delta\phi |\Delta\phi|^{\gamma/\beta} h(x) \qquad (50)$$

where the scaled variable $x = \Delta T/|\Delta\phi|^{1/\beta}$. Using Equation (50) with $h(x)$ given by Equation (26), the fit to the experimental $\Delta\mu,\Delta\phi$ data listed in Table XIV can be made by employing the nonlinear least-squares technique developed by Marquardt[60] to determine simultaneously the six parameters, E_1, E_2, γ, β, T_c, and x_o . In this fitting an initial guess of the values of parameters must be given. It was found that different sets of initial guesses of the parameters converged to slightly different final values but all agreed within their standard errors estimated from the fit. The averages of the values from the various fits were taken as the most probable values of the parameters which are as follows:

$E_1 = 3.902 \pm 0.068$ $\qquad$ $\beta = 0.2746 \pm 0.0029$

$E_2 = 0.143 \pm 0.029$ $\qquad$ $T_c = 150.651^{o} \pm 0.037^{o}K$

$\gamma = 1.101 \pm 0.007$ $\qquad$ $x_o = 0.3259 \pm 0.0068$

The value of T_c determined above contradicts the experimental finding of the liquid-gas coexistence states above this temperature. The value of β is too small compared with other experimental values found for argon and most theoretical predictions. It is felt that these values for the parameters are somewhat unreliable because of (i) a lack of data weighting in the nonlinear least-squares fit and (ii) the $\Delta\mu,\Delta\phi$ data all being above T_c , whereas the exponent β should depend on information below T_c .

A second approach to the analysis of $\Delta\mu,\Delta\phi$ data was then

made using $\beta = 0.3574$ and $x_o = (\frac{2\phi_c}{B_\phi})^{2\beta} \frac{1}{T_c} = 0.1836$, the values determined earlier from the analysis of the coexistence curve in Section IV.5. Equations (50) and (26) were combined and rearranged in the following form:

$$\left[\frac{x_o}{x+x_o} \frac{\Delta\mu}{\Delta\phi|\Delta\phi|^{\gamma/\beta}}\right]^{\frac{2\beta}{\gamma-1}} = E_1^{\frac{2\beta}{\gamma-1}} \left[1 + E_2(\frac{x+x_o}{x_o})^{2\beta}\right] \tag{51}$$

For given values of T_c and γ, $G(x) = \left[\frac{x_o}{x+x_o} \frac{\Delta\mu}{\Delta\phi|\Delta\phi|^{\gamma/\beta}}\right]^{\frac{2\beta}{\gamma-1}}$ and $X = (\frac{x+x_o}{x_o})^{2\beta}$ can be computed from the $\Delta\mu, \Delta\phi$ data and fitted to Equation (51) by using the linear least-squares technique[59] with data weighting. Using propagation of errors, the weights attributed to $G(x)$ and X are, respectively,

$$W_{G(x)} = \frac{(\frac{\gamma-1}{2\beta G(x)})^2}{(\frac{\sigma_{\Delta T}}{\Delta T})^2(\frac{x}{x+x_o})^2 + (\frac{\sigma_{\Delta\phi}}{\Delta\phi})^2[1+\frac{\gamma}{\beta} - \frac{x}{\beta(x+x_o)}]^2 + (\frac{\sigma_{\Delta\mu}}{\Delta\mu})^2} \tag{52}$$

and

$$W_X = \frac{(\frac{x+x_o}{2\beta x})^2}{\{[(\frac{\sigma_{\Delta T}}{\Delta T})^2 + \frac{1}{\beta^2}(\frac{\sigma_{\Delta\phi}}{\Delta\phi})^2]\, X^2\}} \tag{53}$$

where $\sigma_{\Delta T} = \sigma_T/T_c = 0.01^o/T_c$, $\sigma_{\Delta\phi} = \sigma_\phi/\phi_c$ with σ_ϕ computed from Equations (28) and (31), and $\sigma_{\Delta\mu} = 2\sigma_p/P_c = 4.168 \times 10^{-6}\, P$. The fits were performed for a sequence of assumed values of T_c and γ until a minimum of standard deviation of the fit was reached. The values of parameters obtained at the minimum were

$E_1 = 2.396 \pm 0.070$ $\qquad\qquad$ $\gamma = 1.198$

$E_2 = 0.218 \pm 0.014$ $\qquad\qquad$ $T_c = 150.720^{\circ}K$

"Experimental" values of $h(x)$ can be calculated from Equation (50) using the experimental $\Delta\mu, \Delta\phi$ data and the fitted values of exponents β and γ. These values can be compared with the "fitted" function $h(x)$, Equation (26), using the fitted values of all six parameters. These comparisons are made in Figure 20 and yield good agreement. In Figure 21 the relative deviation $[h(x)_{exp't} - h(x)_{fitted}] / h(x)_{exp't}$ is plotted versus $\ln(\frac{x+x_o}{x_o})$. There appears to be a slightly upward trend in this deviation for larger values of $(\frac{x+x_o}{x_o})$. This may be attributed to the fact that the higher order terms in the series expansion of the function $h(x)$ given by Equation (26) do not have the correct forms at large x. However, internal checks have been made by comparing the experimental isothermal compressibility (shown in Table IV) with values calculated from the fitted function $h(x)$ according to

$$K_T = \frac{1}{\rho^2 (\frac{\partial \mu}{\partial \rho})_T} = \frac{\phi_c}{\phi^2 P_c (\frac{\partial \Delta\mu}{\partial \phi})_T} \tag{54}$$

As shown in Figures 22 to 24 for selected isotherms, the calculated values of K_T agree well with the experimental values.

V. CONCLUSIONS

Using refined experimental techniques in the method of angle of minimum deviation, the refractive indices of fluid argon near its critical state were measured along the coexistence curve and along fourteen single phase isotherms from 150.7° to 163°K for $\lambda_{Na} = 5893\text{Å}$. The measurements were carried out to within a few hundredths of a degree both below and above the critical temperature. The accuracy of measurement was improved and estimated to be ±0.010°K in temperature, ±0.01% in pressure, and ±0.00005 in refractive index. Comparison of the measurements along the coexistence curve from the present study with those obtained by Teague[8] showed consistent discrepancies of 0.02°K in the measured temperatures. It is felt that the measurements from the present study are more accurate, since the measuring methods have been improved.

The measured refractive index data were related to the densities by the Lorentz-Lorenz relation, which from previous investigations[6,8] had been verified for argon over a wide range of temperature and pressure. Consequently, the isothermal compressibilities along the single phase isotherms were determined according to Equation (2), in which the derivatives were estimated by the method of cubic spline fit[58].

In analyzing the data to determine the critical constants and exponents, the significance of data weighting in both dependent and independent variables of the fitted equation was considered. The best fit is defined in the sense that the standard deviation of the data from the fitted equation is a minimum.

From the analyses of the data along the coexistence curve according to the law of rectilinear diameter and the simple power law for critical exponent β, the following values of critical constants and exponent were identified: $T_c = 150.725^{0} \pm 0.010^{o}K$, $\beta = 0.3574 \pm 0.0027$, $P_c = 47.983$ atm, and $n_c = 1.08611_{45}$. From the analysis of isothermal compressibility data on the critical isochore, the value of exponent γ was found to be 1.170 ± 0.013 at $T_c = 150.725^{o}K$. If the variation of T_c was included in the analysis, values of $T_c = 150.731^{o}K$ and $\gamma = 1.161 \pm 0.013$ were obtained at the best fit. Values of γ found from the similar analyses of maximum isothermal compressibility on each isotherm do not agree with the above, probably due to the inaccuracy inherent in locating the maximum. It appears that the best value for γ obtained from the present data is 1.170 ± 0.013.

In Table XV, the values of critical constants and exponents determined in this study are compared with those previously reported for argon[8,40,42,64,65,66,67]. For exponents β and γ, the values determined from this study are somewhat lower than those reported previously, yet they are compatible when the error bands are considered. However, they are clearly different from those predicted by the classical theory $\beta = \frac{1}{2}$ and $\gamma = 1$. They appear to correspond much better to those predicted by the three-dimensional lattice gas model, $\beta = 0.313 \pm 0.004$ and $\gamma = 1.250 \pm 0.003$.

The value of exponent β for argon determined in this study is also compared with those reported for other fluids, as shown in Table

XVI. It is worthy of note that the exponent β has a nominal value of 0.352 ± 0.005 for a variety of both nonpolar and polar fluids. The value of β for argon determined in this study is more in line with this nominal value than those previously reported.

The experimental data along the single phase isotherms were also used to compute the reduced chemical potential differences $\Delta\mu$ and the reduced densities $\Delta\phi$. The antisymmetry of $\Delta\mu$ with respect to the critical density is clearly demonstrated by most of the data for which a test is possible. The scaled equation of state, Equation (23) with the form of the function $h(x)$ recently proposed by Vicentini-Missoni *et al*[49], fits the $\Delta\mu,\Delta\phi$ data and predicts reasonable values for the critical temperature, $T_c = 150.720^{\circ}K$, and exponent $\gamma = 1.198$, provided the value of exponent β determined along the coexistence curve is used.

In describing the critical anomalies of a fluid, the simple power laws, e.g., Equations (8) and (9), and the scaled equation of state, Equation (23), are valid only in a neighborhood close to the actual critical point. They should be treated as first order approximations in the expansions of thermodynamic properties about the critical point, as was indicated by Green *et al*[38]. However, the present data even with the improved experimental accuracy and the use of linear regression analysis (no data weighting) were insufficient to resolve the significance of the higher order terms in the expansions. To gain more insight into the critical anomalies, there is much need of further development of a method of nonlinear regression analysis

and/or nonlinear least square fit involving proper data weighting. (The author is not aware of these methods at the present time.) Further improvement in the experimental accuracy will no doubt also be of great value. It is believed that better agreement between the values of critical exponents obtained experimentally for real fluids and those predicted by theoretical models will be reached if the analysis of higher order terms in the expansions is made.

NOMENCLATURE

a - coefficient in Equations (20), (21) and (32)

A - apex angle between the prism faces of the cell

A^+ - coefficient in Equation (11)

A^- - coefficient in Equation (12)

$A^\pm$ - coefficient in Equation (22)

A_{1L} - coefficient in Equation (41)

A_{1G} - coefficient in Equation (42)

A_{2L} - coefficient in Equation (41)

A_{2G} - coefficient in Equation (42)

A_{1K_T} - coefficient in Equation (44)

A_{2K_T} - coefficient in Equation (44)

b - coefficient in Equation (45)

B - coefficient in Equations (3), (16), and (21)

B_ϕ - coefficient in Equations (36), (37), and (40)

B' - coefficient in Equations (8), (17), and (18)

B'_ϕ - coefficient in Equations (38), (39), (41), and (42)

$B_1^\pm$ - coefficient in Equation (19)

$B_2^\pm$ - coefficient in Equation (19)

$C^\pm$ - coefficient in Equation (22)

$C_c^\pm$ - coefficient in Equation (5)

d - coefficient in Equation (33)

d_{cd} - coefficient in Equations (34) and (35)

D - angle of minimum deviation

$D^{\pm}$ - coefficient in Equation (5)

E_1 - coefficient in Equations (26) and (51)

E_2 - coefficient in Equations (26) and (51)

$f(z)$ - arbitrary function, Equations (6) and (7)

$G(x)$ - scaled function $\left(\frac{x_o}{x+x_o} \frac{\Delta\mu}{\Delta\phi|\Delta\phi|^{\gamma/\beta}} \right)^{\frac{2\beta}{\gamma-1}}$

$h(x)$ - scaled function, Equations (23), (26), and (50)

K_T - isothermal compressibility

M - molecular weight

n - refractive index

N_o - Avogadro's number

P - pressure

T - temperature

ΔT - reduced temperature difference $(T-T_c)/T_c$

V - specific volume

x - scaled variable $\Delta T/|\Delta\rho|^{1/\beta}$ or $\Delta T/|\Delta\phi|^{1/\beta}$

x_o - negative value of x on the coexistence curve

X - scaled function $\left(\frac{x+x_o}{x_o}\right)^{2\beta}$

z - arbitrary variable, Equations (6) and (7)

Critical Exponents characterizing the anomaly of

α - specific heat at constant volume

β - density difference on the coexistence curve

γ - isothermal compressibility

δ - pressure along the critical isotherm

Greek Letters

α_m - molecular polarizability

$\beta_1^{\pm}$ - critical exponent in Equation (19)

$\beta_2^{\pm}$ - critical exponent in Equation (19)

λ - critical exponent defined in Equation (7)

λ_{Na} - wavelength of sodium D line

ρ - density

$\Delta\rho$ - reduced density difference $(\rho-\rho_c)/\rho_c$

ϕ - grouping of $(n^2-1)/(n^2+2)$

$\Delta\phi$ - reduced density difference $(\phi-\phi_c)/\phi_c$

Γ - coefficient in Equations (4), (9), (10), (43), and (44)

μ - chemical potential

$\Delta\mu$ - reduced chemical potential difference
$[\mu(\rho,T) - \mu(\rho_c,T)]/(P_c/\rho_c)$

σ - error

Subscripts

c - critical state value

G - gas

L - liquid

Superscript

' - denoting the critical exponent for $T < T_c$

REFERENCES

1. H. A. Lorentz, The Theory of Electrons (B. G. Teubner, Leipzig, Germany, 1909)

2. J. G. Kirkwood, J. Chem. Phys. 4, 592 (1936)

3. J. Yvon, Recherches sur la Theorie Cinetique des Liquids (Herman et Cie., Paris, 1937)

4. P. Mazur and M. Mandel, Physica 22, 289,299 (1956)

5. A. Michels and J. Hamers, Physica 4, 995 (1937)

6. C. P. Abbiss, C. M. Knobler, R. K. Teague, and C. J. Pings, J. Chem. Phys. 42, 4145 (1965)

7. D. E. Diller, J. Chem. Phys. 49, 3096 (1968)

8. R. K. Teague and C. J. Pings, J. Chem. Phys. 48, 4973 (1968)

9. J. M. H. Levelt, doctoral thesis, Amsterdam, 1958

10. S. Y. Larsen, R. D. Mountain, and R. Zwanzig, J. Chem. Phys. 42, 2187 (1965)

11. M. E. Fisher, J. Math. Phys. 5, 944 (1964)

12. D. A. Goldhammer, Z. f. Physik. Chem. 71, 577 (1910)

13. A. Michels, B. Blaisse, and C. Michels, Proc. Roy. Soc. (London) A160, 358 (1937)

14. E. A. Guggenheim, J. Chem. Phys. 13, 253 (1945)

15. M. I. Bagatskii, A. V. Voronel, and B. G. Gusak, Soviet Phys. JETP 16, 517 (1963)

16. A. V. Voronel, Yu. R. Chashkin, V. A. Popov, and V. G. Simkin, Soviet Phys. JETP 18, 568 (1964)

17. A. V. Voronel, F. G. Snigirev, and Yu. R. Chashkin, Soviet Phys. JETP 21, 653 (1965)

18. A. V. Voronel and Yu. R. Chashkin, Soviet Phys. JETP 24, 263 (1967)

19. M. E. Fisher, Rep. Progr. Phys. 30, 615 (1967)

20. G. S. Rushbrooke, J. Chem..Phys. 39, 842 (1963)

21. R. B. Griffiths, Phys. Rev. Letters 14, 623 (1965)

22. G. S. Rushbrooke, J. Chem. Phys. 43, 3439 (1965)

23. T. D. Lee and C. N. Yang, Phys. Rev. 87, 410 (1952)

24. C. Domb, Advan. Phys. 9, Nos. 34, 35 (1960)

25. G. A. Baker, Jr., J. L. Gammel, and J. G. Wills, J. Math. Anal. Appl. 2, 405 (1961)

26. L. Onsager, Phys. Rev. 65, 117 (1944)

27. B. Kaufman and L. Onsager, Phys. Rev. 76, 1244 (1949)

28. G. A. Baker, Jr., Phys. Rev. 122, 1477 (1961)

29. M. E. Fisher, J. Math. Phys. 4, 278 (1963)

30. J. W. Essam and M. E. Fisher, J. Chem. Phys. 38, 802 (1963)

31. G. A. Baker, Jr., Phys. Rev. 129, 99 (1963)

32. M. E. Fisher, Phys. Rev. 136, A1599 (1964)

33. G. A. Baker, Jr., and D. S. Gaunt, Phys. Rev. 155, 545 (1967)

34. M. F. Sykes, J. L. Martin, and D. L. Hunter, Proc. Phys. Soc. (London) 91, 671 (1967)

35. M. A. Weinberger and W. G. Schneider, Can. J. Chem. 30, 422 (1952)

36. J. M. H. Levelt Sengers, J. Straub, and M. Vicentini-Missoni, J. Chem. Phys. 54, 5034 (1971)

37. J. J. van Laar, Proc. Kon. Akad. Amsterdam 14^{I}, 428 (1911/1912); 14^{II}, 1091 (1911/1912)

38. M. S. Green, M. J. Cooper, and J. M. H. Levelt Sengers, Phys. Rev. Letters 26, 492 (1971)

39. J. Straub, doctoral thesis, München, Germany, 1965

40. J. M. H. Levelt Sengers, Ind. Eng. Chem. Fundam. 9, 470 (1970)

41. H. W. Habgood and W. G. Schneider, Can. J. Chem. 32, 98 (1954)

42. A. F. Grigor and W. A. Steele, Phys. and Chem. of Liq. 1, 129 (1968)

43. C. Edwards, J. A. Lipa, and M. J. Buckingham, Phys. Rev. Letters 20, 496 (1968)

44. B. Widom, J. Chem. Phys. 43, 3898 (1965)

45. R. B. Griffiths, Phys. Rev. 158, 176 (1967)

46. C. Domb and D. L. Hunter, Proc. Phys. Soc. (London) 86, 1147 (1965)

47. L. P. Kadanoff, Physics (Long Island City, N. Y.) 2, 263 (1966)

48. A. Z. Patashinskii and V. L. Pokrovoskii, Soviet Phys. JETP 23, 292 (1966)

49. M. Vicentini-Missoni, J. M. H. Levelt Sengers, and M. S. Green, J. Res. Nat. Bur. Std. 73A, 563 (1969)

50. M. Vicentini-Missoni, R. I. Joseph, M. S. Green, and J. M. H. Levelt Sengers, Phys. Rev. B1, 2312 (1970)

51. P. R. Roach, Phys. Rev. 170, 213 (1968)

52. H. A. Houston, A Treatise on Light (Longmans Green and Co., London, 1921), p. 98

53. B. L. Smith, Rev. Sci. Instr. 34, 19 (1963)

54. R. K. Teague, doctoral thesis, California Institute of Technology, Pasadena, California, 1968

55. C. M. Knobler, W. I. Honeywell, and C. J. Pings, Rev. Sci. Instr. 34, 1437 (1963)

56. W. I. Honeywell, doctoral thesis, California Institute of Technology, Pasadena, California, 1964

57. H. L. Daneman and G. C. Mergner, Rev. Sci. Instr. 39, 1498 (1968)

58. R. H. Pennington, Introductory Computer Methods and Numerical Analysis (The Macmillan Co., New York, 1965), pp. 404-412

59. J. H. Williamson, Can. J. Phys. 46, 1845 (1968)

60. D. W. Marquardt, J. Soc. Indust. Appl. Math. 11, 431 (1963)

61. A. Ralston and H. F. Wilf, Mathematical Methods for Digital Computers (John Wiley and Sons, Inc., New York, 1965) Section 17

62. B. Widom and J. S. Rowlinson, J. Chem. Phys. 52, 1670 (1970)

63. H. S. Salzer, Mathematical Tables and Other Aids to Computation, V, No. 36, pp. 213-215 (1951)

64. C. A. Crommelin, Communications from the Physical Laboratory, University of Leiden, No. 115a (1910)

65. E. Mathias, H. Kamerlingh Onnes, and C. A. Crommelin, Communications from the Physical Laboratory, University of Leiden, No. 131a (1912)

66. W. D. McCain, Jr., and W. T. Ziegler, J. Chem. Eng. Data 12, 199 (1967)

67. H. D. Bale, B. C. Dobbs, J. S. Lin, and P. W. Schmidt, Phys. Rev. Letters 25, 1556 (1970)

68. Esin Gulari, work in progress, Chemical Engineering Laboratory, California Institute of Technology (1971)

69. L. A. Weber, Phys. Rev. A2, 2379 (1970)

70. L. W. Tilton and J. K. Taylor, J. Res. Nat. Bur. Std. 20, 419 (1938)

71. J. L. Walsh, J. H. Ahlberg, and E. N. Nilson, J. Math. and Mech. 11(2), 225 (1962)

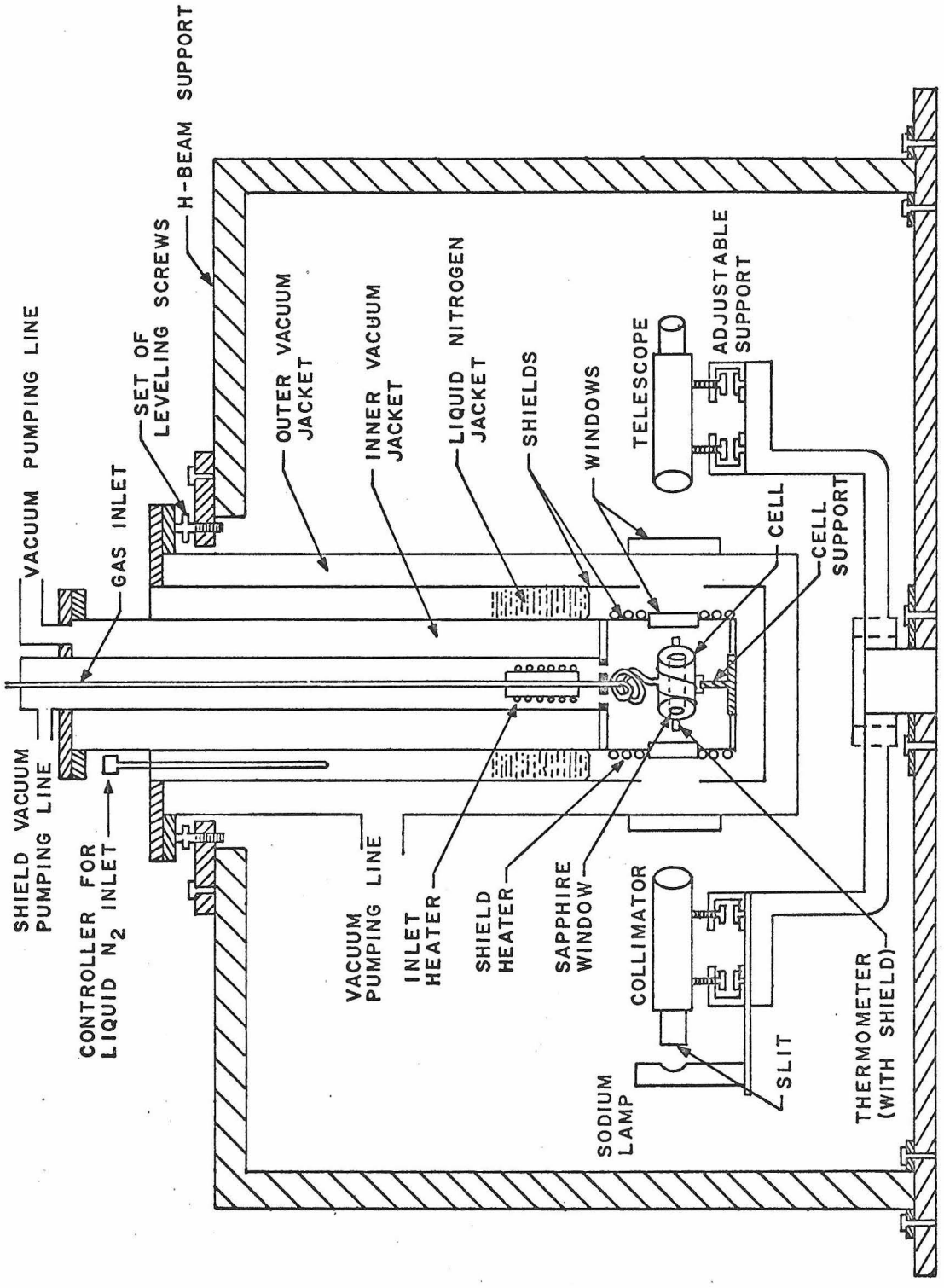

Figure 1. Optical Cell, Cryostat, and Spectrometer Apparatus

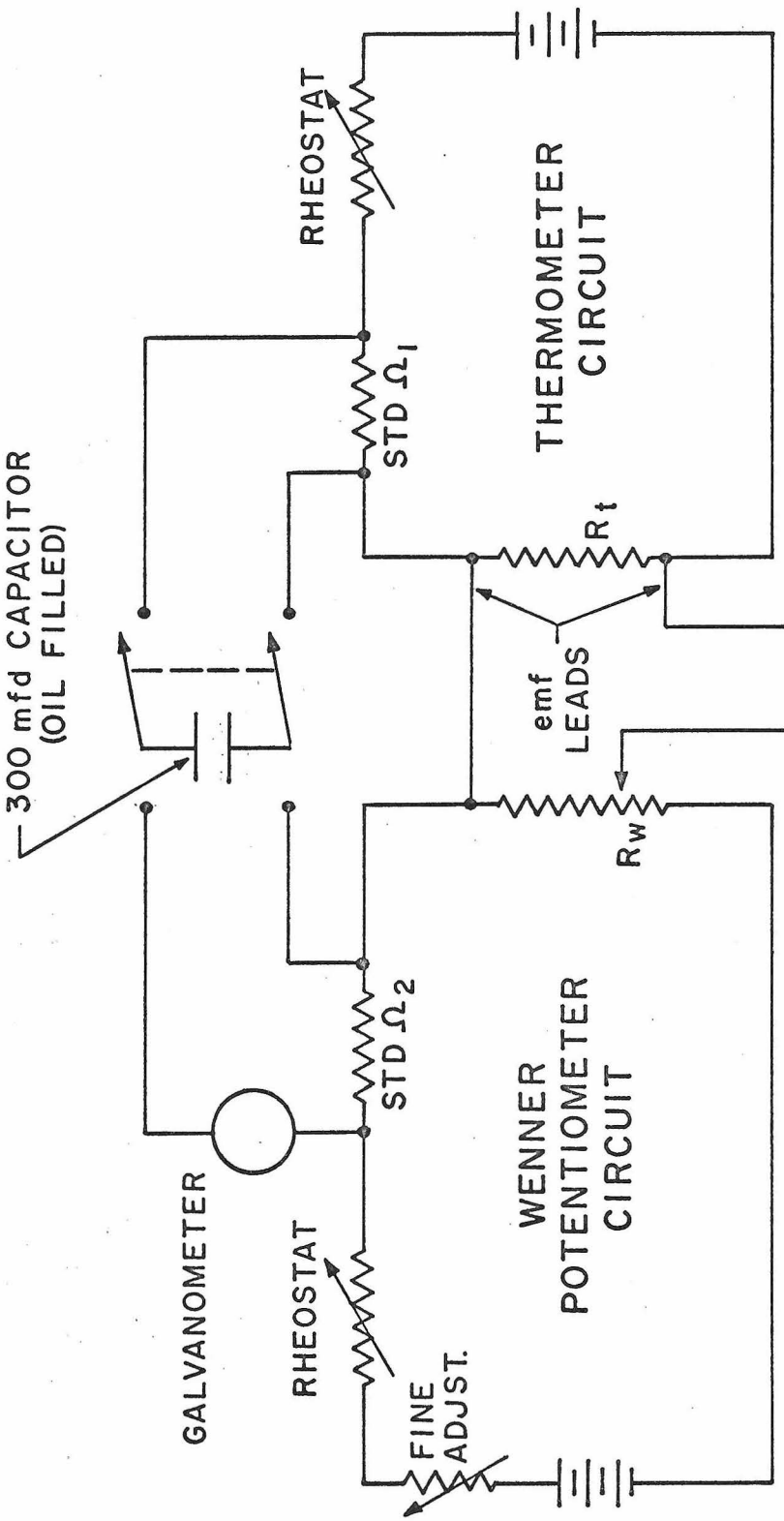

Figure 2. Diagram of Temperature Measurement System

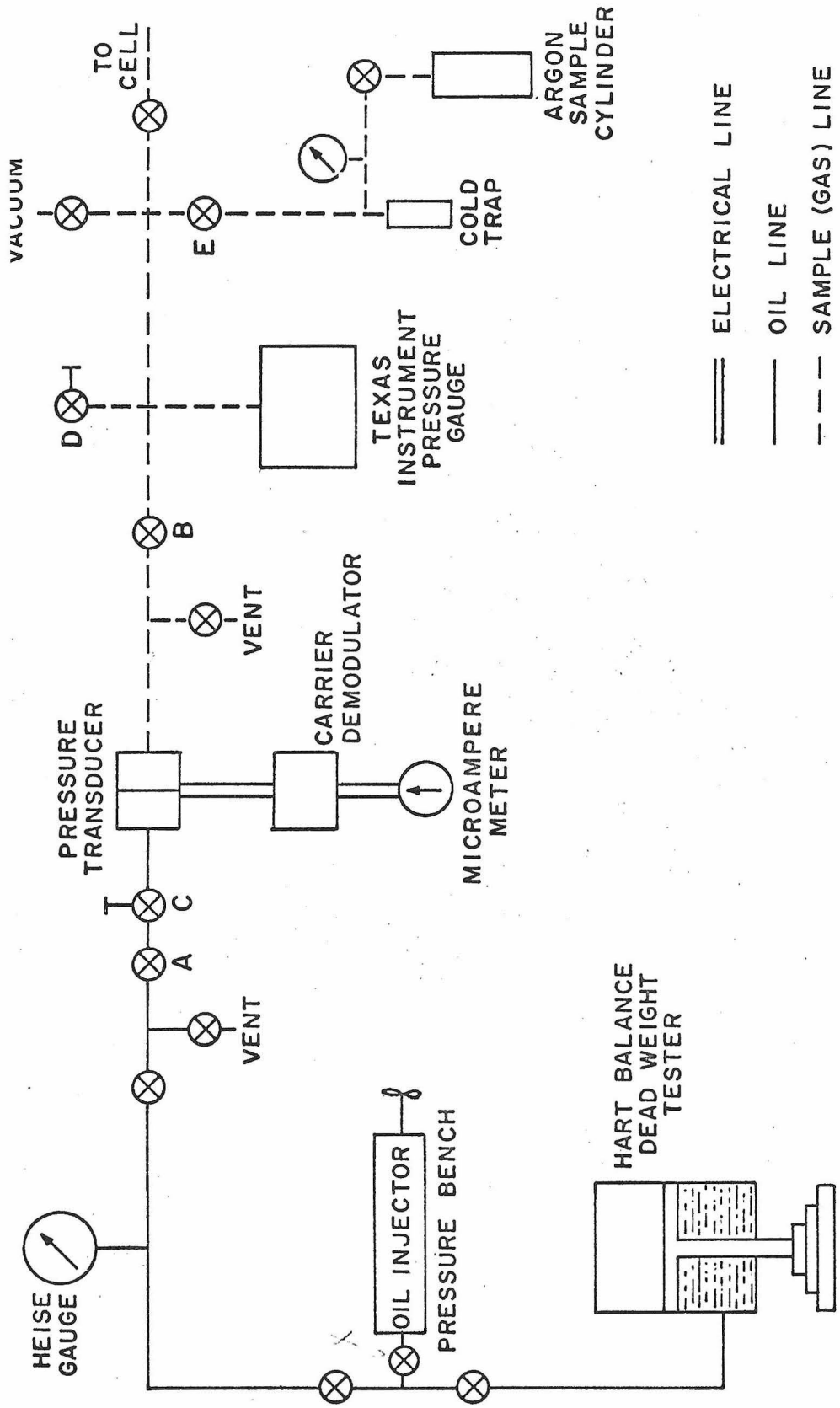

Figure 3. Diagram of Pressure Measurement System

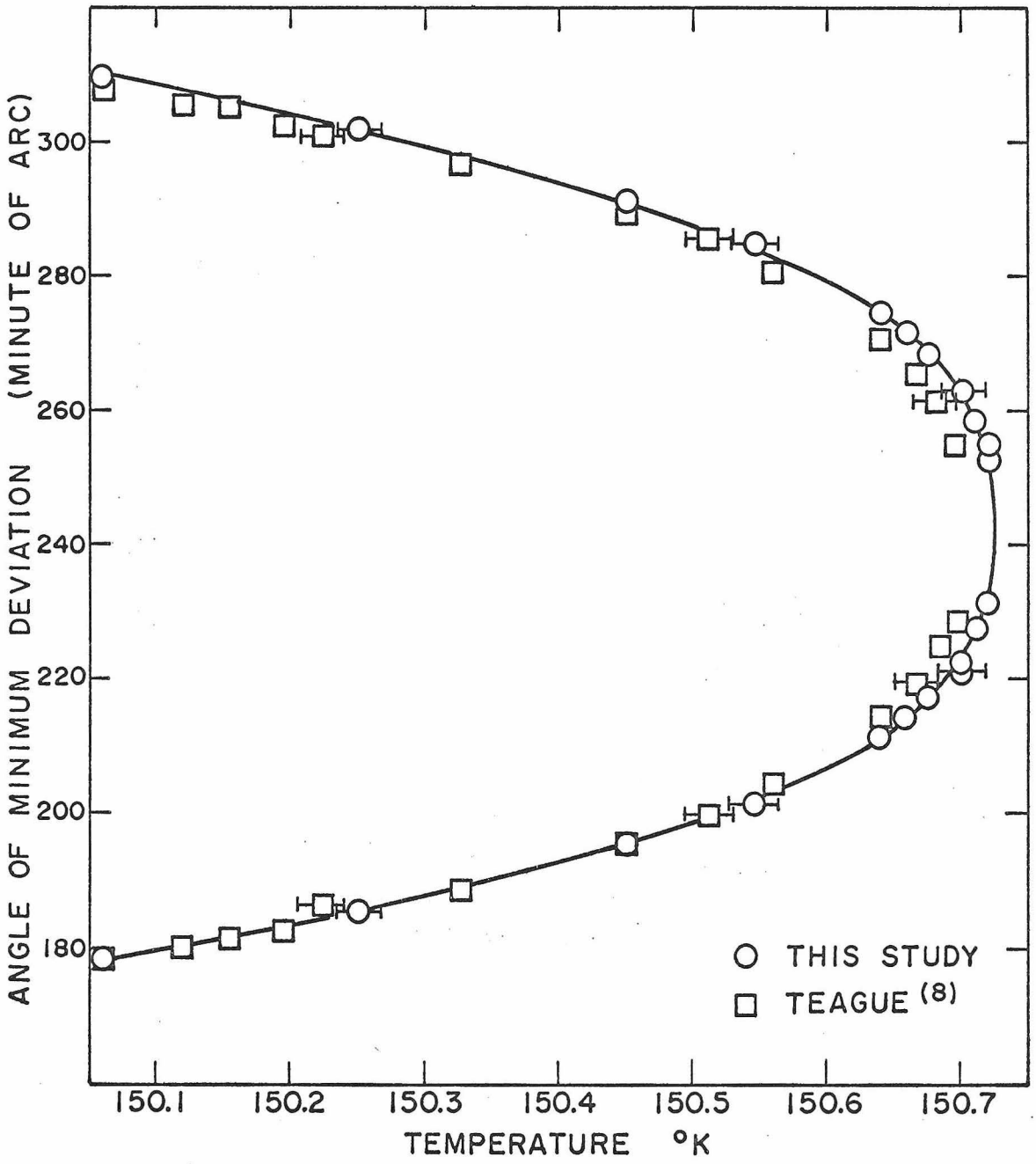

Figure 4. Comparison of Experimental Values of Angle of Minimum Deviation for Coexisting Gas-Liquid States

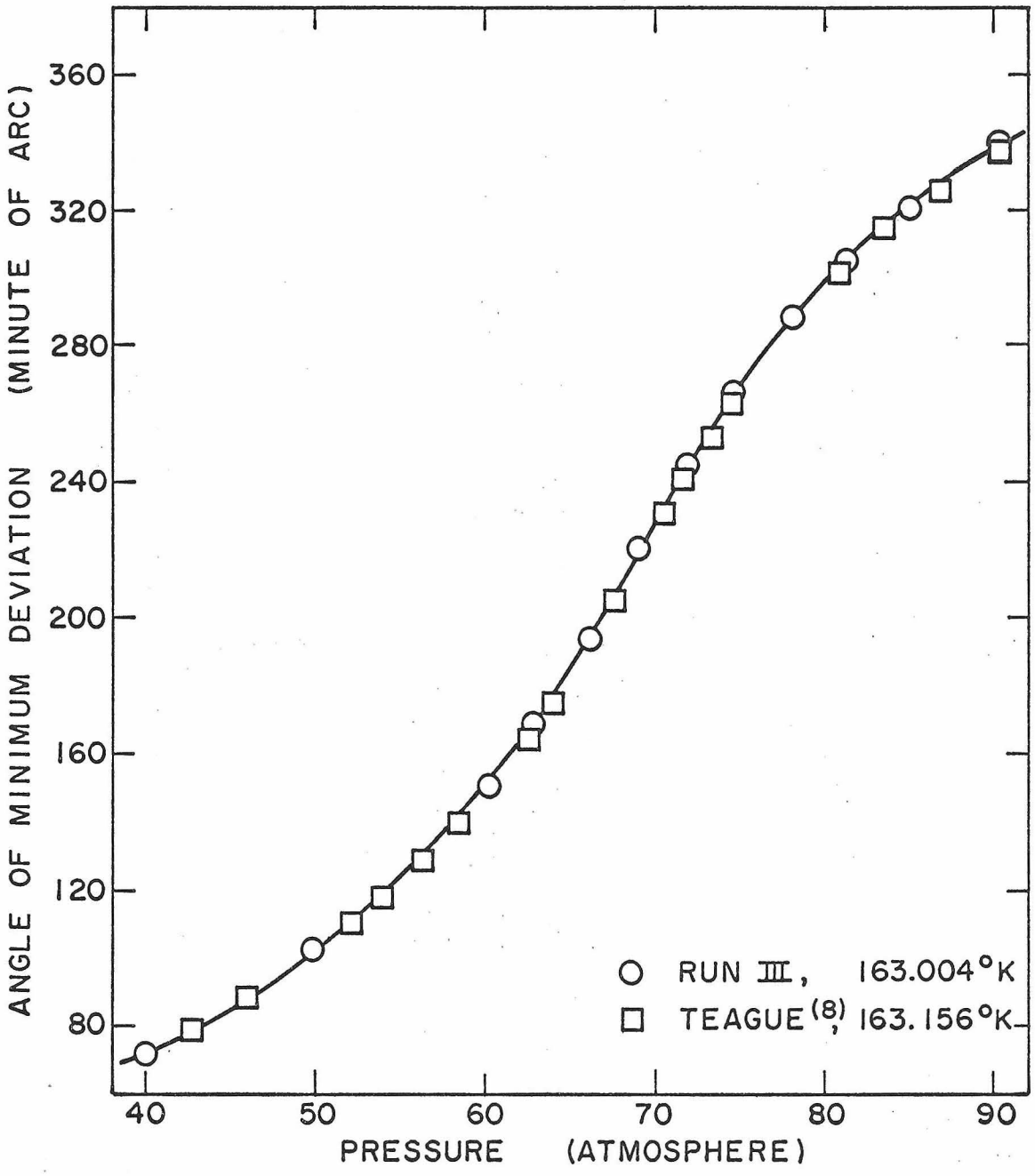

Figure 5. Comparison of Experimental Values of Angle of Minimum Deviation along the 163°K Isotherm

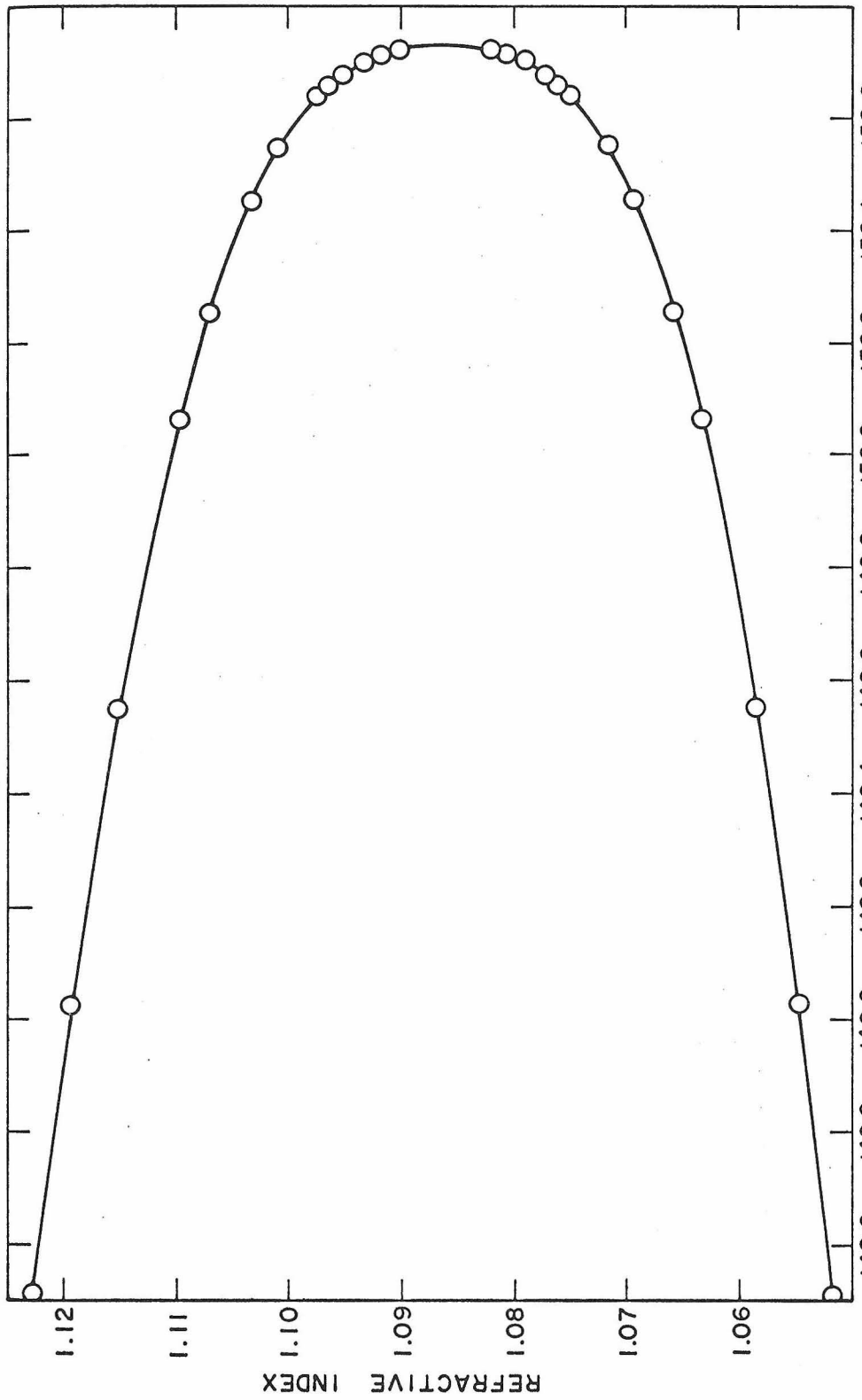

Figure 6. Refractive Index of Argon for Coexisting Gas-Liquid States.
Solid line is a visual line of best fit of the data.

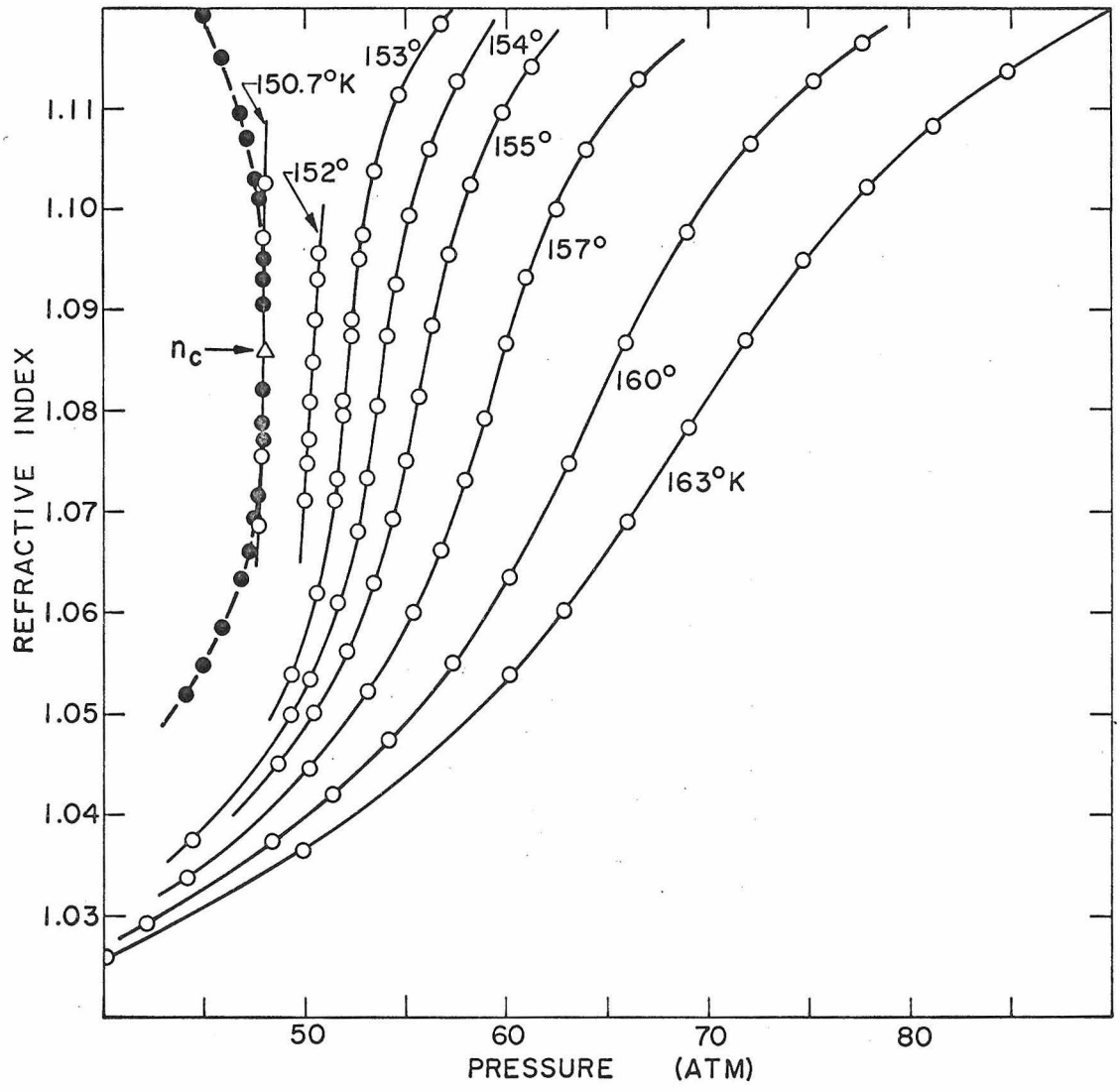

Figure 7. Refractive Index of Argon along the 152° to 163°K Isotherms. ● data along the coexistence curve; ○ data along the single phase isotherms. Solid line represents the cubic spline fit of the data along each isotherm.

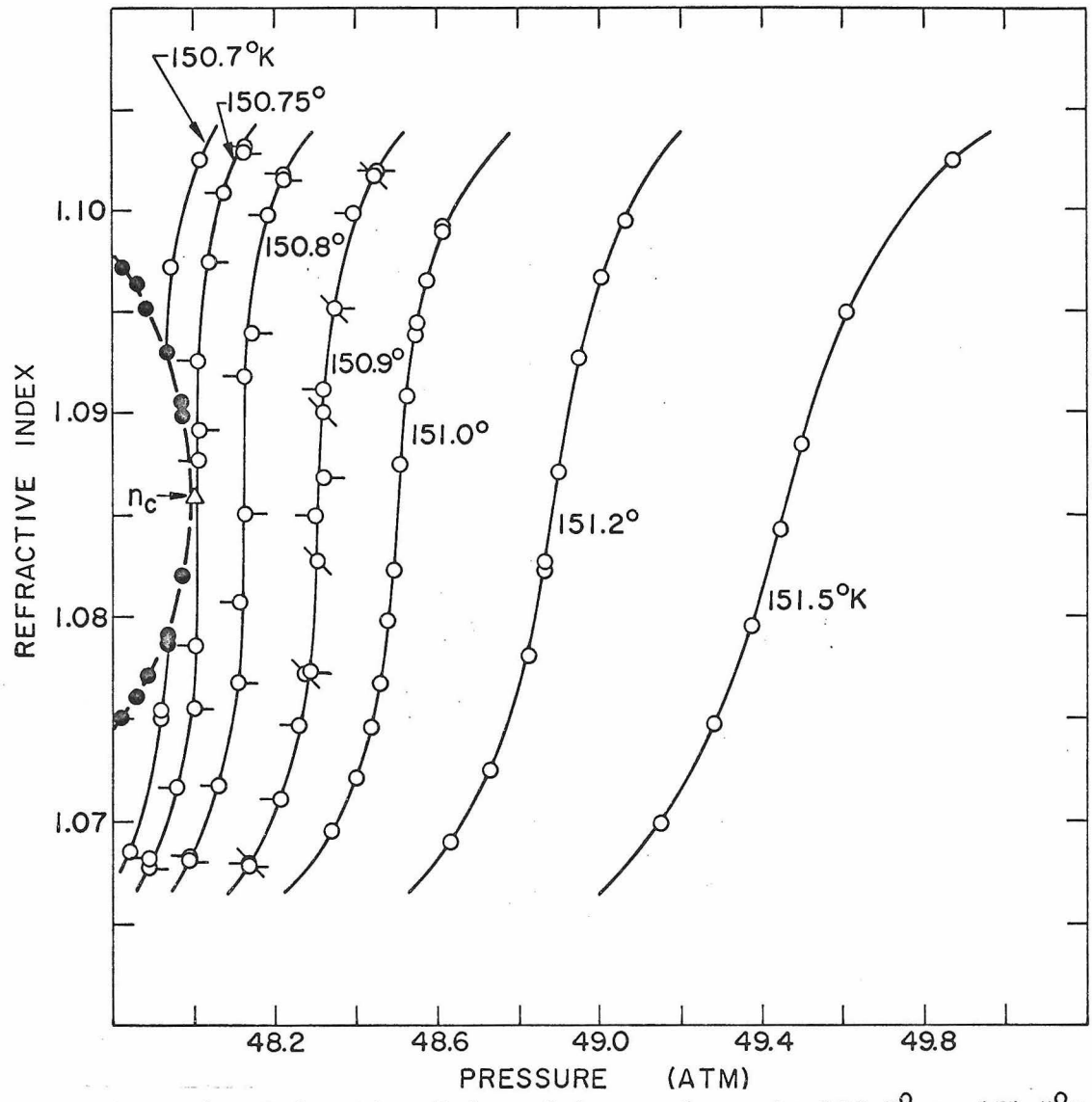

Figure 8. Refractive Index of Argon along the 150.7° to 151.5°K Isotherms. ● data along the coexistence curve; ○ data along the single phase isotherms. ○- , -○, and ○ correspond to data Set I, II, and III of the isotherms, respectively. Solid line represents the cubic spline fit of the data along each isotherm or data Set II of the isotherm.

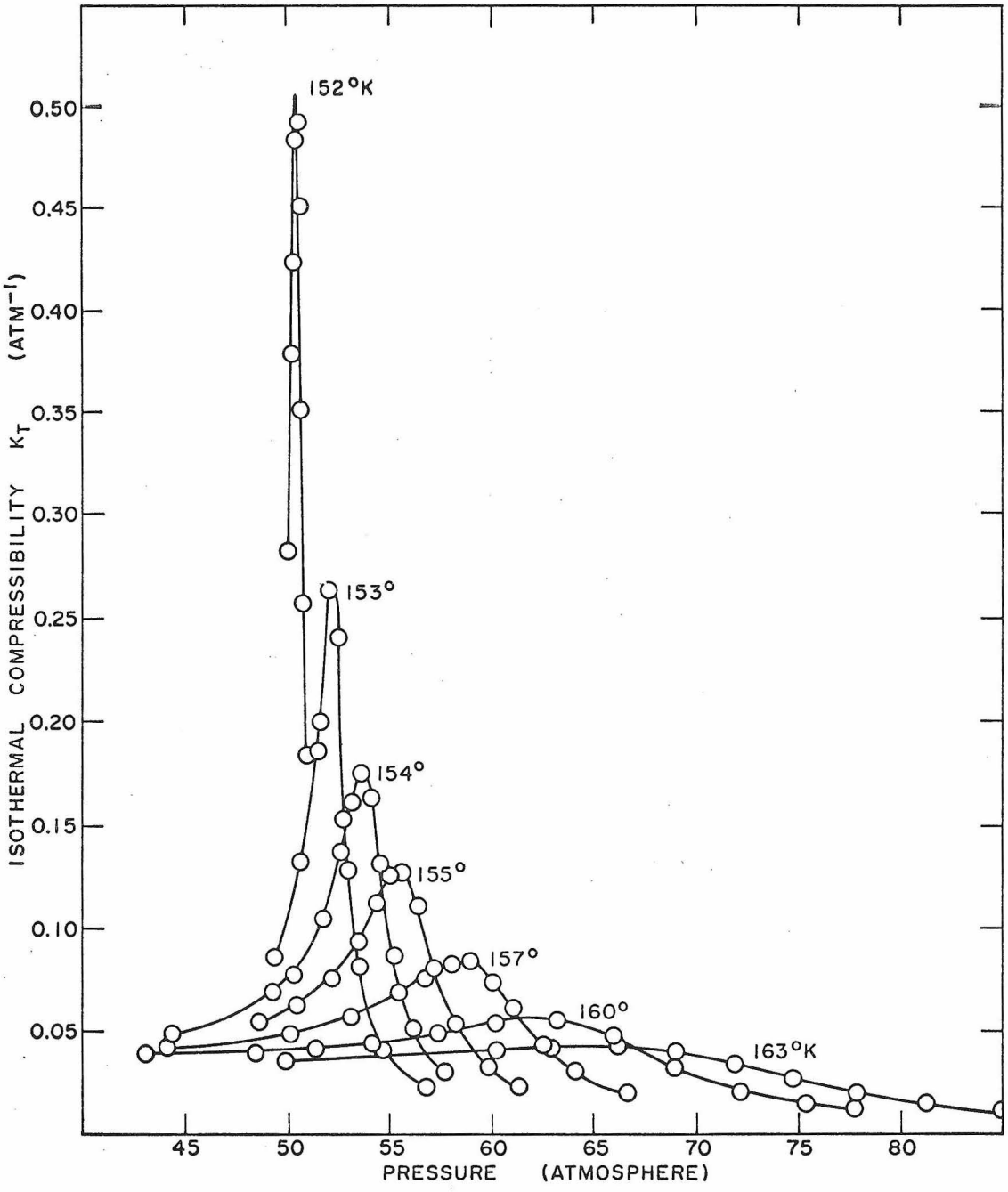

Figure 9. Isothermal Compressibility of Argon along the 152° to 163°K Isotherms

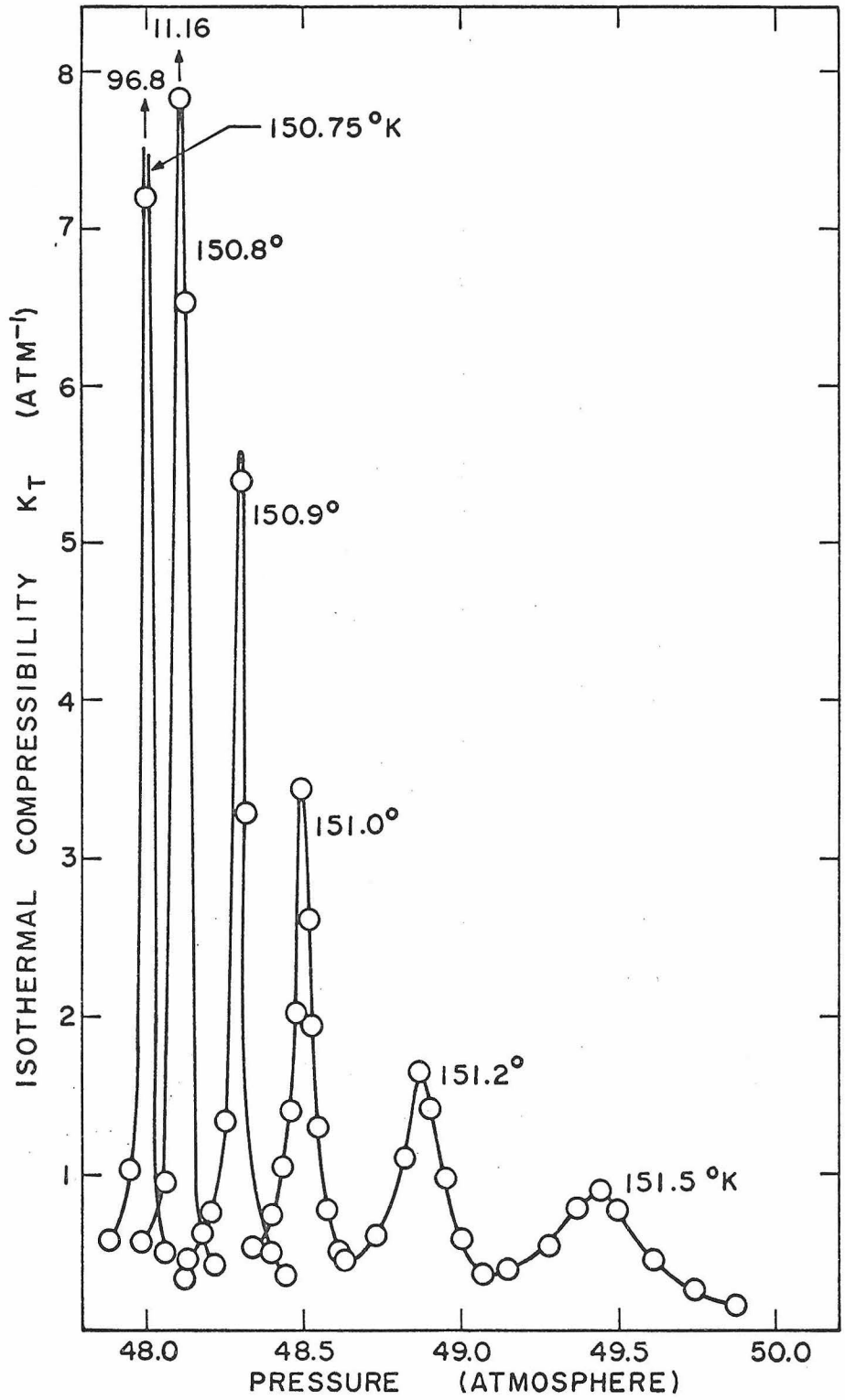

Figure 10. Isothermal Compressibility of Argon along the 150.75° to 151.5°K Isotherms

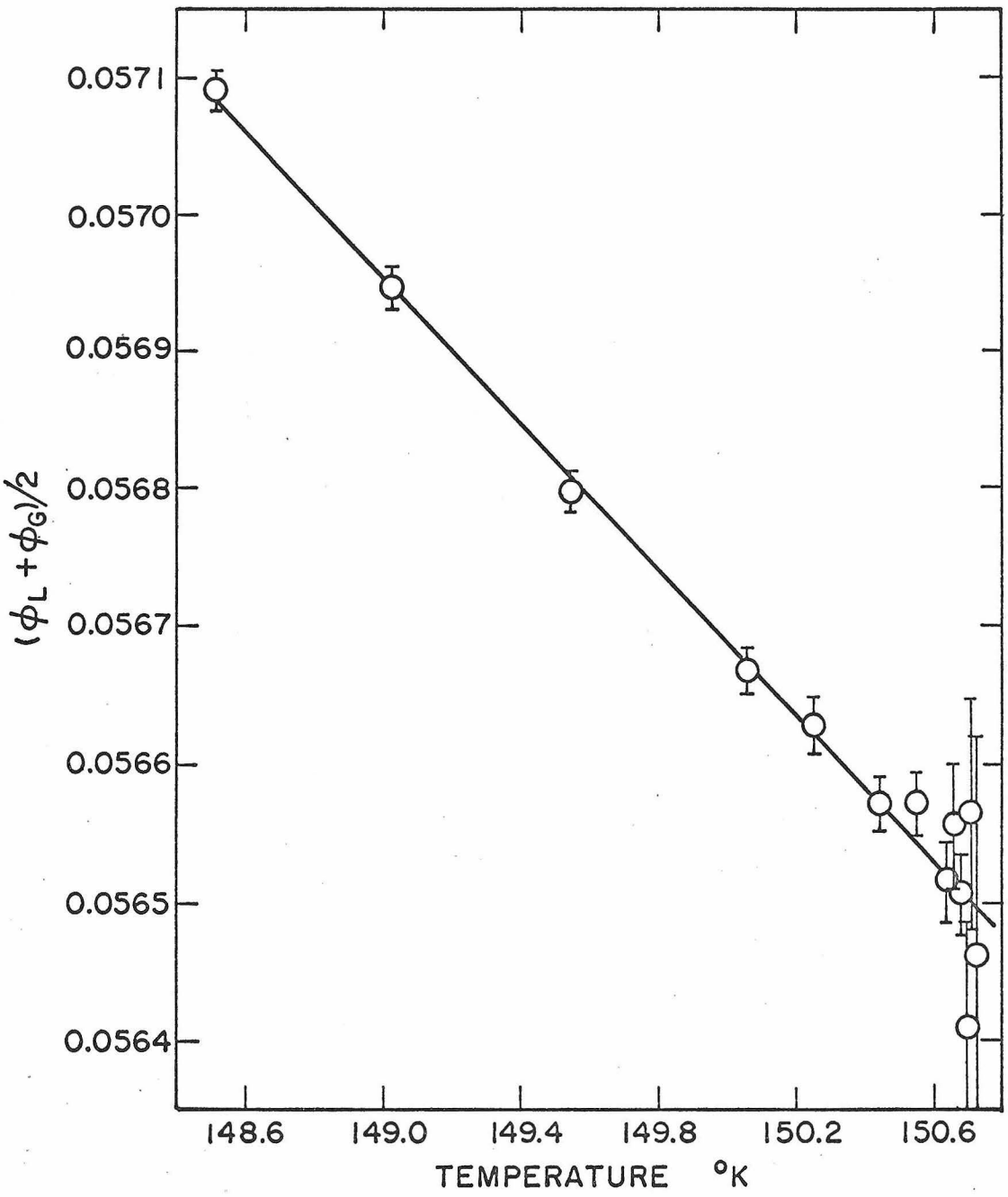

Figure 11. The Locus of Rectilinear Diameter in Terms of ϕ. The line is a least-squares fit to Equation (33).

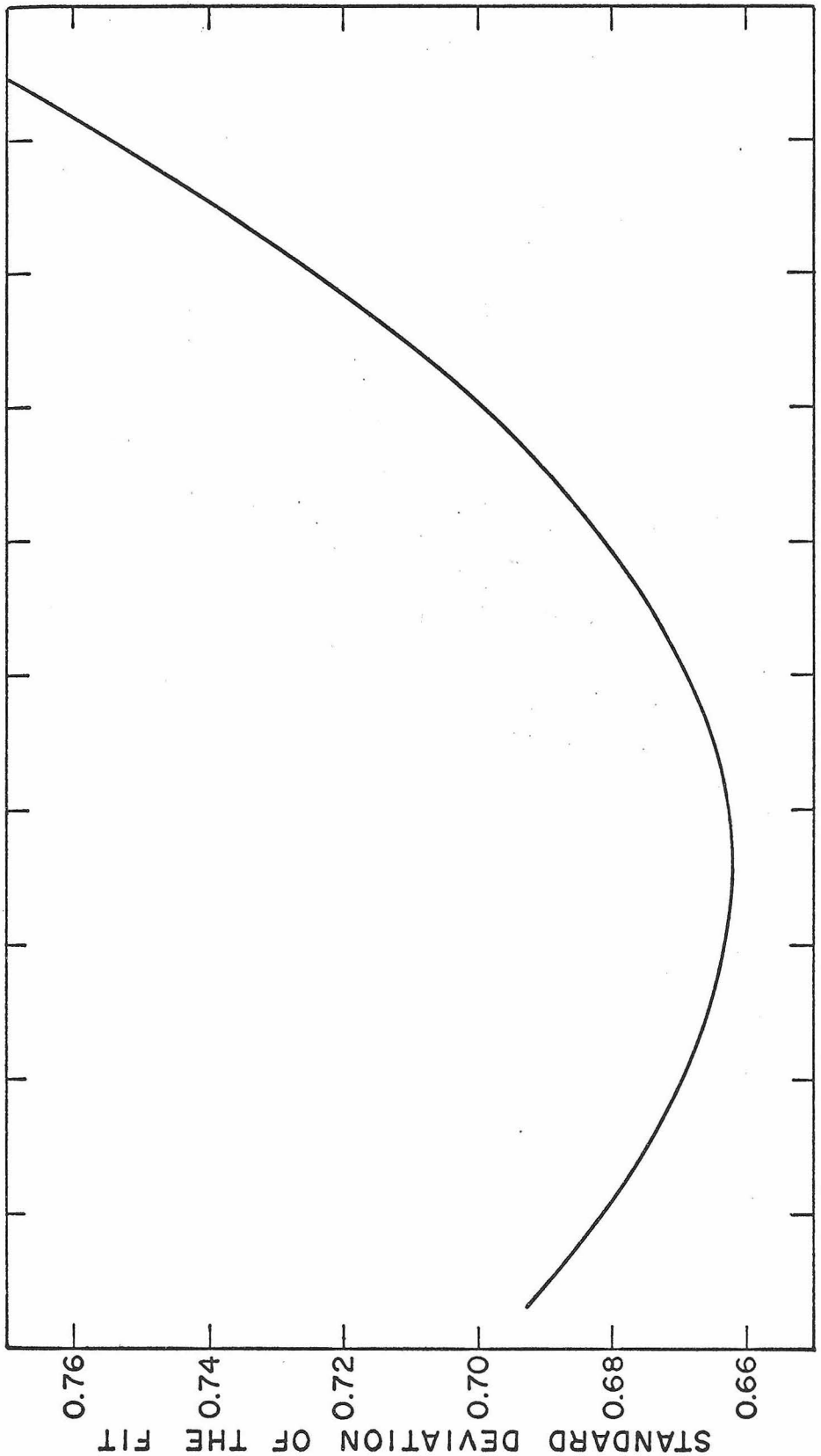

Figure 12. Standard Deviation of the Fit to Equation (35) for Various Values of α.

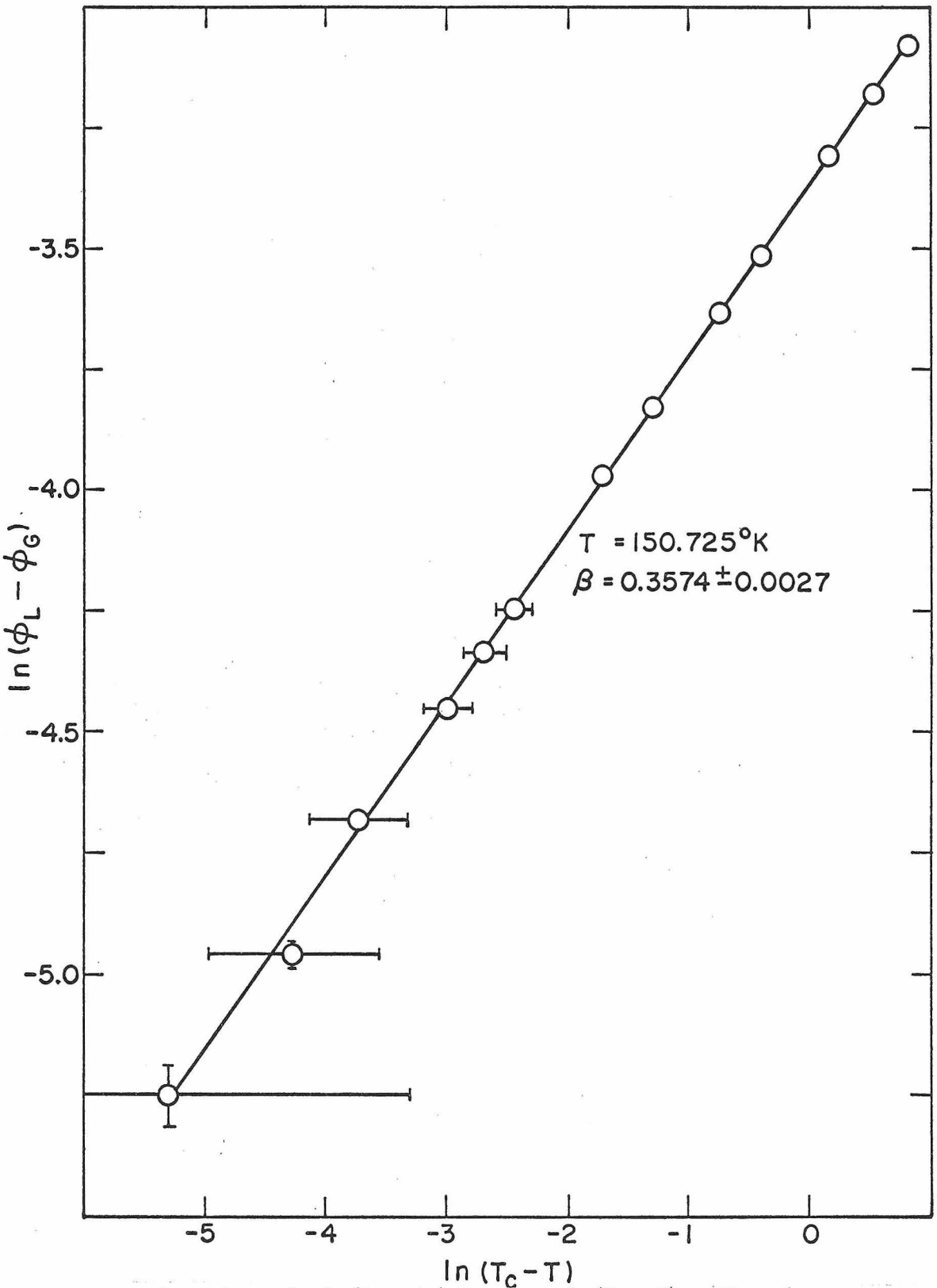

Figure 13. Plot of $\ln(\phi_L - \phi_G)$ versus $\ln(T_c - T)$. The slope of the fitted line, Equation (37), is the exponent β.

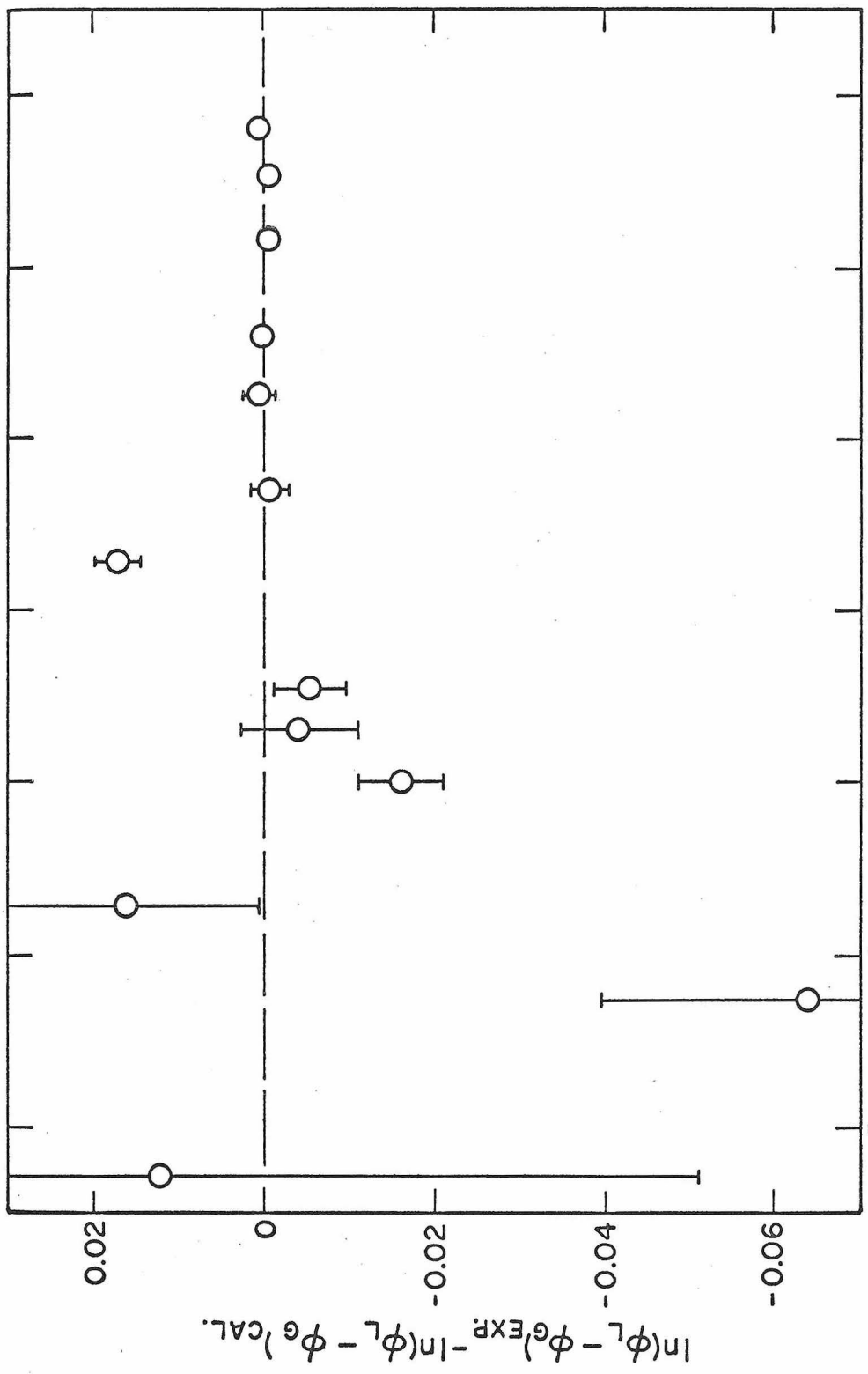

Figure 14. Differences of the Experimental and Calculated $(\phi_L - \phi_G)$ from Equation (37)

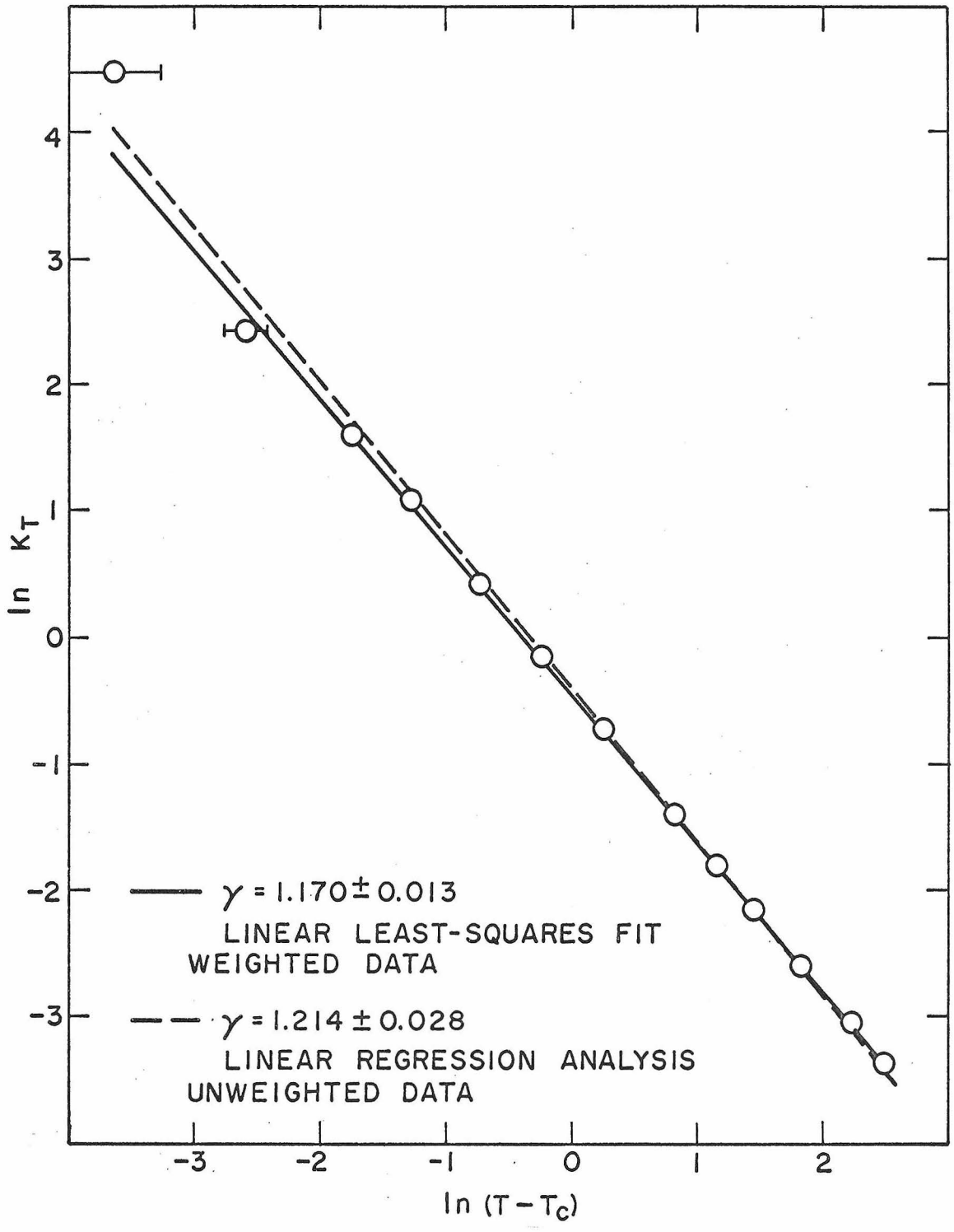

Figure 15. Plot of $\ln K_T$ versus $\ln(T - T_c)$ on the critical Isochore $\phi_c = 0.0564984$ for $T_c = 150.725^{\circ}K$. The slope of each fit evaluates the exponent γ .

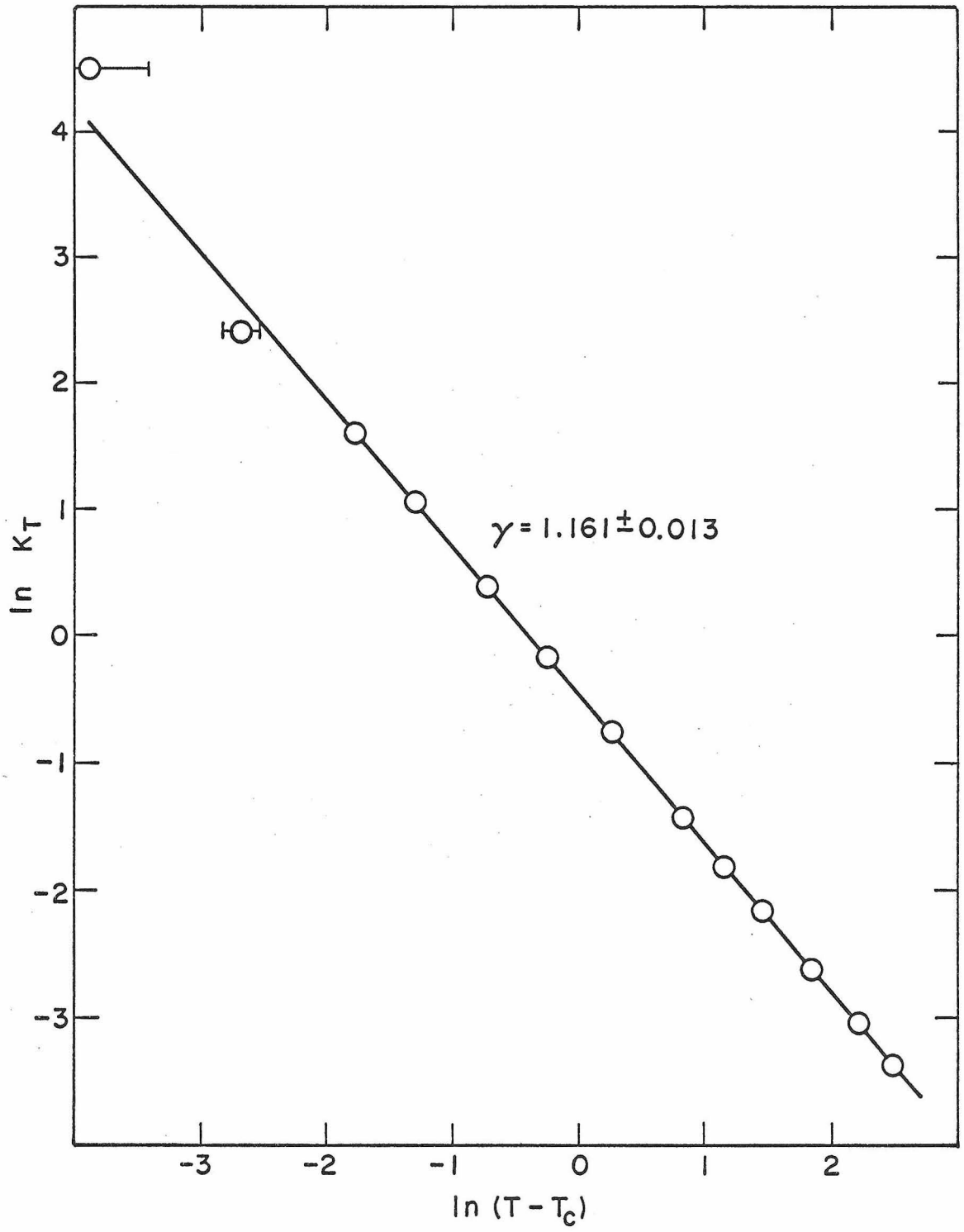

Figure 16. Plot of $\ln K_T$ versus $\ln(T - T_c)$ on the Critical Isochore $\phi_c = 0.0564969$ for $T_c = 150.731^{\circ}K$. The slope of the fitted line, Equation (43), is the exponent γ .

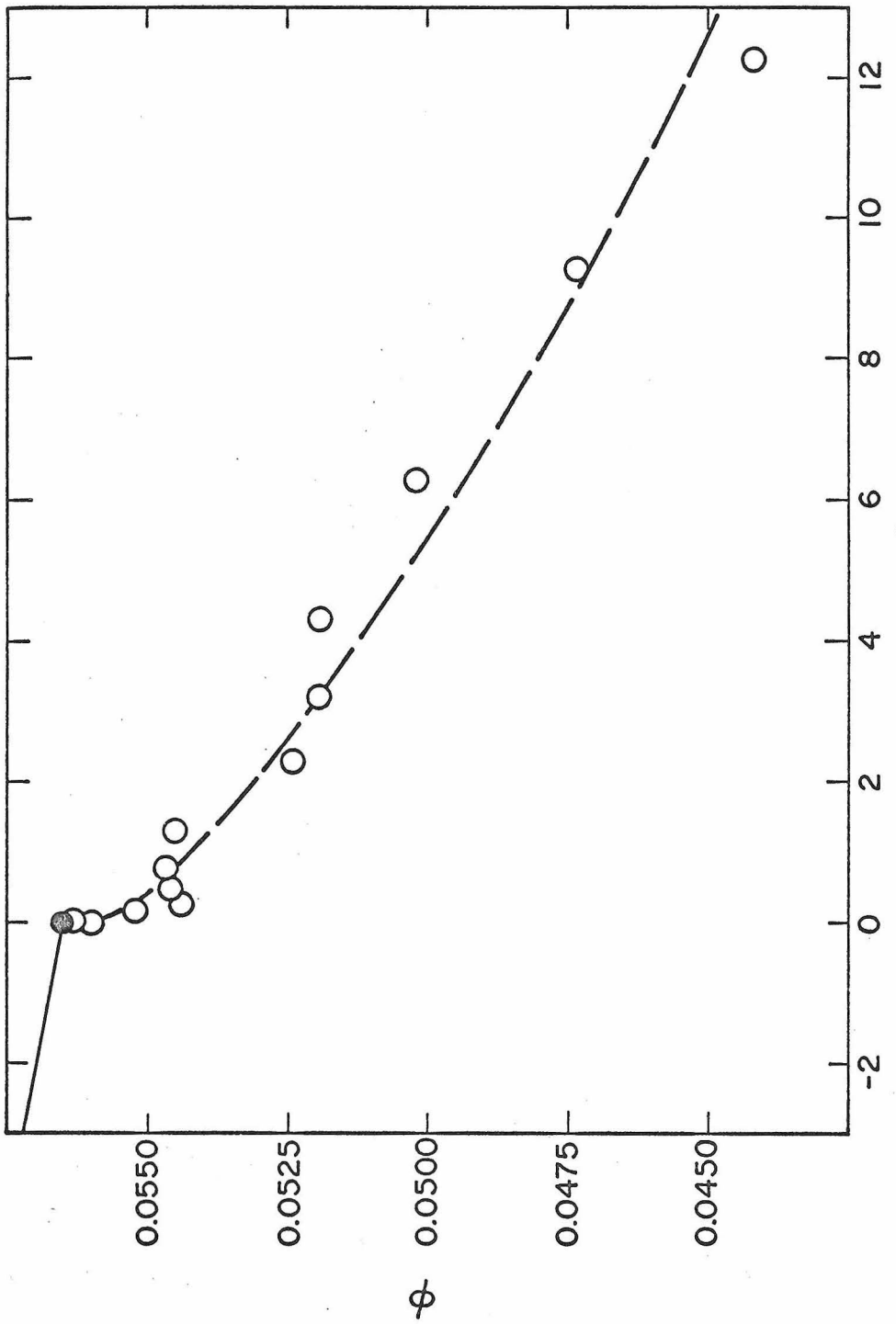

Figure 17. The Locus of Maximum Isothermal Compressibility in the $T-\phi$ plane. The dashed curve is a least-squares fit to Equation (45) with $T_c = 150.725^{\circ}K$ and $\beta = 0.3574$. The solid line is the rectilinear diameter, Equation (33).

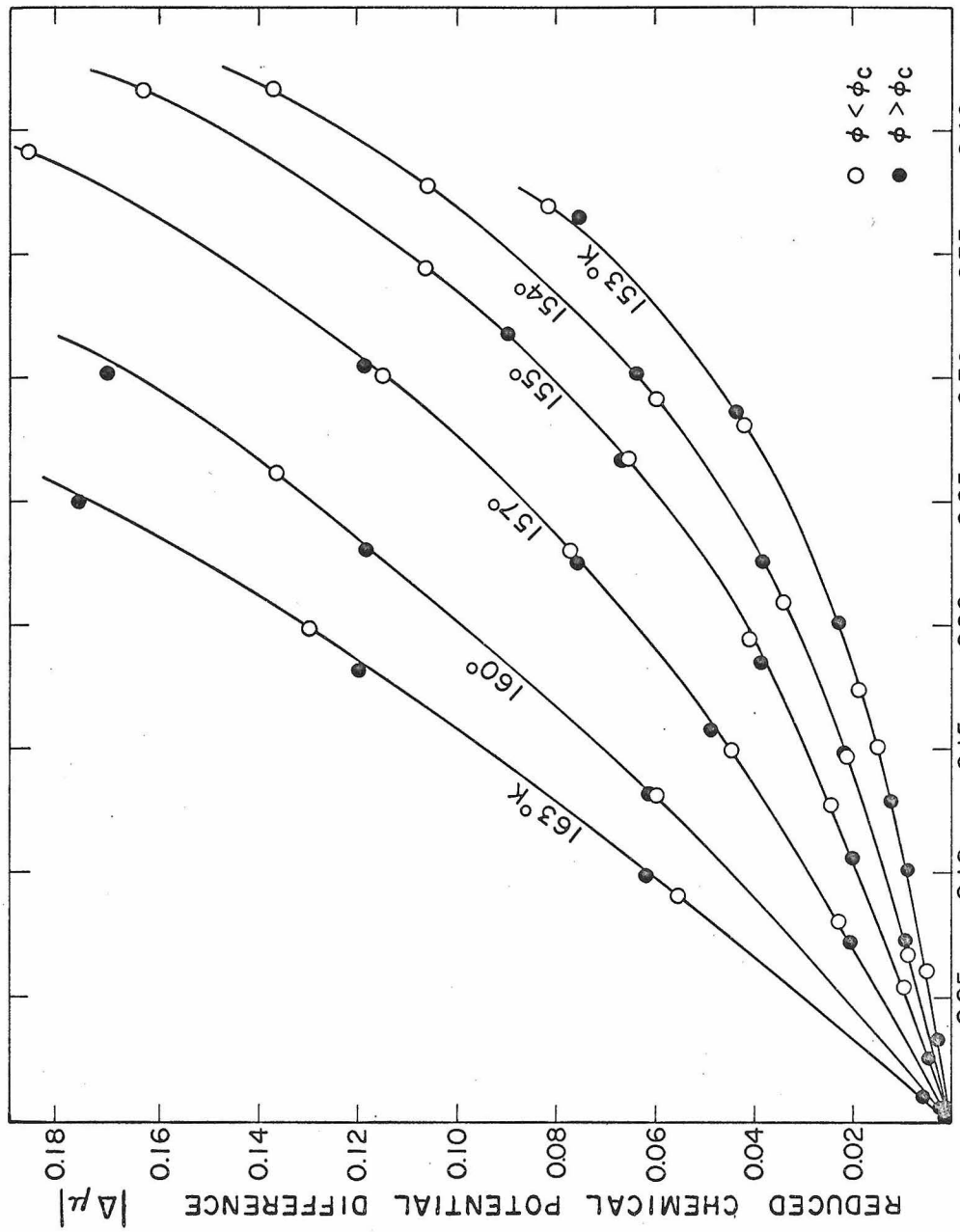

Figure 18. The Reduced Chemical Potential Difference versus the Reduced Density Difference for the 153° to 163°K Isotherms

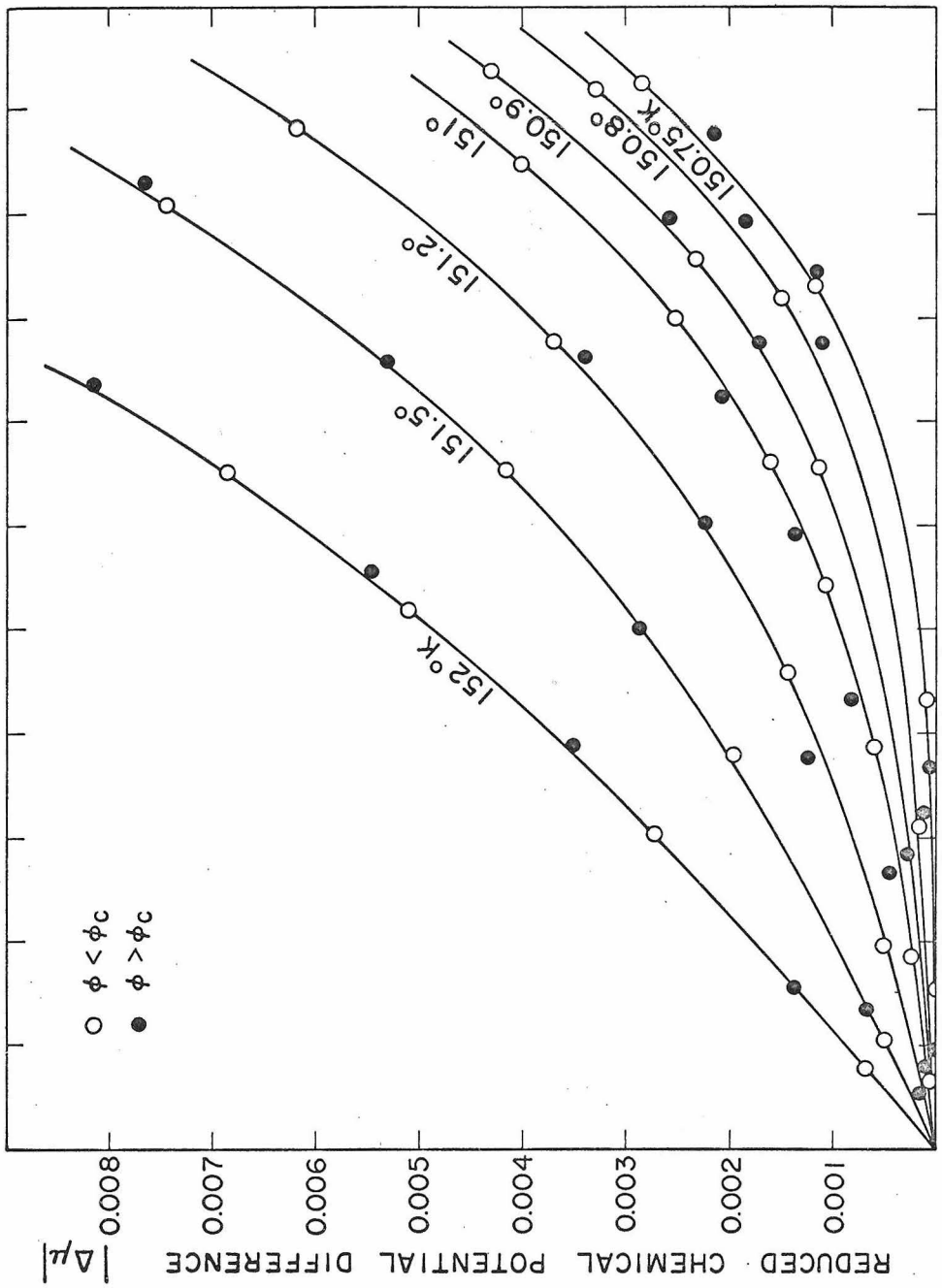

Figure 19. The Reduced Chemical Potential Difference versus the Reduced Density Difference for the 150.75° to 152°K Isotherms

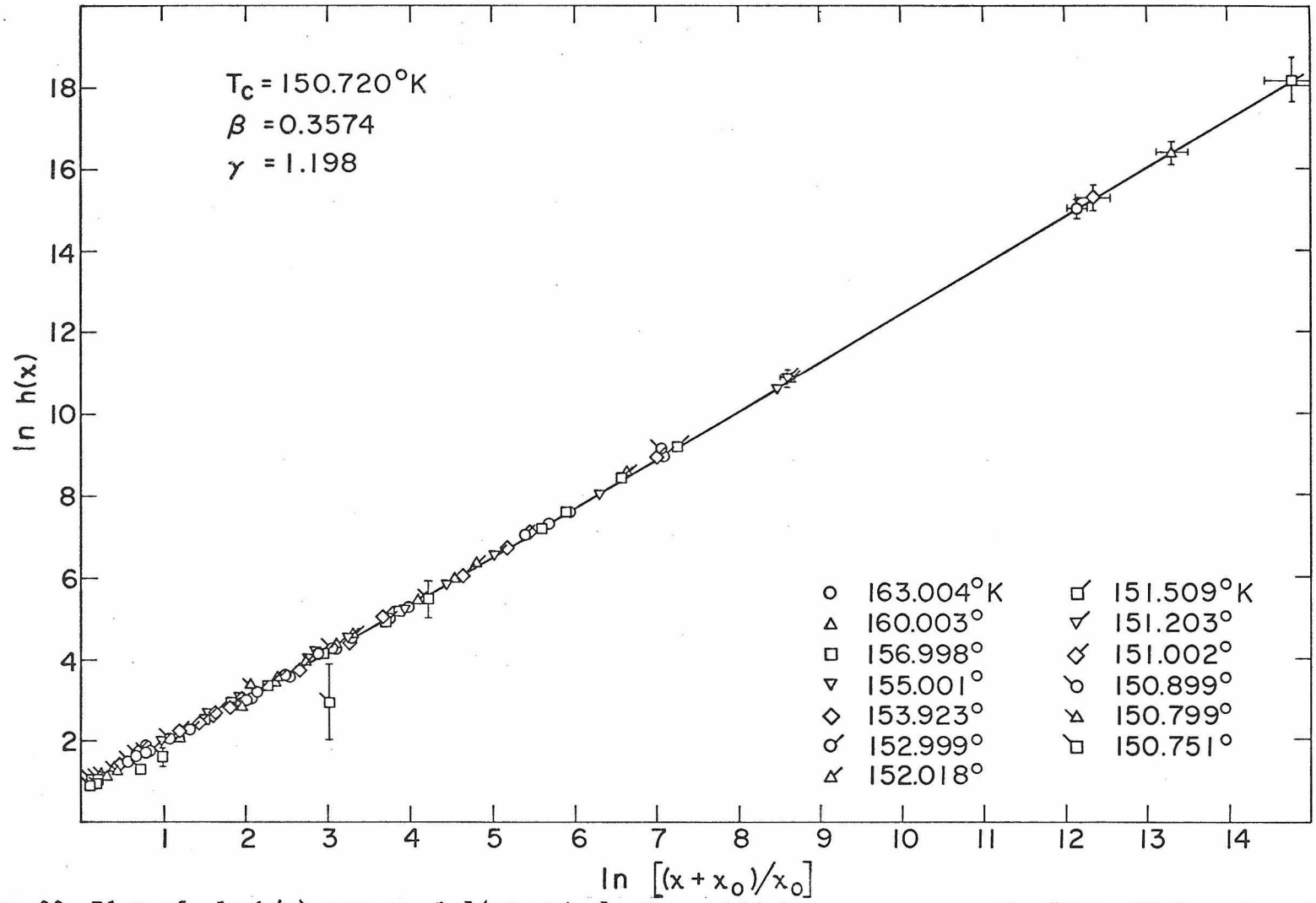

Figure 20. Plot of ln h(x) versus $\ln[(x+x_o)/x_o]$. The solid line represents the "fitted" function h(x), Equation (26), using the fitted values of all six parameters. The points are the "experimental" values of h(x) calculated from the experimental $\Delta\mu, \Delta\phi$ data and the fitted values of β and γ.

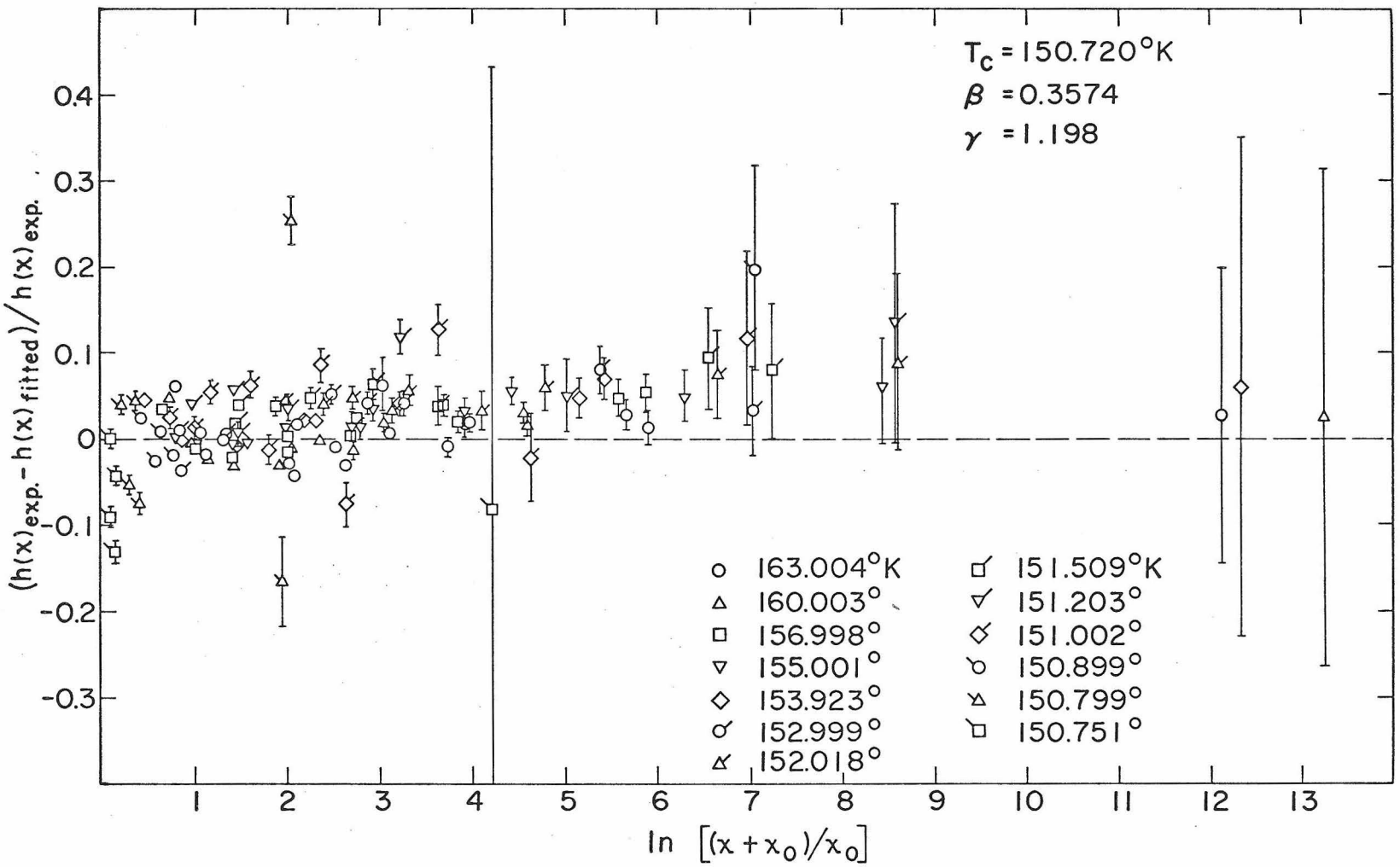

Figure 21. Plot of Relative Deviation $[h(x)_{exp't} - h(x)_{fitted}] / h(x)_{exp't}$ versus $\ln[(x+x_o)/x_o]$

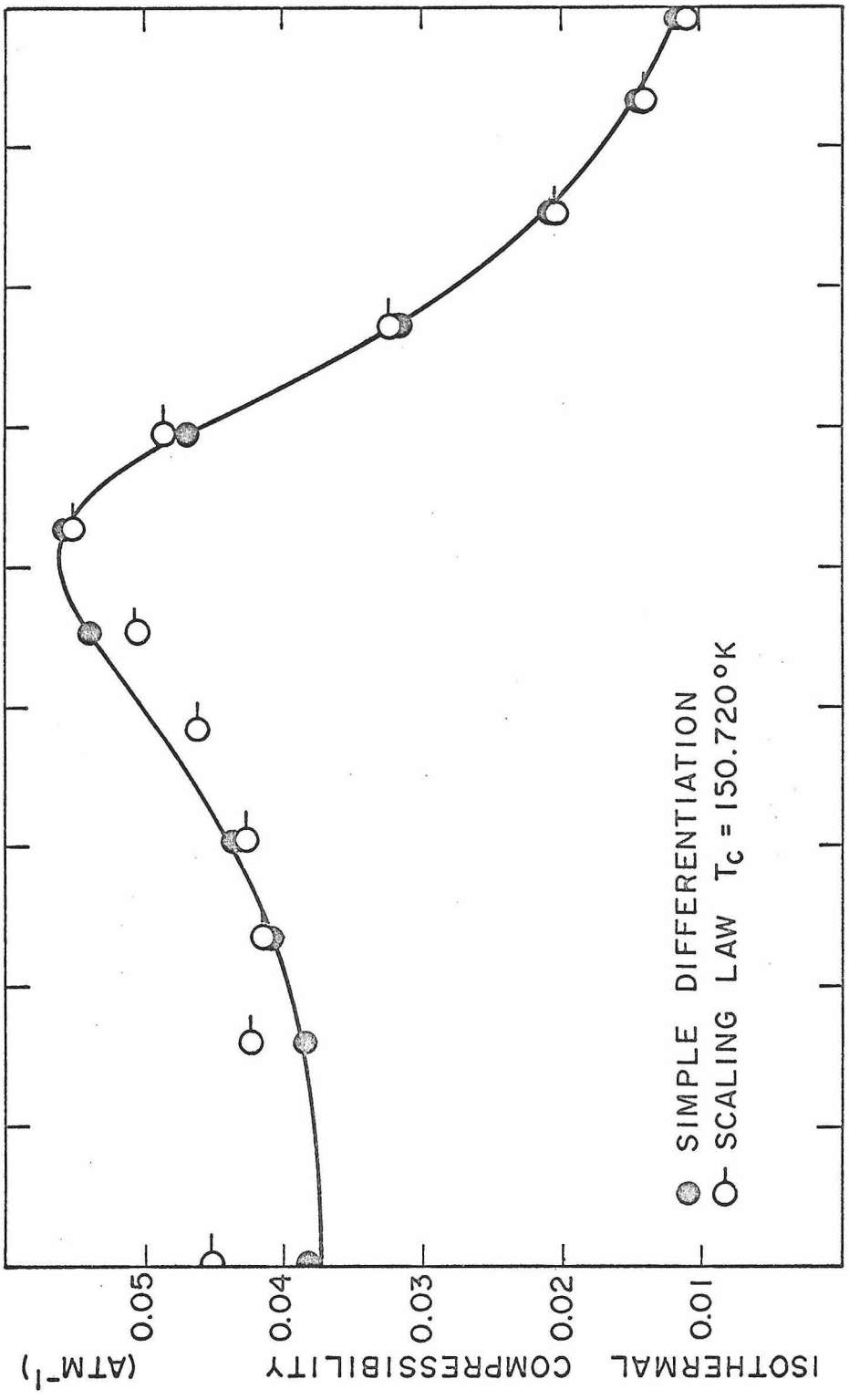

Figure 22. Comparison of the Experimental and Calculated Isothermal Compressibility along the 160.003°K Isotherm. ● estimated from experimental data, Equation (30); O- calculated, Equation (54)

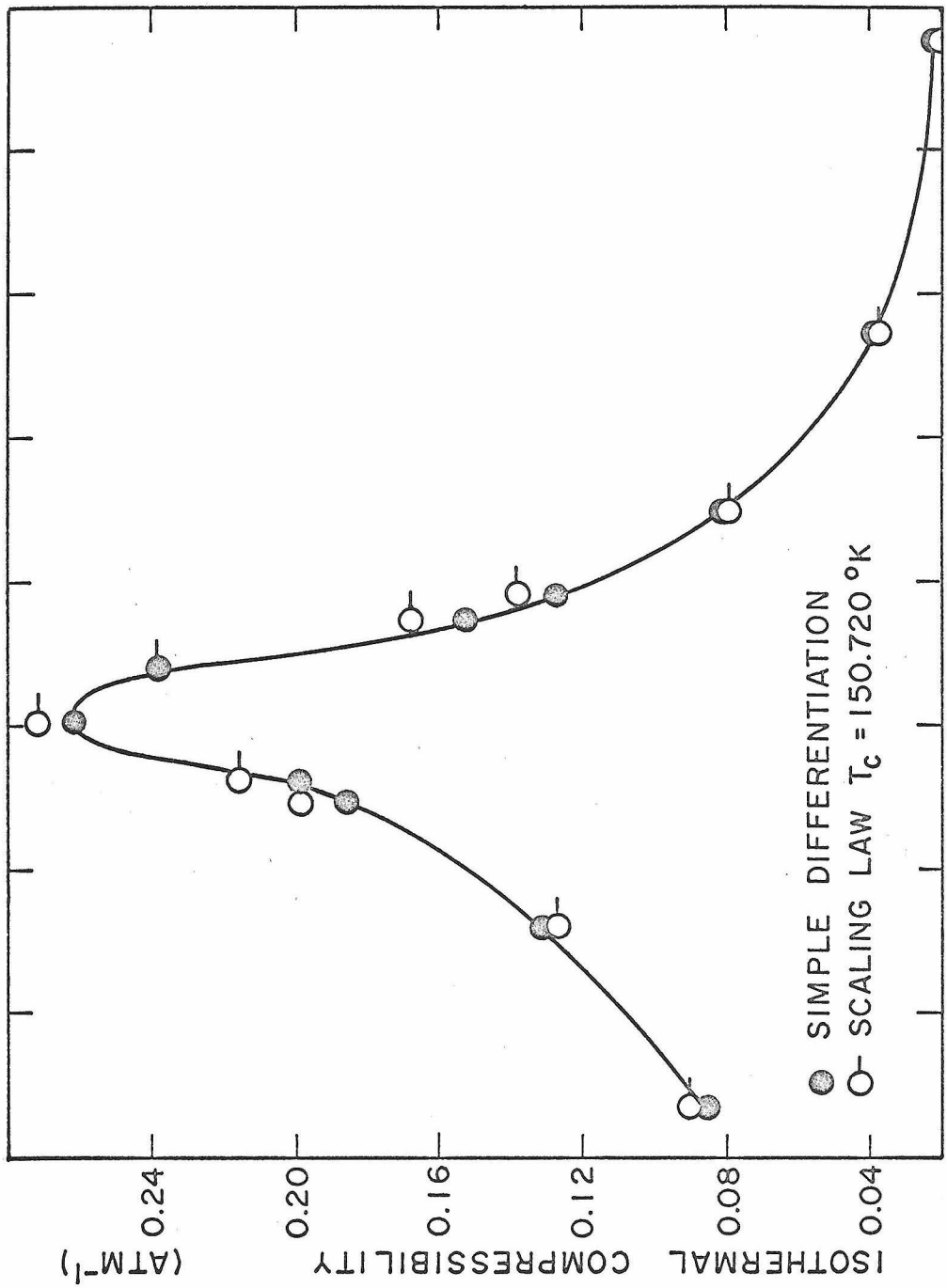

Figure 23. Comparison of the Experimental and Calculated Isothermal Compressibility along the 152.999°K Isotherm. ● estimated from experimental data, Equation (30); O— calculated, Equation (54)

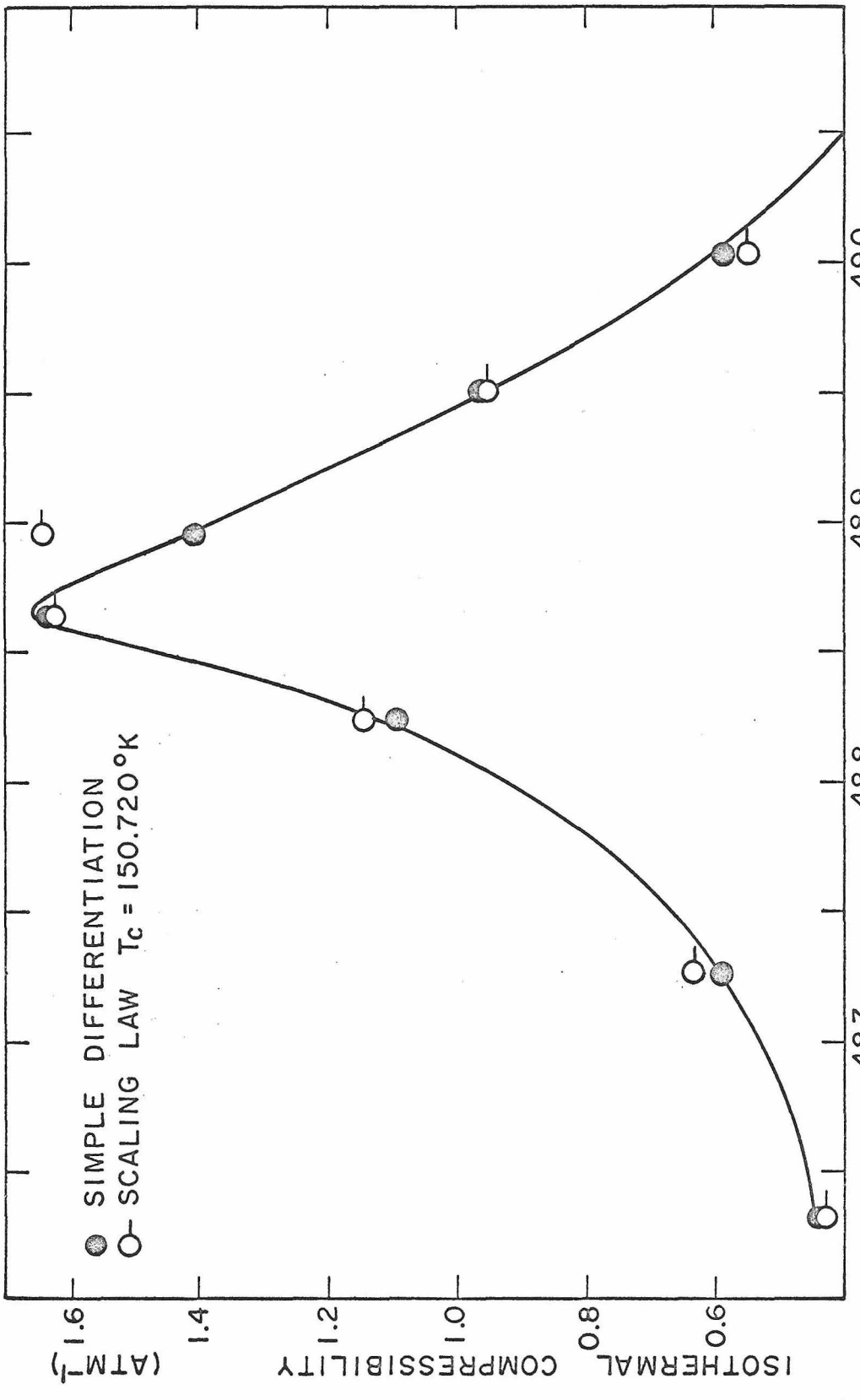

Figure 24. Comparison of the Experimental and Calculated Isothermal Compressibility along the 151.203°K Isotherm. ● estimated from experimental data, Equation (30); O- calculated, Equation (54)

TABLE I

EXPERIMENTAL VALUES OF ANGLE OF MINIMUM DEVIATION OF ARGON ALONG THE SINGLE PHASE ISOTHERMS

Pressure (atm)	Angle D (minute of arc)
RUN III 163.004°K	
40.078_8	72.28
49.869_7	102.49
60.120_3	150.77
62.834_9	168.80
65.998_0	193.49
69.036_5	220.14
71.870_1	245.07
74.700_4	267.31
77.861_3	287.96
81.157_3	305.22
84.922_6	321.10
90.265_6	338.67
RUN IV 160.003°K	
42.093_6	82.13
48.395_8	104.65
51.360_4	117.82
54.144_8	132.82
57.345_2	154.05
60.128_2	177.98
63.072_5	210.14
65.867_5	244.10
68.890_0	275.75
72.109_2	300.28
75.303_8	318.33
77.756_7	329.17
RUN V 156.998°K	
44.123_8	95.09
50.159_4	124.89
53.133_2	146.18
55.367_1	168.25
56.687_1	185.62
57.943_4	205.54
58.865_4	222.74
59.961_5	243.38
60.944_3	260.56
62.449_4	282.15
64.012_1	298.98
66.611_6	319.09
RUN XXXIII 155.001°K	
48.627_{36}	126.146
53.423_{83}	176.664
55.019_{36}	211.150
55.648_{22}	229.175
57.113_{53}	269.000
61.233_{12}	322.234

†Excluded in the final results for smoothness by cubic spline fit (see p. 29 and p. 39)

*Excluded in the final results due to possible errors in the measurements (see p. 29)

#Coexisting gas-liquid state.

TABLE I (continued)

Pressure (atm)	Angle D (minute of arc)
RUN XXXIV	155.001°K
†48.629$_{20}$	126.150
50.405$_{08}$	140.152
52.088$_{60}$	157.672
54.344$_{52}$	194.566
56.319$_{40}$	248.863
58.153$_{23}$	288.716
59.790$_{96}$	309.500
†61.235$_{37}$	322.271
RUN VI	153.923°K
44.350$_{1}$	105.37
49.307$_{1}$	139.95
50.210$_{2}$	149.63
51.670$_{3}$	170.70
52.585$_{3}$	190.81
53.096$_{8}$	206.14
53.624$_{7}$	226.05
54.065$_{1}$	244.03
54.502$_{1}$	260.91
55.137$_{9}$	279.78
56.105$_{5}$	299.06
57.645$_{8}$	318.35
RUN XXX	152.999°K
49.329$_{48}$	151.595
51.450$_{30}$	199.648
†51.933$_{29}$	223.623
†52.296$_{80}$	245.884
52.708$_{75}$	267.793
53.477$_{88}$	292.930
†56.755$_{92}$	334.668

Pressure (atm)	Angle D (minute of arc)
RUN XXXI	152.999°K
*49.326$_{91}$	152.013
*50.329$_{91}$	168.835
*51.022$_{98}$	186.138
*51.731$_{58}$	215.312
*52.120$_{21}$	238.814
*52.520$_{17}$	262.161
*53.074$_{06}$	284.186
*54.226$_{99}$	308.937
*55.226$_{99}$	321.815
*56.754$_{07}$	335.393
*58.931$_{21}$	348.923
RUN XXXII	152.999°K
†49.329$_{97}$	151.511
50.594$_{72}$	173.354
51.601$_{05}$	205.575
52.015$_{84}$	227.772
52.394$_{26}$	250.876
52.893$_{38}$	274.854
54.720$_{85}$	314.442
56.752$_{48}$	334.476
RUN VII	152.018°K
*45.886$_{14}$	125.07
*49.971$_{53}$	200.85
*50.287$_{51}$	228.70
*50.455$_{64}$	248.81
*50.575$_{71}$	261.14
*50.854$_{41}$	280.91

TABLE I (continued)

Pressure (atm)	Angle D (minute of arc)
RUN VIII	152.018°K
49.971_{70}	200.00
50.126_{56}	210.40
50.398_{95}	238.79
50.852_{83}	279.07
RUN IX	152.018°K
49.971_{97}	199.45
50.200_{86}	216.92
50.498_{00}	250.39
50.854_{54}	279.04
RUN X	152.018°K
49.972_{36}	199.95
50.304_{73}	227.54
50.605_{85}	262.02
50.707_{17}	270.34
50.854_{54}	279.83
RUN XI	151.509°K
49.145_{53}	197.92
49.372_{74}	223.75
49.495_{10}	249.32
49.871_{30}	289.11
RUN XII	151.509°K
49.146_{29}	197.42
49.278_{67}	210.24
49.438_{61}	237.38
49.607_{79}	267.64
49.738_{55}	280.53
49.871_{33}	289.28

Pressure (atm)	Angle D (minute of arc)
RUN XIV	151.203°K
48.630_{33}	193.91
48.823_{03}	219.83
48.895_{91}	245.35
49.064_{82}	280.84
RUN XV	151.203°K
48.631_{69}	194.03
48.728_{59}	204.04
48.863_{57}	232.89
48.949_{46}	261.42
49.002_{60}	272.71
49.065_{45}	280.72
RUN XVI	151.002°K
†48.338_{88}	195.396
RUN XVII	151.002°K
48.339_{53}	195.660
†48.476_{99}	224.750
48.511_{64}	246.620
†48.550_{98}	265.615
†48.618_{75}	280.250
RUN XVIII	151.002°K
48.340_{17}	195.770
48.435_{87}	209.845
*48.493_{57}	231.491
48.527_{69}	255.916
*48.575_{88}	271.534
†48.619_{64}	279.760

TABLE I (continued)

Pressure (atm)	Angle D (minute of arc)
RUN XIX	151.002°K
48.340_{54}	195.380
48.398_{10}	202.990
48.457_{81}	215.730
*48.510_{82}	240.335
48.546_{83}	264.180
48.575_{95}	272.160
48.614_{29}	278.818
RUN XX	151.002°K
48.338_{53}	196.036
†48.511_{48}	245.620
RUN XXI	151.002°K
48.340_{17}	195.549
48.478_{97}	223.397
48.494_{27}	233.397
†48.511_{26}	246.133
†48.527_{81}	256.783
*48.551_{77}	266.823
†48.618_{83}	280.369
RUN XXII	150.899°K
48.134_{19}	190.697
48.288_{05}	217.472
48.320_{03}	244.662
48.352_{01}	268.309
48.448_{38}	286.968

Pressure (atm)	Angle D (minute of arc)
RUN XXIII	150.899°K
48.131_{30}	191.270
48.208_{27}	200.168
48.256_{32}	210.087
48.302_{98}	239.331
48.319_{28}	256.789
48.396_{33}	281.484
48.444_{78}	287.522
RUN XXIV	150.899°K
48.130_{30}	190.694
48.280_{86}	217.314
48.302_{70}	233.302
48.320_{90}	254.322
48.348_{39}	269.589
48.444_{86}	286.762
RUN XXV	150.799°K
47.988_{64}	191.431
48.108_{96}	216.139
48.124_{73}	239.383
48.142_{18}	267.014
48.221_{55}	286.296
RUN XXVI	150.799°K
47.987_{40}	192.139
48.057_{14}	202.026
48.112_{20}	227.180
48.125_{73}	258.778
48.178_{72}	281.379
48.220_{35}	287.378

TABLE I (continued)

Pressure (atm)	Angle D (minute of arc)
RUN XXVII	150.751°K
47.889_{81}	190.634
48.000_{47}	212.639
48.014_{18}	246.917
48.015_{91}	251.197
48.035_{76}	274.915
48.122_{57}	290.307
RUN XXVIII	150.751°K
47.890_{49}	191.804
47.955_{60}	201.431
47.999_{92}	221.188
48.004_{37}	247.512
48.006_{88}	260.966
48.066_{52}	284.930
48.122_{56}	291.609

Pressure (atm)	Angle D (minute of arc)
RUN XXIX	150.701°K
47.840_{26}	192.875
47.921_{82}	211.898
47.936_{14}	#222.430
	#262.266
47.943_{82}	274.169
48.015_{82}	289.305

TABLE II

EXPERIMENTAL VALUES OF ANGLE OF MINIMUM DEVIATION OF ARGON FOR THE COEXISTING GAS-LIQUID STATES

Temperature (°K)	Pressure (atm)	Angle of Minimum Deviation (minutes of arc) D_{gas}	D_{liquid}
RUN 1			
148.513	44.015_{94}	$145.28_2 \pm 0.05$*	$347.41_0 \pm 0.08$*
150.546	47.637_{11}	201.37_2 0.06	284.91_6 0.15
RUN 2			
148.513	44.016_{34}	$145.39_0 \pm 0.05$	$347.42_4 \pm 0.04$
149.026	44.907_{22}	153.73_9 0.06	337.32_5 0.05
149.548	45.828_{08}	164.16_6 0.05	325.16_1 0.05
150.061	46.755_{98}	178.21_7 0.07	309.47_5 0.05
RUN 3			
148.513	44.019_{38}	$145.41_6 \pm 0.06$	$347.38_1 \pm 0.05$
150.252	47.108_{08}	185.40_5 0.12	301.75_1 0.05
150.450	47.475_{96}	195.34_8 0.12	291.05_6 0.05
150.639	47.824_{22}	211.36_7 0.15	274.24_1 0.15
RUN 4			
148.513	44.017_{53}	$145.32_1 \pm 0.05$	$347.37_6 \pm 0.05$
150.658	47.861_{65}	214.19_3 0.27	271.76_2 0.25
150.675	47.893_{75}	217.12_4 0.15	268.34_4 0.15
150.711	47.959_{27}	227.45_4 0.50	258.44_0 0.50
RUN 5			
150.701	47.934_{19}	$221.45_0 \pm 0.08$	
150.701	47.936_{14}	222.43_0 0.07	$262.26_6 \pm 0.09$
150.720	47.969_{48}	230.68_6 0.90	255.11_6 0.50
150.720	47.969_{48}	231.13_6 0.70	252.97_6 0.50
150.701	47.931_{64}	$221.93_3 \pm 0.05$	$262.99_9 \pm 0.07$

*Relative error in D estimated from uncertainty in the readings V (see Appendix B).

TABLE III

REFRACTIVE INDEX OF ARGON FOR COEXISTING GAS-LIQUID STATES

Temperature (Deg K)	Pressure (atm)	GAS STATE Refractive Index	GAS STATE Error*	LIQUID STATE Refractive Index	LIQUID STATE Error*
148.513	44.017_{30}	1.05174_{59}	$\pm 0.00002_{44}$	1.12288_{89}	$\pm 0.00003_{35}$
149.026	44.907_{22}	1.05471_{79}	0.00002_{84}	1.11936_{66}	0.00003_{31}
149.548	45.828_{08}	1.05841_{13}	0.00002_{53}	1.11510_{53}	0.00003_{25}
150.061	46.755_{98}	1.06338_{27}	0.00003_{30}	1.10960_{99}	0.00003_{18}
150.252	47.108_{08}	1.06592_{50}	0.00005_{10}	1.10689_{85}	0.00003_{15}
150.450	47.475_{96}	1.06943_{79}	0.00005_{14}	1.10314_{67}	0.00003_{10}
150.546	47.637_{11}	1.07156_{43}	0.00003_{05}	1.10099_{06}	0.00006_{58}
150.639	47.824_{22}	1.07509_{47}	0.00006_{27}	1.09723_{80}	0.00006_{54}
150.658	47.861_{65}	1.07608_{99}	0.00010_{52}	1.09636_{63}	0.00010_{04}
150.675	47.893_{75}	1.07712_{37}	0.00006_{29}	1.09516_{39}	0.00006_{51}
150.701	47.933_{89}	1.07882_{03}	0.00018_{66}	1.09315_{57}	0.00013_{88}
150.711	47.959_{27}	1.08076_{68}	0.00018_{68}	1.09168_{17}	0.00018_{79}
150.720	47.969_{48}	1.08198_{66}	$\pm 0.00036_{31}$	1.09013_{69}	$\pm 0.00036_{37}$

*Computed by Equation (28)

TABLE IV

REFRACTIVE INDEX AND ISOTHERMAL COMPRESSIBILITY OF ARGON ALONG THE SINGLE PHASE ISOTHERMS

Pressure (atm)	Angle D (minute of arc)	Refractive Index	Derivative* $(\partial D/\partial P)_T$ (min./atm)	Isothermal† Compressibility (atm^{-1})
163.004°K Isotherm				
40.078_8	72.28	1.02578_{93}	2.636_{13}	0.0362241
49.869_7	102.49	1.03653_{47}	3.655_{62}	0.0353188
60.120_3	150.77	1.05366_{58}	6.131_{27}	0.0400636
62.834_9	168.80	1.06005_{00}	7.174_{87}	0.0417925
65.998_0	193.49	1.06878_{07}	8.399_{84}	0.0425665
69.036_5	220.14	1.07818_{90}	8.980_{48}	0.0398773
71.870_1	245.07	1.08697_{54}	8.435_{06}	0.0335466
74.700_4	267.31	1.09480_{17}	7.245_{62}	0.0262480
77.861_3	287.96	1.10205_{82}	5.837_{71}	0.0196562
81.157_3	305.22	1.10811_{58}	4.708_{21}	0.0149244
84.922_6	321.10	1.11368_{30}	3.770_{90}	0.0113393
90.265_6	338.67	1.11983_{56}	2.880_{80}	0.0081949
160.003°K Isotherm				
42.093_6	82.13	1.02929_{50}	3.176_{24}	0.0383738
48.395_8	104.65	1.03730_{22}	4.079_{29}	0.0385902
51.360_4	117.82	1.04197_{98}	4.874_{24}	0.0409002
54.144_8	132.82	1.04730_{26}	5.911_{45}	0.0439321
57.345_2	154.05	1.05482_{77}	7.525_{82}	0.0481118
60.128_2	177.98	1.06329_{78}	9.739_{30}	0.0537490
63.072_5	210.14	1.07466_{06}	11.957_{16}	0.0556863
65.867_5	244.10	1.08663_{38}	11.817_{18}	0.0471896
68.890_0	275.75	1.09776_{88}	8.953_{77}	0.0315305
72.109_2	300.28	1.10638_{28}	6.507_{31}	0.0209796
75.303_8	318.33	1.11271_{23}	4.878_{61}	0.0148032
77.756_7	329.17	1.11650_{98}	4.011_{63}	0.0117554

†Calculated by Equation (30)

*Obtained from the spline fit

#Interpolated from a large graph of angle D versus pressure

**Coexisting gas-liquid state

TABLE IV (continued)

Pressure (atm)	Angle D (minute of arc)	Refractive Index	Derivative $(\partial D/\partial P)_T$ (min./atm.)	Isothermal Compressibility (atm^{-1})
156.998°K Isotherm				
44.123$_8$	95.09	1.0339044	4.05316	0.0422391
50.159$_4$	124.89	1.0444892	6.14478	0.0486065
53.133$_2$	146.18	1.0520393	8.413$_{22}$	0.0567289
55.367$_1$	168.25	1.0598554	11.73739	0.0685967
56.687$_1$	185.62	1.0659993	14.50962	0.0767137
57.943$_4$	205.54	1.0730367	17.53451	0.0835326
58.865$_4$	222.74	1.0791060	19.18470	0.0841687
59.961$_5$	243.38	1.0863802	18.34605	0.0734845
60.944$_3$	260.56	1.0924276	16.37057	0.0611222.
62.449$_4$	282.15	1.1000175	12.40554	0.0426614
64.012$_1$	298.98	1.1059266	9.33923	0.0302456
66.611$_6$	319.09	1.1129786	6.48171	0.0196187
155.001°K Isotherm				
48.62736	126.146	1.0449349	6.97980	0.0546548
50.40508	140.152	1.0499026	8.94804	0.0629709
52.08860	157.672	1.0561106	12.15571	0.0758951
53.42383	176.664	1.0628323	16.84191	0.0936528
54.34452	194.566	1.0691609	22.28847	0.1123094
55.01936	211.150	1.0750170	26.92297	0.1247700
55.64822	229.175	1.0813750	29.79988	0.1269738
56.31940	248.863	1.0883110	28.08758	0.1099532
57.11353	269.000	1.0953959	22.44373	0.0810852
58.15323	288.716	1.1023237	15.91898	0.0534555
59.79096	309.500	1.1096169	10.19195	0.0318432
61.23312	322.234	1.1140803	7.71353	0.0231101

TABLE IV (continued)

Pressure (atm)	Angle D (minute of arc)	Refractive Index	Derivative $(\partial D/\partial P)_T$ (min./atm)	Isothermal Compressibility (atm^{-1})
153.923°K Isotherm				
44.350_1	105.37	1.03755_{80}	5.224_{27}	0.0490804
49.307_1	139.95	1.04983_{10}	9.776_{79}	0.0689040
50.210_2	149.63	1.05326_{18}	11.784_{62}	0.0776006
51.670_3	170.70	1.06072_{24}	18.065_{18}	0.1040337
52.585_3	190.81	1.06783_{37}	26.628_{63}	0.1368785
53.096_8	206.14	1.07324_{86}	33.792_{01}	0.1605020
53.624_7	226.05	1.08027_{32}	40.453_{86}	0.1748161
54.065_1	244.03	1.08660_{92}	40.809_{37}	0.1630125
54.502_1	260.91	1.09255_{07}	35.178_{60}	0.1311634
55.137_9	279.78	1.09918_{49}	24.936_{31}	0.0865051
56.105_5	299.06	1.10595_{47}	15.963_{68}	0.0516849
57.645_8	318.35	1.11271_{93}	10.057_{28}	0.0305148
152.999°K Isotherm				
49.329_{48}	151.595	1.05395_{80}	13.110_{81}	0.0851962
50.594_{72}	173.354	1.06166_{14}	23.267_{04}	0.1319000
51.450_{30}	199.648	1.07095_{61}	37.855_{98}	0.1857894
51.601_{05}	205.575	1.07304_{91}	41.878_{54}	0.1994702
52.015_{84}	227.772	1.08088_{04}	61.420_{96}	0.2633629
52.394_{26}	250.876	1.08901_{97}	61.809_{56}	0.2399637
52.708_{75}	267.793	1.09497_{15}	42.055_{69}	0.1526469
52.893_{38}	274.854	1.09745_{38}	36.280_{00}	0.1281898
53.477_{88}	292.930	1.10380_{32}	24.570_{29}	0.0812769
54.720_{85}	314.442	1.11134_{95}	12.867_{70}	0.0395467
56.755_{92}	334.476	1.11836_{75}	7.842_{99}	0.0225891

TABLE IV (continued)

Pressure (atm)	Angle D (minute of arc)	Refractive Index	Derivative $(\partial D/\partial P)_T$ (min./atm.)	Isothermal Compressibility (atm^{-1})
152.018°K Isotherm				
49.972_{01}	199.80	1.07100_{98}	57.665_{41}	0.2827899
50.126_{56}	210.40	1.07475_{23}	81.249_{27}	0.3779110
50.200_{86}	216.92	1.07705_{31}	93.733_{39}	0.4225547
50.304_{73}	227.54	1.08079_{86}	112.513_{21}	0.4829430
50.398_{95}	238.79	1.08476_{34}	120.475_{44}	0.4921038
50.498_{00}	250.39	1.08884_{36}	115.730_{39}	0.4501993
50.605_{85}	262.02	1.09294_{12}	94.570_{32}	0.3510950
50.707_{17}	270.34	1.09586_{71}	71.530_{32}	0.2571033
50.853_{97}	279.31	1.09901_{98}	52.684_{67}	0.1830834
151.509°K Isotherm				
49.145_{91}	197.67	1.07025_{74}	78.557_{04}	0.3894877
49.278_{67}	210.24	1.07469_{59}	116.243_{53}	0.5410997
49.372_{74}	223.75	1.07946_{22}	179.704_{51}	0.7847634
49.438_{61}	237.38	1.08426_{66}	220.457_{46}	0.9059986
49.495_{10}	249.32	1.08847_{19}	199.998_{63}	0.7814476
49.607_{79}	267.64	1.09491_{77}	126.137_{87}	0.4581049
49.738_{55}	280.53	1.09944_{84}	77.596_{95}	0.2584426
49.871_{32}	289.195	1.10249_{19}	55.568_{31}	0.1862766
151.203°K Isotherm				
48.631_{01}	193.97	1.06895_{03}	87.988_{65}	0.4447584
48.728_{59}	204.04	1.07250_{71}	123.380_{34}	0.5921940
48.823_{03}	219.83	1.07807_{97}	245.234_{26}	1.0905246
48.863_{57}	232.89	1.08268_{44}	392.379_{13}	1.6444934
48.895_{91}	245.35	1.08707_{40}	354.528_{76}	1.4083196
48.949_{46}	261.42	1.09273_{01}	260.728_{20}	0.9701685
49.002_{60}	272.71	1.09669_{85}	163.704_{20}	0.5831351
49.065_{23}	280.78	1.09953_{62}	103.381_{54}	0.3573136

TABLE IV (Continued)

Pressure (atm)	Angle D (minute of arc)	Refractive Index	Derivative $(\partial D/\partial P)_T$ (min./atm.)	Isothermal Compressibility (atm^{-1})
151.002°K Isotherm				
48.339_{53}	195.660	1.0695_{474}	106.542_{67}	0.5337899
48.398_{10}	202.990	1.0721_{364}	150.292_{20}	0.7251826
48.435_{87}	209.845	1.0745_{565}	226.380_{56}	1.0558059
48.457_{81}	215.730	1.0766_{332}	308.307_{58}	1.3977251
48.478_{97}	223.397	1.0793_{377}	463.522_{14}	2.0274672
48.494_{27}	233.397	1.0828_{631}	822.337_{70}	3.4387932
48.511_{64}	246.620	1.0875_{212}	662.492_{68}	2.6177178
48.527_{69}	255.916	1.0907_{936}	511.771_{20}	1.9465461
48.546_{83}	264.180	1.0937_{009}	353.505_{26}	1.3012142
48.575_{95}	272.160	1.0965_{069}	215.094_{05}	0.7677776
48.614_{29}	278.818	1.0988_{469}	143.001_{53}	0.4978486
150.899°K Isotherm				
Set I				
48.134_{19}	190.697	1.0677_{938}	103.948_{61}	0.5346480
48.288_{05}	217.472	1.0772_{478}	374.589_{40}	1.6842730
48.320_{03}	244.662	1.0868_{317}	1981.929_{70}	7.8957454
48.352_{01}	268.309	1.0951_{530}	342.768_{02}	1.2426528
48.448_{38}	286.968	1.1017_{098}	127.247_{19}	0.4299878
Set II				
48.131_{30}	191.270	1.0679_{963}	90.588_{28}	0.4645047
48.208_{27}	200.168	1.0711_{398}	152.903_{91}	0.7484274
48.256_{32}	210.087	1.0746_{419}	286.164_{47}	1.3330548
48.302_{98}	239.331	1.0849_{540}	1321.452_{52}	5.3851662
48.319_{28}	256.789	1.0911_{008}	865.518_{41}	3.2805038
48.396_{33}	281.484	1.0997_{836}	149.869_{27}	0.5166471
48.444_{78}	287.522	1.1019_{044}	105.587_{75}	0.3560854

TABLE IV (continued)

Pressure (atm)	Angle D (minute of arc)	Refractive Index	Derivative $(\partial D/\partial P)_T$ (min./atm.)	Isothermal Compressibility (atm^{-1})
150.899°K Isotherm (continued)				
Set III				
48.130_{30}	190.694	1.06779_{27}	98.620_{85}	0.5072535
48.280_{86}	217.314	1.07719_{21}	434.715_{12}	1.9560743
48.302_{76}	233.302	1.08282_{96}	1181.701_{01}	4.9436207
48.320_{90}	254.322	1.09023_{26}	952.695_{44}	3.6470329
48.348_{39}	269.589	1.09560_{30}	328.563_{45}	1.1843622
48.444_{86}	286.762	1.10163_{75}	113.455_{75}	0.3836696
150.799°K Isotherm				
Set I				
47.988_{64}	191.431	1.06805_{31}		
48.108_{96}	216.139	1.07677_{75}		
48.124_{73}	239.383	1.08497_{23}		
48.142_{18}	267.014	1.09469_{76}		
48.221_{55}	286.296	1.10147_{38}		
Set II				
47.987_{40}	192.139	1.06830_{33}	109.236_{55}	0.5575383
48.057_{14}	202.026	1.07179_{59}	193.858_{21}	0.9399623
48.112_{20}	227.180	1.08067_{16}	1820.904_{51}	7.8286263
48.125_{73}	258.778	1.09180_{06}	1737.268_{26}	6.5324497
48.178_{72}	281.379	1.09974_{67}	179.048_{03}	0.6174739
48.220_{35}	287.378	1.10185_{38}	119.082_{19}	0.4018026

TABLE IV (continued)

Pressure (atm)	Angle D (minute of arc)	Refractive Index	Derivative $(\partial D/\partial P)_T$ (min./atm.)	Isothermal Compressibility (atm^{-1})
150.751°K Isotherm				
Set I				
47.889_{81}	190.634	1.06777_{15}		
48.000_{47}	212.639	1.07554_{25}		
48.014_{18}	246.917	1.08762_{58}		
48.015_{91}	251.197	1.08913_{27}		
48.035_{76}	274.915	1.09747_{53}		
48.122_{57}	290.307	1.10288_{30}		
Set II				
47.890_{49}	191.804	1.05818_{50}	111.968	0.5725011
47.955_{60}	201.431	1.07158_{58}	207.447	1.0088907
47.999_{92}	221.188	1.07855_{86}	1628.915	7.1979628
#48.003_{70}	235.000	1.08342_{80}	14365.380	
48.004_{37}	247.512	1.08783_{53}	12058.666	47.4708272
48.006_{88}	260.966	1.09257_{04}	3191.075	11.8952862
48.066_{52}	284.930	1.10099_{41}	152.154	0.5179595
48.122_{56}	291.609	1.10333_{94}	96.554	0.3208939
150.701°K Isotherm				
47.840_{26}	192.875	1.06856_{34}		
47.921_{82}	211.898	1.07528_{10}		
47.936_{14}	**222.430	1.07899_{67}		
	**262.266	1.09302_{77}		
47.943_{82}	274.169	1.09721_{31}		
48.015_{82}	289.305	1.10253_{05}		

TABLE V

COMPARISON OF THE ESTIMATED VALUES OF THE DERIVATIVES $(\partial D/\partial P)_T$

Pressure (atm)	Angle D (minute of arc)	Derivative $(\partial D/\partial P)_T$ (minute/atm) Visual Estimate	Numerical[58] Estimate	Percentage† Difference %
163.004°K Isotherm				
40.079	72.28	2.760	2.636	4.70
49.870	102.49	3.670	3.656	0.38
60.120	150.77	5.950	6.131	-2.96
62.835	168.80	7.270	7.175	1.32
65.998	193.49	8.435	8.400	0.42
69.037	220.14	8.895	8.981	-0.96
71.870	245.07	8.455	8.435	0.24
74.700	267.31	7.305	7.246	0.81
77.861	287.96	5.730	5.838	-1.85
81.157	305.22	4.665	4.708	1.33
84.923	321.10	3.820	3.771	1.30
90.266	338.67	3.070	2.881	6.56
152.999°K Isotherm				
49.329	151.595	14.250	13.111	8.69
50.595	173.354	22.630	23.267	-2.73
51.450	199.648	38.750	37.856	2.36
51.601	205.575	44.370	41.878	5.95
52.016	227.772	60.450	61.419	-1.58
52.394	250.876	57.050	61.815	-7.11
52.709	267.793	45.600	42.048	8.45
52.893	274.854	37.150	36.296	2.35
53.478	292.930	22.950	24.525	-6.42
54.721	314.442	13.300	12.920	2.94
56.756	334.668	7.520	7.927	-5.13

† $100\left[\left(\frac{\partial D}{\partial P}\right)_{T_{visual}} - \left(\frac{\partial D}{\partial P}\right)_{T_{numerical}}\right] / \left(\frac{\partial D}{\partial P}\right)_{T_{numerical}}$

TABLE V (continued)

Pressure (atm)	Angle D (minute of arc)	Derivative $(\partial D/\partial P)_T$ (minute/atm) Visual Estimate	Numerical Estimate	Percentage Difference %
151.203°K Isotherm				
48.631	193.970	95.100	87.989	8.08
48.728	204.040	121.100	123.380	-1.85
48.823	219.830	259.800	245.234	5.94
48.864	232.890	394.800	392.379	0.62
48.896	245.350	364.500	354.529	2.81
48.949	261.420	257.600	260.728	-1.20
49.003	272.710	161.500	163.704	-1.35
49.065	280.780	118.400	103.381	14.53
150.799°K Isotherm				
47.987	192.139	95.000	109.237	-13.03
48.057	202.026	214.000	193.858	10.39
48.112	227.180	1500.000	1820.905	-17.62
48.126	258.778	1240.000	1737.268	-28.62
48.179	281.379	210.000	179.048	17.28
48.220	287.378	102.000	119.082	-14.34

TABLE VI

RECTILINEAR DIAMETER ANALYSIS $(\phi_L + \phi_G)/2 = \overline{\phi} = \phi_o - dT$

Coefficients obtained from the least squares fit of the weighted data to the equation above:

$\phi_o = 0.0963753$, $d = 0.000264567$

Standard deviation of the data from the fitted equation $\sigma_{fit} = 0.7239$

E X P E R I M E N T A L D A T A

Temperature (deg.K)	ϕ_L †	ϕ_G †	$\overline{\phi}_{Exp't}$	Error*	$\overline{\phi}_{Cal'd}$	$\Delta\overline{\phi}$ #
148.513	0.0341802	0.0800028	0.0570915 ±	0.0000133	0.0570836	0.0000079
149.026	0.0361229	0.0777691	0.0569460	0.0000140	0.0569479	-0.0000019
149.548	0.0385338	0.0750618	0.0567978	0.0000132	0.0568098	-0.0000120
150.061	0.0417732	0.0715620	0.0566677	0.0000148	0.0566741	-0.0000064
150.252	0.0434272	0.0698321	0.0566297	0.0000194	0.0566235	0.0000061
150.450	0.0457097	0.0674346	0.0565721	0.0000194	0.0565711	0.0000010
150.546	0.0470897	0.0660549	0.0565723	0.0000233	0.0565457	0.0000265
150.639	0.0493780	0.0636503	0.0565142	0.0000292	0.0565211	-0.0000070
150.658	0.0500225	0.0630911	0.0565568	0.0000469	0.0565161	0.0000407
150.675	0.0506916	0.0623195	0.0565055	0.0000292	0.0565116	-0.0000061
150.701	0.0517891	0.0610297	0.0564095	0.0000750	0.0565047	-0.0000953
150.711	0.0530473	0.0600823	0.0565648	0.0000854	0.0565021	0.0000627
150.720	0.0538352	0.0590887	0.0564619 ±	0.0001656	0.0564997	-0.0000378

† $\phi_L = [(n^2-1)/(n^2+2)]_{Liquid}$; $\phi_G = [(n^2-1)/(n^2+2)]_{Gas}$

* $\sigma_{\overline{\phi}_{exp't}} = (\sigma^2_{\phi_L} + \sigma^2_{\phi_G})^{1/2} / 2$; σ_{ϕ_L} and σ_{ϕ_G} are computed using Equation (31).

$\overline{\phi}_{exp't} - \overline{\phi}_{cal'd}$

TABLE VII

RESULTS OF THE LEAST SQUARES FIT OF THE WEIGHTED DATA TO THE EQUATION $\ln(\phi_L - \phi_G) = \ln B_\phi + \beta \ln(T_c - T)$

Coefficients of the equation at best fit†: $B_\phi = 0.03448$, $\beta = 0.3574 \pm 0.0027$, $T_c = 150.725^\circ K$

Temperature (Deg.K)	$\ln(T_c - T)$	Error*	$\ln(\phi_L - \phi_G)$ exp't	Error#	$\ln(\phi_L - \phi_G)$ cal'd	$\Delta \ln(\phi_L - \phi_G)$**
148.513	0.794	± 0.005	-3.08298	± 0.00058	-3.08350	0.00053
149.026	0.530	0.006	-3.17854	0.00067	-3.17781	-0.00073
149.548	0.163	0.009	-3.30968	0.00072	-3.30901	-0.00067
150.061	-0.409	0.015	-3.51362	0.00099	-3.51361	-0.00001
150.252	-0.749	0.021	-3.63420	0.00147	-3.63484	0.00064
150.450	-1.291	0.036	-3.82929	0.00179	-3.82868	-0.00062
150.546	-1.720	0.056	-3.96515	0.00246	-3.98215	0.01700
150.639	-2.453	0.116	-4.24943	0.00409	-4.24415	-0.00528
150.658	-2.703	0.149	-4.33754	0.00717	-4.33338	-0.00415
150.675	-2.996	0.200	-4.45435	0.00502	-4.43799	-0.01636
150.701	-3.730	0.417	-4.68415	0.01624	-4.70032	0.01618
150.711	-4.269	0.714	-4.95686	0.02427	-4.89297	-0.06389
150.720	-5.298	± 2.000	-5.24885	± 0.06306	-5.26098	0.01212

†Using T_c as a variable parameter, the best fit is obtained when the standard deviation of the data from the fitted equation reaches a minimum.

#$\sigma_{\ln(\phi_L-\phi_G)} = (\sigma^2_{\phi_L} + \sigma^2_{\phi_G})^{1/2} / (\phi_L-\phi_G)$; σ_{ϕ_L} and σ_{ϕ_G} are computed using Equation (31)

*$\sigma_{\ln(T_c-T)} = \sigma_T/(T_c-T)$; $\sigma_T = \pm 0.01^\circ K$

**$\ln(\phi_L-\phi_G)_{exp't} - \ln(\phi_L-\phi_G)_{cal'd}$

TABLE VIII

COMPARISON OF THE VALUES OF B_ϕ, β, AND T_c OBTAINED FROM LEAST SQUARES FITS AND LINEAR REGRESSION ANALYSES

Least squares fit† to the equation

$$\ln \phi_F = \ln B_\phi + \beta \ln(T_c - T)$$

ϕ_F	B_ϕ	β	T_c (°K)	σ_{fit}*
$\phi_L - \phi_G$	0.03448	0.3574 ± 0.0027	150.725	0.3192
$\phi_L - \phi_C$#	0.01750	0.3694 ± 0.0028	150.728	0.5165
#$\phi_C - \phi_G$	0.01699	0.3445 ± 0.0027	150.721	0.2552
$\phi_L - \phi_C$**	0.01753	0.3677 ± 0.0028	150.725	0.5475
$\phi_C - \phi_G$**	0.01696	0.3466 ± 0.0027	150.725	0.3546

Linear regression analysis*** of the equation

$$\ln \phi_F = \ln B_\phi + \beta \ln(T_c - T) + A_{1\phi}^{****}(T_c - T) + A_{2\phi}^{****}(T_c - T)^2$$

$\phi_L - \phi_G$	0.03452	0.3600 ± 0.0032	150.725	0.0215
$\phi_L - \phi_C$#	0.01755	0.3648 ± 0.0022	150.725	0.0148
#$\phi_C - \phi_G$	0.01698	0.3551 ± 0.0044	150.725	0.0292

†Weighted data

*Standard deviation of the data from the fitted equation

#Computed from the fitted line of rectilinear diameter (Equation (33))

**Value of T_c fixed at 150.725°K

***Unweighted data

****$A_{1\phi} = A_{2\phi} = 0$ obtained for the best fit at minimum of σ_{fit} (see Table IX)

TABLE IX

COEFFICIENTS OF THE EQUATION $\ln(\phi_L - \phi_G) = \ln B_\phi + \beta \ln(T_c - T) + A_{1\phi}(T_c - T) + A_{2\phi}(T_c - T)^2$

OBTAINED BY THE LINEAR REGRESSION ANALYSIS OF UNWEIGHTED DATA FOR VARIOUS ASSUMED VALUES OF T_c

T_c (°K)	B_ϕ	β	$A_{1\phi}$	$A_{2\phi}$	σ_{fit} †	σ_β *
150.721	0.02475	0.2411	0.5167	-0.154	0.0779	0.0203
150.722	0.03075	0.3035	0.0857	0.0	0.0598	0.0135
150.723	0.03409	0.3408	0.0	0.0	0.0444	0.0063
150.724	0.03435	0.3513	0.0	0.0	0.0287	0.0042
150.725	0.03452	0.3600	0.0	0.0	0.0215	0.0032
150.726	0.03466	0.3674	0.0	0.0	0.0228	0.0035
150.727	0.03643	0.3877	-0.0416	0.0	0.0237	0.0068
150.728	0.03966	0.4157	-0.2019	0.055	0.0241	0.0105
150.729	0.04114	0.4315	-0.2549	0.069	0.0273	0.0124
150.730	0.04257	0.4464	-0.3037	0.082	0.0306	0.0144

† Standard deviation of the data from the fitted equation

* Standard error of β

TABLE X

RESULTS OF THE LEAST SQUARES FIT TO THE EQUATION $\ln K_T = \ln \Gamma - \gamma \ln(T - T_c)$ USING THE WEIGHTED DATA OF ISOTHERMAL COMPRESSIBILITY K_T ON THE CRITICAL ISOCHORE $\phi_c = 0.0564984$ FOR $T_c = 150.725^{\circ}K$

Least squares fit coefficients of the equation: $\Gamma = 0.6409$, $\gamma = 1.170 \pm 0.013$

Temperature (Deg.K)	$\ln(T - T_c)$		Error†	$K_T(atm^{-1})$* exp't	$\ln K_T$# exp't	$\ln K_T$ cal'd	$\Delta \ln K_T$**
163.004	2.508	±	0.0008	0.0343966	-3.37271	-3.37850	0.00579
160.003	2.228		0.0011	0.0477655	-3.04145	-3.05069	0.00924
156.998	1.836		0.0016	0.0738977	-2.60507	-2.59287	-0.01220
155.001	1.453		0.0023	0.1170841	-2.14486	-2.14458	-0.00028
153.923	1.163		0.0031	0.1642119	-1.80660	-1.80478	-0.00182
152.999	0.822		0.0044	0.2447089	-1.40769	-1.40592	-0.00177
152.018	0.257		0.0077	0.4725413	-0.74963	-0.74552	-0.00411
151.509	-0.243		0.0128	0.8576162	0.15360	0.16029	0.00669
151.203	-0.738		0.0209	1.5050593	0.40883	0.41850	-0.00967
151.002	-1.284		0.0361	2.9574693	1.08433	1.05669	0.02764
150.899	-1.749		0.0575	4.9522075	1.59983	1.60058	-0.00075
150.799	-2.604		0.1351	11.1342123	2.41002	2.60069	-0.19067
150.751	-3.650	±	0.3846	89.0415607	4.48910	3.82419	0.66491

† $\sigma_{\ln(T-T_c)} = \sigma_T/(T-T_c)$; $\sigma_T = \pm 0.010^{\circ}K$

*Computed at $\phi_c = 0.0564984$ along each isotherm

$\sigma_{\ln K_T} = \sigma_{K_T}/K_T$; $\sigma_{K_T} = \pm 0.05\ K_T$ (see p.40)

** $\ln K_T$ exp't - $\ln K_T$ cal'd

TABLE XI

COEFFICIENTS OF THE EQUATION $\ln K_T = \ln \Gamma - \gamma \ln(T - T_c)$ OBTAINED FROM THE LEAST SQUARES FITS OF THE WEIGHTED DATA OF ISOTHERMAL COMPRESSIBILITY ON THE CRITICAL ISOCHORE ϕ_c FOR VARIOUS ASSUMED VALUES OF T_c

T_c (°K)	ϕ_c †	Γ	γ	σ_{fit} *	σ_γ #
150.723	0.0564990	0.6442	1.1729	0.6431	0.01249
150.724	0.0564987	0.6425	1.1713	0.6148	0.01251
150.725	0.0564984	0.6409	1.1697	0.5894	0.01253
150.726	0.0564982	0.6393	1.1682	0.5672	0.01256
150.727	0.0564979	0.6377	1.1667	0.5483	0.01258
150.728	0.0564976	0.6361	1.1652	0.5331	0.01260
150.729	0.0564974	0.6345	1.1638	0.5217	0.01262
150.730	0.0564971	0.6330	1.1623	0.5142	0.01264
150.731	0.0564969	0.6315	1.1609	0.5106	0.01266
150.732	0.0564966	0.6300	1.1596	0.5108	0.01268
150.733	0.0564963	0.6286	1.1582	0.5144	0.01270
150.734	0.0564961	0.6271	1.1569	0.5214	0.01272

† Computed from the fitted line of Eq. (33) for each assumed value of T_c

* Standard deviation of the data from the fitted equation.

Standard error of the exponent γ

TABLE XII

VALUES OF P, D_m, n, AND ϕ ALONG THE LOCUS OF MAXIMUM ISOTHERMAL COMPRESSIBILITY AND COMPARISON OF THE NUMERICAL AND VISUAL ESTIMATED VALUES OF MAXIMUM ISOTHERMAL COMPRESSIBILITY

Temperature (Deg.K)	Pressure P (atm)	Angle D_m (minute of arc)	Refractive Index n	ϕ †	Maximum Compressibility $K_T(atm^{-1})$ Numerical*	Visual#	ΔK_T** %
163.004	65.417	188.668	1.06707_{68}	0.0441759	0.04262_{83}	0.0429	0.64
160.003	62.415	202.403	1.07192_{92}	0.0473264	0.05597_{56}	0.0576	2.90
156.998	58.459	214.977	1.07636_{76}	0.0502023	0.08601_{89}	0.0873	1.49
155.001	55.425	222.576	1.07904_{80}	0.0519364	0.12827_{95}	0.1312	2.28
153.923	53.543	222.768	1.07911_{59}	0.0519803	0.17552_{02}	0.1756	0.05
152.999	51.963	224.557	1.07974_{51}	0.0523881	0.26616_{64}	0.2612	-1.87
152.018	50.359	233.938	1.08305_{37}	0.0545241	0.50681_{21}	0.5038	-0.59
151.509	49.426	234.513	1.08325_{64}	0.0546549	0.91749_{05}	0.9235	0.66
151.203	48.867	234.296	1.08318_{00}	0.0546056	1.64911_{50}	1.666	1.02
151.002	48.494	233.278	1.08282_{11}	0.0543740	3.44018_{73}	2.980	-13.38
150.899	48.301	236.856	1.08408_{21}	0.0551877	5.55076_{57}	6.255	12.69
150.799	48.118	241.505	1.08571_{99}	0.0562440	11.16530_{05}	9.402	-15.79
150.751	48.004	240.528	1.08537_{56}	0.0560220	96.82052_{79}	--	--

† $\phi = (n^2-1)/(n^2+2)$

*Computed at the angle D_m from the spline fit of angle D versus pressure

#Estimated from large graph of compressibility K_T versus pressure along each isotherm

**$100(K_{T\ visual} - K_{T\ numerical}) / K_{T\ numerical}$

TABLE XIII

COEFFICIENTS OF THE EQUATION $\ln K_T = \ln \Gamma - \gamma \ln(T - T_c)$ OBTAINED FROM THE LEAST SQUARES FITS OF THE WEIGHTED DATA OF MAXIMUM ISOTHERMAL COMPRESSIBILITY

T_c	Γ	γ	$\sigma_{fit}^{\dagger}$	σ_{γ}^{*}
150.723	0.7099	1.1524	1.1427	0.01230
150.724	0.7080	1.1508	1.1172	0.01232
150.725	0.7062	1.1492	1.0925	0.01235
150.726	0.7044	1.1477	1.0706	0.01237
150.727	0.7027	1.1462	1.0502	0.01239
150.728	0.7009	1.1447	1.0319	0.01241
150.729	0.6992	1.1432	1.0154	0.01243
150.730	0.6975	1.1418	1.0009	0.01245
150.731	0.6958	1.1404	0.9884	0.01247
150.732	0.6942	1.1390	0.9779	0.01249
150.733	0.6925	1.1376	0.9692	0.01251
150.734	0.6909	1.1363	0.9624	0.01252
150.735	0.6893	1.1349	0.9573	0.01254
150.736	0.6878	1.1336	0.9537	0.01256
150.737	0.6862	1.1324	0.9517	0.01258
150.738	0.6847	1.1311	0.9510	0.01259
150.739	0.6832	1.1299	0.9514	0.01261
150.740	0.6818	1.1287	0.9528	0.01263

†Standard deviation of the data from the fitted equation

*Standard error of the exponent γ

TABLE XIV

REDUCED CHEMICAL POTENTIAL DIFFERENCE $\Delta\mu$ AND REDUCED DENSITY DIFFERENCE $\Delta\phi$ COMPUTED FROM THE REFRACTIVE INDEX DATA FOR $\phi_c = 0.0564984$ AND $P_c = 47.983$ atm

Pressure (atm)	Refractive Index n	ϕ †	$\Delta\phi$*	$\Delta\mu$#
163.004°K Isotherm				
40.078_8	1.02578_{93}	0.0171165	-0.69705	-1.288230
49.869_7	1.03653_{47}	0.0242012	-0.57165	-0.719462
60.120_3	1.05366_{58}	0.0354354	-0.37281	-0.303180
62.834_9	1.06005_{00}	0.0396023	-0.29905	-0.217776
65.998_0	1.06878_{07}	0.0452829	-0.19851	-0.129743
69.036_5	1.07818_{90}	0.0513809	-0.09058	-0.055574
71.870_1	1.08697_{54}	0.0570532	0.00982	0.005982
74.700_4	1.09480_{17}	0.0620870	0.09892	0.061897
77.861_3	1.10205_{82}	0.0667383	0.18124	0.119624
81.157_3	1.10811_{58}	0.0706091	0.24975	0.176094
84.922_6	1.11368_{30}	0.0741569	0.31255	0.237299
90.265_6	1.11983_{56}	0.0780668	0.38175	0.319883

† $\phi = (n^2-1) / (n^2+2)$

* $\Delta\phi = (\phi - \phi_c) / \phi_c$

\# $\Delta\phi = [\mu(\rho,T) - \mu(\rho_c,T)] / (P_c/\rho_c) = [\mu(\phi,T) - \mu(\phi_c T)] / (P_c/\phi_c)$

TABLE XIV (continued)

Pressure (atm)	Refractive Index n	ϕ †	$\Delta\phi$*	$\Delta\mu$#
160.003°K Isotherm				
42.093_6	1.02929_{50}	0.0194310	-0.65608	-0.917151
48.395_8	1.03730_{22}	0.0247061	-0.56271	-0.577911
51.360_4	1.04197_{98}	0.0277802	-0.50830	-0.444503
54.144_8	1.04730_{26}	0.0312715	-0.44651	-0.333133
57.345_2	1.05482_{77}	0.0361946	-0.35937	-0.220890
60.128_2	1.06329_{78}	0.0417179	-0.26161	-0.136382
63.072_5	1.07466_{06}	0.0490968	-0.13101	-0.059659
65.867_5	1.08663_{38}	0.0568331	0.00592	0.002572
68.890_0	1.09776_{88}	0.0639907	0.13261	0.061371
72.109_2	1.10638_{28}	0.0695028	0.23017	0.118066
75.303_8	1.11271_{23}	0.0735390	0.30161	0.170598
77.756_7	1.11650_{98}	0.0759547	0.34437	0.209222
156.998°K Isotherm				
44.123_8	1.03390_{44}	0.0224696	-0.60230	-0.574649
50.159_4	1.04448_{92}	0.0294270	-0.47915	-0.296667
53.133_2	1.05203_{93}	0.0343721	-0.39163	-0.186237
55.367_1	1.05985_{54}	0.0394755	-0.30130	-0.114612
56.687_1	1.06599_{93}	0.0434755	-0.23050	-0.077048
57.943_4	1.07303_{67}	0.0480445	-0.14963	-0.044643
58.865_4	1.07910_{60}	0.0519739	-0.08008	-0.022912
59.961_5	1.08638_{02}	0.0566696	0.00303	0.000854
60.944_3	1.09242_{76}	0.0605618	0.07192	0.020590
62.449_4	1.10001_{75}	0.0654318	0.15812	0.048684
64.012_1	1.10592_{66}	0.0692115	0.22502	0.075984
66.611_6	1.11297_{86}	0.0737085	0.30461	0.118754

TABLE XIV (continued)

Pressure (atm)	Refractive Index n	ϕ	$\Delta\phi$	$\Delta\mu$
155.001°K Isotherm				
48.627_{36}	1.04493_{49}	0.0297194	-0.47398	-0.230020
50.405_{08}	1.04990_{26}	0.0329741	-0.41637	-0.163039
52.088_{60}	1.05611_{06}	0.0370324	-0.34454	-0.106179
53.423_{83}	1.06283_{23}	0.0414149	-0.26697	-0.065933
54.344_{52}	1.06916_{09}	0.0455298	-0.19414	-0.040923
55.019_{36}	1.07501_{70}	0.0493277	-0.12692	-0.024140
55.648_{22}	1.08137_{50}	0.0534402	-0.05413	-0.009713
56.319_{40}	1.08831_{10}	0.0579134	0.02505	0.004483
57.113_{53}	1.09539_{59}	0.0624684	0.10567	0.020002
58.153_{23}	1.10232_{37}	0.0669081	0.18425	0.038897
59.790_{96}	1.10961_{69}	0.0715666	0.26670	0.066685
61.233_{12}	1.11408_{03}	0.0744097	0.31702	0.089934
153.923°K Isotherm				
44.350_{1}	1.03755_{80}	0.0248744	-0.55973	-0.343128
49.307_{1}	1.04983_{10}	0.0329273	-0.41720	-0.136918
50.210_{2}	1.05326_{18}	0.0351714	-0.37748	-0.105645
51.670_{3}	1.06072_{24}	0.0400405	-0.29130	-0.059654
52.585_{3}	1.06783_{37}	0.0446678	-0.20940	-0.034103
53.096_{8}	1.07324_{86}	0.0481818	-0.14720	-0.021104
53.624_{7}	1.08027_{32}	0.0527284	-0.06673	-0.008761
54.065_{1}	1.08660_{92}	0.0568172	0.00564	0.000712
54.502_{1}	1.09255_{07}	0.0606410	0.07332	0.009468
55.137_{9}	1.09918_{49}	0.0648984	0.14868	0.021377
56.105_{5}	1.10595_{47}	0.0692294	0.22533	0.038327
57.645_{8}	1.11271_{93}	0.0735434	0.30169	0.063686

TABLE XIV (continued)

Pressure (atm)	Refractive Index n	ϕ	$\Delta\phi$	$\Delta\mu$
152.999°K Isotherm				
49.329_{48}	1.05395_{80}	0.0356264	-0.36943	-0.081351
50.594_{72}	1.06166_{14}	0.0406523	-0.28047	-0.041941
51.450_{30}	1.07095_{61}	0.0466951	-0.17351	-0.018720
51.601_{05}	1.07304_{91}	0.0480525	-0.14949	-0.014971
52.015_{84}	1.08088_{04}	0.0531207	-0.05978	-0.005280
52.394_{26}	1.08901_{97}	0.0583697	0.03312	0.002722
52.708_{75}	1.09497_{15}	0.0621960	0.10085	0.008852
52.893_{38}	1.09745_{38}	0.0637887	0.12904	0.012302
53.477_{88}	1.10380_{32}	0.0678545	0.20100	0.022739
54.720_{85}	1.11134_{95}	0.0726710	0.28625	0.043497
56.755_{92}	1.11836_{75}	0.0771350	0.36526	0.075370
152.018°K Isotherm				
49.972_{01}	1.07100_{98}	0.0467299	-0.17290	-0.010639
50.126_{56}	1.07475_{23}	0.0491563	-0.12995	-0.006836
50.200_{86}	1.07705_{31}	0.0506459	-0.10359	-0.005083
50.304_{73}	1.08079_{86}	0.0530678	-0.06072	-0.002722
50.398_{95}	1.08476_{34}	0.0556272	-0.01542	-0.000680
50.498_{00}	1.08884_{86}	0.0582596	0.03117	0.001368
50.605_{85}	1.09294_{12}	0.0608919	0.07776	0.003499
50.707_{17}	1.09586_{71}	0.0627708	0.11102	0.005427
50.853_{97}	1.09901_{98}	0.0647926	0.14680	0.008135

TABLE XIV (continued)

Pressure (atm)	Refractive Index n	ϕ	$\Delta\phi$	$\Delta\mu$
151.509°K Isotherm				
49.145_{91}	1.07025_{74}	0.0462417	-0.18154	-0.007433
49.278_{67}	1.07469_{59}	0.0491197	-0.13060	-0.004147
49.372_{74}	1.07946_{22}	0.0522042	-0.07601	-0.001955
49.438_{61}	1.08426_{66}	0.0553068	-0.02109	-0.000510
49.495_{10}	1.08847_{19}	0.0580171	0.02688	0.000663
49.607_{79}	1.09491_{77}	0.0621615	0.10023	0.002866
49.738_{55}	1.09944_{84}	0.0650672	0.15166	0.005282
49.871_{32}	1.10249_{19}	0.0670157	0.18615	0.007648
151.203°K Isotherm				
48.631_{01}	1.06895_{03}	0.0453931	-0.19656	-0.006163
48.728_{59}	1.07250_{71}	0.0477011	-0.15571	-0.003691
48.823_{03}	1.07807_{97}	0.0513101	-0.09183	-0.001434
48.863_{57}	1.08268_{44}	0.0542858	-0.03916	-0.000528
48.895_{91}	1.08707_{40}	0.0571167	0.01094	0.000156
48.949_{46}	1.09273_{01}	0.0607563	0.07536	0.001224
49.002_{60}	1.09669_{85}	0.0633043	0.12046	0.002231
49.065_{23}	1.09953_{62}	0.0651235	0.15266	0.003379
151.002°K Isotherm				
48.339_{53}	1.06954_{74}	0.0457808	-0.18970	-0.003997
48.398_{10}	1.07213_{64}	0.0474607	-0.15996	-0.002516
48.435_{87}	1.07455_{65}	0.0490294	-0.13220	-0.001593
48.457_{81}	1.07663_{32}	0.0503742	-0.10840	-0.001073
48.478_{97}	1.07933_{77}	0.0521237	-0.07743	-0.000586
48.494_{27}	1.08286_{31}	0.0544011	-0.03712	-0.000247
48.511_{64}	1.08752_{12}	0.0574048	0.01604	0.000118
48.527_{69}	1.09079_{36}	0.0595112	0.05333	0.000441
48.546_{83}	1.09370_{09}	0.0613800	0.08640	0.000814
48.575_{95}	1.09650_{69}	0.0631814	0.11829	0.001364
48.614_{29}	1.09884_{69}	0.0646818	0.14484	0.002069

TABLE XIV (continued)

Pressure (atm)	Refractive Index n	ϕ	$\Delta\phi$	$\Delta\mu$
150.899°K Isotherm				
48.131_{30}	1.06799_{63}	0.0447734	-0.20753	-0.004295
48.208_{27}	1.07113_{98}	0.0468143	-0.17141	-0.002312
48.256_{32}	1.07464_{19}	0.0490847	-0.13122	-0.001129
48.302_{98}	1.08495_{40}	0.0557501	-0.01324	-0.000062
48.319_{28}	1.09110_{08}	0.0597088	0.05682	0.000270
48.396_{33}	1.09978_{36}	0.0652819	0.15547	0.001702
48.444_{78}	1.10190_{44}	0.0666398	0.17950	0.002567
150.799°K Isotherm				
47.987_{40}	1.06830_{33}	0.0449729	-0.20400	-0.003273
48.057_{14}	1.07179_{59}	0.0472399	-0.16387	-0.001487
48.112_{20}	1.08067_{16}	0.0529858	-0.06217	-0.000168
48.125_{73}	1.09180_{06}	0.0601588	0.06479	0.000116
48.178_{72}	1.09974_{67}	0.0652583	0.15505	0.001095
48.220_{35}	1.10185_{38}	0.0666075	0.17893	0.001838
150.751°K Isotherm				
47.890_{49}	1.06818_{50}	0.0448960	-0.20536	-0.002833
47.956_{60}	1.07158_{58}	0.0471036	-0.16628	-0.001162
47.999_{92}	1.07855_{86}	0.0516199	-0.08635	-0.000090
48.003_{70}	1.08342_{80}	0.0547657	-0.03067	-0.000005
48.004_{37}	1.08783_{53}	0.0576071	0.01962	0.000009
48.006_{88}	1.09257_{04}	0.0606536	0.07355	0.000059
48.066_{52}	1.10099_{41}	0.0660571	0.16919	0.001146
48.122_{56}	1.10333_{94}	0.0675579	0.19575	0.002133

TABLE XV

CRITICAL CONSTANTS AND EXPONENTS FOR ARGON

	T_c (Deg. K)	P_c (atm)	β	γ
Crommelin, et al[64,65]	150.72	47.996		
McCain and Ziegler[66]	150.65 ± 0.02	47.92 ± 0.05		
Grigor and Steele[42]	150.6 ± 0.1	48.0 ± 0.15	0.38 ± 0.02	1.22 ± 0.04
Teague and Pings[8]†	150.704 ± 0.015	48.18 ± 0.03	0.3643 ± 0.0066	
Sengers[40]	150.76 ± 0.02	48.13	0.362 ± 0.001	
Bale, et al[67]*	150.6 ± 0.05		0.35 ± 0.01	1.20 ± 0.05
This study†	150.725 ± 0.010	47.983	0.3574 ± 0.0027	1.170 ± 0.013

†Based on refractive index data

*X-ray scattering study

TABLE XVI

COMPARISON OF THE CRITICAL EXPONENT β FOR VARIOUS FLUIDS

Fluid	β	Reference
Argon	0.38 ± 0.02	Grigor and Steele[42]
	0.3643 ± 0.0066	Teague and Pings[8]
	0.362 ± 0.001	Sengers[40]
	0.35 ± 0.01†	Bale, et al[67]
	0.3574 ± 0.0027	This study
Krypton	0.355 ± 0.004	Gulari[68]
Xenon	0.350 ± 0.07*	Vicentini-Missoni et al[50]
He^4	0.355 ± 0.009*	Vicentini-Missoni et al[50]
CO_2	0.352 ± 0.008*	Vicentini-Missoni et al[50]
	0.3475 ± 0.0006	Sengers et al[36]
N_2O	0.3482 ± 0.0007	Sengers et al[36]
$CClF_3$	0.354 ± 0.007	Sengers et al[36]
Oxygen	0.353 ± 0.005	Weber[69]

†X-ray scattering study

*From the analysis using the scaled equation of state (Equation (23))

APPENDIX A

ALIGNMENT OF OPTICAL SYSTEM AND DETERMINATION OF APEX ANGLE OF CELL

The spectrometer was first properly adjusted[52] such that the optical axes of the viewing and the collimating telescopes, both focused for parallel light, were co-planar. This plane is called the optical plane of the spectrometer and is perpendicular to the axis of rotation of the spectrometer.

The cryostat, with its outer vacuum jacket and both shields removed, was mounted on the H-beam support (see Figure 1). A square-shaped bracket attached to the bottom of the inner vacuum jacket was used to hold the cell with the fluid inlet line to the cryostat.

Using a Gauss eyepiece on the viewing telescope, the faces of both windows of the cell were set to be perpendicular to the optical plane, as shown in the sketch of Figure A. A new small front-aluminized flat mirror was first held in position on one of the outside edges of the cell such that the face of the mirror was also perpendicular to the optical plane and approximately parallel to the bisector plane of cell windows (within 30'), and then sealed to the cell with G.E. varnish (No. 7031).

After the bracket was removed, the outer vacuum jacket and both shields were fixed to the cryostat. The cell, now seated on the cell support inside the inner shield, had to be adjusted in position so that the faces of both windows of the cell were perpendicular to the optical plane.

By adjusting the set of leveling screws on top of the H-beam support, the face of the small mirror on the cell was set to be perpendicular to the optical plane using the Gauss eyepiece. In this way the perpendicularity of the bisector plane of cell windows to the optical plane was obtained.

The telescopes were then lined up with the light beam passing through the evacuated cell. A horizontal reference mark was placed on the slit of the collimating telescope by observing the position of the horizontal cross hair through the viewing telescope. The cell was then pressurized with the sample gas such that a reasonably large angle of minimum deviation was observed. If the cell were tilted, the light passing through the cell would be refracted vertically from the optical plane and the image of the horizontal mark moved accordingly. Using the set of leveling screws on top of the H-beam support, the cell was rotated around an axis perpendicular to its bisector plane until the image of the horizontal mark coincided with the horizontal cross hair of the viewing telescope.

In this way the faces of both windows of the cell were set perpendicular to the optical plane and the cell was in proper position for measuring the angle of minimum deviation. For each experimental run the cell position was rechecked and the leveling screws adjusted, if necessary, to restore the cell to its proper position.

The apex angle of the cell can be determined indirectly by calibration with water, the refractive index of which is known[70]. The measurements were made by filling the triple distilled water

into the cell and measuring the angle of minimum deviation D along with temperature. The apex angle A of the cell can be calculated from the angle D and the known refractive index n of water using the formula:

$$n = \sin \tfrac{1}{2}(A+D) \,/\, \sin \tfrac{1}{2} A$$

or

$$A = 2 \cot^{-1}[(n - \cos \tfrac{1}{2} D) \,/\, \sin \tfrac{1}{2} D]$$

The experimental results are as follows:

	Run I	Run II
D	16° 2.69' ± 0.13'	16° 2.42' ± 0.13'
t	20.822°C ± 0.015°C	20.928°C ±0.015°C
$n_{water-air}$	1.3329136 ± 0.0000015	1.3329044 ± 0.0000015
n_{air}	1.0002718	1.0002717
n_{water}	1.3332759	1.3332660
A	44° 16.42' ± 0.31'	44° 15.86' ± 0.31'

The average value of the apex angle A is 44° 16.14' ± 0.31' , which included both the experimental errors in angle D and in temperature.

Before the cell was enclosed in the cryostat, the apex angle A was measured by the direct reflection method[52]. The viewing telescope with Gauss eyepiece was first set to face one window until the direct and reflected images of the cross hairs coincided; then the telescope was rotated to face the other window and the images were made to coincide again. The angle through which the telescope

was rotated is the supplement of the apex angle between the two windows of the cell. However, there were two distinct reflected images of the cross hairs observed from each window. The readings on the spectrometer were recorded when the telescope was at its sharpest focus. Coincidently, this also produced the smallest separation of the two images. The experimental results are as follows:

	Reflected Images	
	1 (left)	2 (right)
Window I	301° 34.80'	301° 33.19'
Window II	165° 52.84'	165° 51.04'
	135° 41.96'	135° 42.15'
Apex angle A	44° 18.04'	44° 17.85'

One possible explanation for the two images is that they are the separate reflections from the inner and outer faces of each window if the two faces are not exactly parallel to each other.

The refractive index of argon was determined by the angle of minimum deviation measured in the same way as that of water. Thus, the final value of apex angle A used to calculate the refractive index was the one determined by calibration with water, rather than the one determined by the direct reflection method.

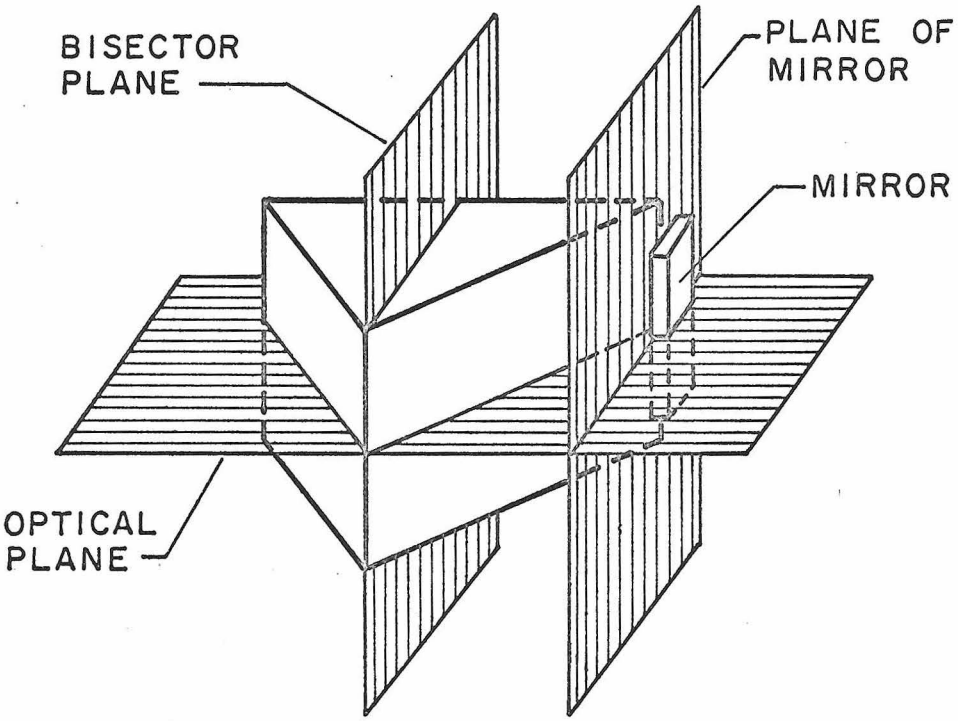

Figure A. Orientation of Prism Cell

APPENDIX B

ANGLE DETERMINATION ON THE SPECTROMETER

A Gaertner spectrometer model L114 was used for angle measurements. It had a graduated circle and vernier that gave readings accurate to 0.33'. For angles smaller than 5^{o}, a micrometer tangent screw accurate to 0.02' per degree was used. Since the maximum of the angle of minimum deviation to be measured in this study was larger than 5^{o} but the range of variation of the angle was smaller than 5^{o}, a special procedure described below was established to make use of the micrometer accuracy over this range.

With the cell evacuated, the viewing telescope was moved until the image of the slit was in the field of view. The micrometer was then clamped to the base of the spectrometer and used to move the telescope until the cross hairs on the telescope coincided with the left edge of the slit image. The reading on the micrometer was recorded as instrument zero V_o. Next, looking through a microscope mounted above the graduate circle and the vernier, a line on the vernier was marked and the micrometer was advanced approximately 2^{o} until the marked line was exactly opposite to a line on the graduated circle, which was also marked. This second reading on the micrometer was recorded as V_1. The micrometer was then backed to a reading near the beginning of the micrometer scale and unclamped from the base. The telescope was freely moved to set the two marked lines on the graduated circle and the vernier approximately opposite to each other. The micrometer was clamped again to move the

telescope until the two marked lines were exactly in line. This reading on the micrometer was recorded as V_2 .

After the cell was filled with the sample fluid and under temperature control, the refracted light image of slit was found and set near the cross hairs of the viewing telescope by advancing the micrometer. Since it was not feasible to rotate the prism cell seated inside the cryostat, the angle of incidence for the angle of minimum deviation was found by rotating the spectrometer with its telescopes fixed relative to each other. The viewing telescope was then moved until the cross hairs coincided with the left edge of the slit image and the reading on micrometer was recorded as V .

The angle of minimum deviation D for the refraction of the fluid in the cell is the sum of the two differences $(V - V_2)$ and $(V_1 - V_o)$.

From a large number of repeated observations, the uncertainties in the readings V_o, V_1 and V_2 on the spectrometer were found to be ±0.05, ±0.03 and ±0.03 minutes of arc, respectively. The uncertainty in determining the reading V depended on the state and stability of the sample system in the cell and was found in general to be ±0.06 minutes of arc, except when the temperature was within $0.1^{o}K$ of critical temperature and the stability of the sample system decreased. From the sum of the variances of four readings, the total uncertainty in determining angle D absolutely was estimated to be ±0.09 minutes of arc.

For each isotherm studied, several readings of V_o, V_1, and

V_2 were taken at the beginning and the averages of the readings were used throughout. Relative errors in the angles D determined on the isotherm could be estimated from the uncertainty in the readings of V alone.

APPENDIX C

CALIBRATION OF TEXAS INSTRUMENT PRESSURE GAUGE

A Texas Instrument model 141 precision pressure gauge monitored the pressure by a Bourdon tube. Attached to the free end of the tube was a mirror, the movement of which was followed by an optical transducer mounted on a gear concentric with the tube. The position of the transducer was converted to a digital readout which was then multiplied by a scale factor to determine the pressure.

For this study a metallic Bourdon tube with a maximum deflection of 100 degrees at 5000 psi was used in the gauge and calibrated using a Hart balance dead weight tester as a primary pressure standard. The schematic diagram of calibration was the same as the one shown in Figure 3 in Section II.C. For convenience, a separate gas line filled with nitrogen gas direct from a high pressure cylinder was employed in place of the sample gas line connected to the cell. The calibration procedure is much the same as the one described in Section II.C for the precise pressure measurement.

The experimental data for the calibration are listed in Table C. The pressure above the atmosphere, in the unit of psig, was calculated from the oil pressure with the addition of hydrostatic oil and gas heads. Since the chamber around the Bourdon tube used in the T.I. gauge was open to the atmosphere, at the beginning of each calibration test the zero readout was taken with the Bourdon tube vented to the atmosphere and then subtracted from the observed degree of deflection to indicate the pressure measured above the atmosphere

by the gauge. In Test No. 4 the calibration was performed after the Bourdon tube had been initially pressurized and vented three times as suggested by the manufacturer for better accuracy. Test No. 5 was done with the argon sample on the sample gas line connected to the cell. No systematic difference among the data of different tests could be noted.

A tube constant of 50.1 psi per degree of deflection was assumed and the residual pressures of the calibration data were calculated from the following equation

$$\Delta_{psig} = P - 50.1 \cdot \text{degree} \qquad \text{(C-1)}$$

In Figure C, the residual pressures vs. degree of deflection were plotted for all tests. In Tests No. 1, 2, and 4, the pressures were first increased and then decreased. In general the residual pressures for the same degree of deflection differed by 2 to 3 psi between the increasing and the decreasing pressures. This can be attributed to the hysteresis effect of the metallic Bourdon tube. To eliminate the hysteresis, the actual pressure measurements by the gauge were taken with increasing pressure only. As shown in Figure C, a smooth curve was drawn through those data points with increasing pressure. The average deviation of data points from the curve was estimated to be ±0.3 psi and this was used as the accuracy of the pressure measurements by the gauge.

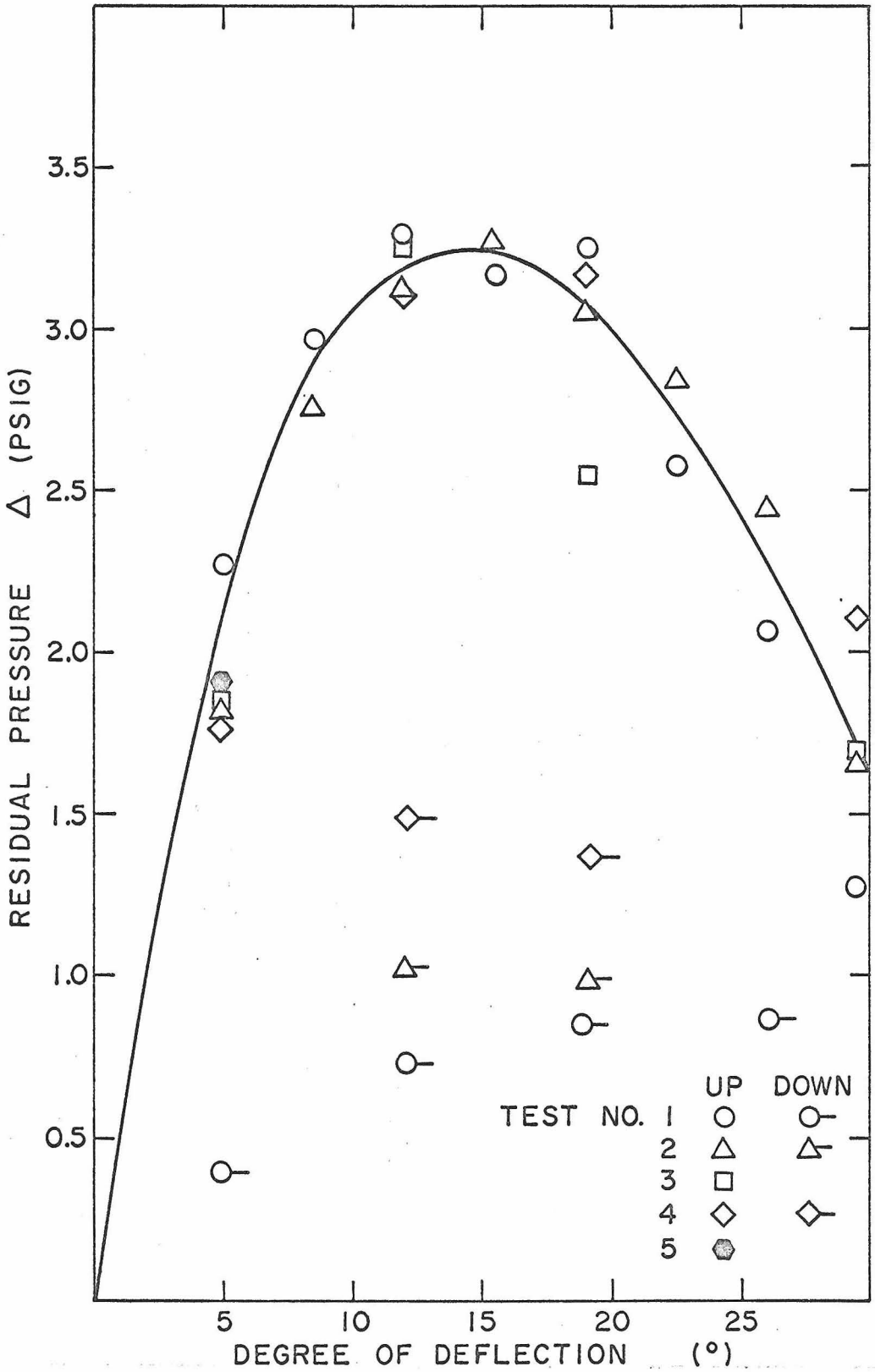

Figure C. Residual Pressure Δ (psig) versus Degree of Deflection of the Texas Instrument Pressure Gauge

TABLE C

CALIBRATION DATA OF TEXAS INSTRUMENT PRESSURE GAUGE

$$\Delta_{psig} = P - 50.1 \cdot degree$$

P(psig)	Degree*	psig
Test No. 1		
Up		
252.4191	4.993	2.2698
426.3606	8.451	2.9655
596.0218	11.831	3.2887
776.6552	15.439	3.1613
956.2415	19.022	3.2393
1126.6220	22.436	2.5784
1305.5131	26.017	2.0614
1481.5739	29.547	1.2692
Down		
1306.5763	26.062	0.8701
952.3487	18.992	0.8495
600.6270	11.974	0.7296
246.3883	4.910	0.3973
Test No. 2		
Up		
242.2000	4.798	1.8202
419.6964	8.322	2.7642
594.6672	11.807	3.1365
770.9083	15.322	3.2761
950.8493	18.918	3.0575
1125.8324	22.415	2.8409
1302.3870	28.947	2.4423
1482.2011	29.552	1.6459

P (psig)	Degree*	psig
Test No. 2		
Down		
954.7442	19.037	0.9905
600.1212	11.958	1.0254
Test No. 3		
Up		
242.2108	4.798	1.8310
596.0954	11.833	3.2621
948.8794	18.889	2.5405
1480.7971	29.523	1.6954
Test No. 4		
Up		
241.1507	4.778	1.7729
597.5139	11.864	3.1275
950.1562	18.902	3.1660
1482.3578	29.546	2.1032
Down		
958.0878	19.096	1.3782
599.9862	11.946	1.4916
Test No. 5		
243.1938	4.816	1.9122

*Observed degree of deflection on T.I. gauge minus the zero readout

APPENDIX D

AN ALGORITHM FOR CUBIC SPLINE FIT

The method of cubic spline fit[58] which is essentially the numerical analogue of the draftsman's spline, consists of joining the assigned points by sections of cubics, requiring that the slopes and curvatures be continuous at the junction points. The marked superiority of the quality of the derivatives over those obtained from polynomials of interpolation is a consequence of the relaxation of the overall requirement of analyticity.

For a set of data points $(x_1,y_1),(x_2,y_2),\cdots,(x_m,y_m)$ let $Z_1,Z_2,\cdots,Z_m$ be the values of the second derivative of the approximating function $F(x)$ at each point. Then assume the linear relationship of second derivative between the points (x_k,y_k) and (x_{k+1},y_{k+1})

$$F'' = \frac{x_{k+1} - x}{d_k} Z_k + \frac{x - x_k}{d_k} Z_{k+1} \qquad \text{(D-1)}$$

where $d_k = x_{k+1} - x_k$.

Integrating twice, we obtain a third degree polynomial as the equation of curve for this interval

$$F = \frac{Z_k}{6d_k}(x_{k+1} - x)^3 + \frac{Z_{k+1}}{6d_k}(x - x_k)^3 + a_1 x + a_2 \qquad \text{(D-2)}$$

The constants a_1 and a_2 of integration can be evaluated from the fact that the curve passes through the two end points (x_k,y_k) and (x_{k+1},y_{k+1}) . Then we have the equation of the curve:

$$F = C_{1,k}(x_{k+1} - x)^3 + C_{2,k}(x - x_k)^3 + C_{3,k}(x_{k+1} - x) + C_{4,k}(x - x_k) \tag{D-3}$$

where $C_{1,k} = Z_k/6d_k$, $C_{2,k} = Z_{k+1}/6d_k$, $C_{3,k} = \frac{y_k}{d_k} - \frac{Z_k d_k}{6}$, and $C_{4,k} = \frac{y_{k+1}}{d_k} - \frac{Z_{k+1} d_k}{6}$.

The only unknown quantities in Equation (D-3) are Z_k and Z_{k+1}, the values of the second derivatives at the end points of the interval. These values can be determined from the condition that the slope F' at the end point (x_k,y_k) as determined from Equation (D-3) must be the same as that determined by the corresponding equation for the interval of (x_{k-1},y_{k-1}) and (x_k,y_k), i.e., the first derivative must be continuous, $F'(x_k^+) = F'(x_k^-)$. Thus, we obtain

$$-\frac{Z_k d_k}{2} + \frac{y_{k+1} - y_k}{d_k} - \frac{d_k(Z_{k+1} - Z_k)}{6} = \frac{Z_k d_{k-1}}{2} + \frac{y_k - y_{k-1}}{d_{k-1}} - \frac{d_{k-1}(Z_k - Z_{k-1})}{6} \tag{D-4}$$

or, rearranging,

$$Z_{k-1}\frac{d_{k-1}}{6} + Z_k\frac{d_{k-1} + d_k}{3} + Z_{k+1}\frac{d_k}{6} = \frac{y_{k+1} - y_k}{d_k} - \frac{y_k - y_{k-1}}{d_{k-1}} \tag{D-5}$$

There are (m-2) equations like Equation (D-5) for $k=2,3,\cdots,m-1$. For the very end points of the data set, there are several reasonable choices for these values Z_1 and Z_m , and the particular choice for these values will influence the shape of fit, especially near the end points. One reasonable choice is to require the third derivative to be continuous at (x_2,y_2)

$$-\frac{Z_1}{d_1}+\frac{Z_2}{d_1}=F_2'''=-\frac{Z_2}{d_2}+\frac{Z_3}{d_2} \tag{D-6}$$

or

$$-\frac{Z_1}{d_1}+Z_2\left(\frac{1}{d_1}+\frac{1}{d_2}\right)-\frac{Z_3}{d_2}=0 \tag{D-7}$$

and also at (x_{m-1},y_{m-1})

$$-\frac{Z_{m-2}}{d_{m-2}}+Z_{m-1}\left(\frac{1}{d_{m-2}}+\frac{1}{d_{m-1}}\right)-\frac{Z_m}{d_{m-1}}=0 \tag{D-8}$$

Equations (D-7) and (D-8), along with Equations (D-5), constitute m equations in m unknowns for the quantities $Z_1,Z_2,\cdots,Z_m$ and can be written in the matrix form

$$RZ = b \tag{D-9}$$

where

$$R=\begin{bmatrix}
\frac{-1}{d_1} & \frac{1}{d_1}+\frac{1}{d_2} & \frac{-1}{d_2} & 0 & \cdots & 0 & 0\\
\frac{d_1}{6} & \frac{d_1+d_2}{3} & \frac{d_2}{6} & 0 & \cdots & 0 & 0\\
0 & \frac{d_2}{6} & \frac{d_2+d_3}{3} & \frac{d_3}{6} & \cdots & 0 & 0\\
\cdots & \cdots & \cdots & \cdots & \cdots & \cdots & \cdots\\
0 & 0 & \cdots & \cdots & \frac{d_{m-2}}{6} & \frac{d_{m-2}+d_{m-1}}{3} & \frac{d_{m-1}}{6}\\
0 & 0 & \cdots & \cdots & \frac{-1}{d_{m-2}} & \frac{1}{d_{m-2}}+\frac{1}{d_{m-1}} & \frac{-1}{d_{m-1}}
\end{bmatrix}$$

and

$$b = \begin{bmatrix} 0 \\ \frac{y_3-y_2}{d_2} - \frac{y_2-y_1}{d_1} \\ \vdots \\ \frac{y_m-y_{m-1}}{d_{m-1}} - \frac{y_{m-1}-y_{m-2}}{d_{m-2}} \\ 0 \end{bmatrix}$$

Making use of the special nature of the tridiagonal matrix R, the unknown Z_k can be found by the elimination method from Equation (D-9) and then the $C_{i,j}$ in Equation (D-3) can be determined.

For interpolation we must determine between which two points (x_k,y_k) and (x_{k+1},y_{k+1}) the given value of x lies, and then find F from Equation (D-3).

For the first derivative, differentiating Equation (D-3) we get

$$F' = -3C_{1,k}(x_{k+1} - x)^2 + 3C_{2,k}(x - x_k)^2 - C_{3,k} + C_{4,k} \qquad \text{(D-10)}$$

Integrating Equation (D-3), we can obtain the integral as follows:

$$\int F\,dx = -\frac{C_{1,k}}{4}(x_{k+1} - x)^4 + \frac{C_{2,k}}{4}(x - x_k)^4 - \frac{C_{3,k}}{2}(x_{k+1} - x)^2 + \frac{C_{4,k}}{2}(x - x_k)^2 \qquad \text{(D-11)}$$

It can be proved[71] that the fundamental property of the spline fit lies in its minimization of the integral-square measure of

approximation to the second derivative, i.e., minimizing the norm:

$$N = \int_{x_1}^{x_m} [y'' - F'']^2 \, dx \qquad \text{(D-12)}$$

PROPOSITION I

It is proposed that the concept of residual viscosity, the principle of corresponding states, and the concept of an acentric factor can be combined to produce a new correlation of relatively high accuracy for the viscosity of nonpolar dense gases.

1. Concept of Residual Viscosity

The residual viscosity is defined as the difference between the viscosity at a given pressure and temperature, and the dilute gas viscosity at the same temperature. In general, dense gas theories[1,2] predict that a relationship exists between the residual viscosity and the density of a gas. Experimental studies[3-12] have also shown that the residual viscosity is a function of density for a number of gases. This can be expressed as follows:

$$\eta - \eta_o = \phi(\rho) \qquad (1)$$

where η is the viscosity, η_o is dilute gas viscosity at the same temperature as η, and ρ is the density of the gas. However, the function $\phi(\rho)$ was found to vary from gas to gas.

2. Principle of Corresponding States for Viscosity

The principle of corresponding states has formed the basis of many semi-empirical correlations[13-15] for the dense gas viscosity, in which the reduced viscosity is related to the reduced temperature and pressure or density. All of these have used the critical constants as the reducing parameters. The viscosity has been reduced with respect to either the critical or the atmospheric viscosity. None of these correlations has proved to be entirely satisfactory. The deviations of predicted viscosities from experimental values may range from about 2% to 10%.

Using a dimensional analysis approach and the concept of residual viscosity, Thodos and co-workers[16,17] have developed a viscosity correlation for nonpolar gases, which was later modified by Dean and Stiel[18] on the basis of more recent viscosity data and was expressed in the following generalized relationship:

$$(\eta - \eta_o)\xi = 10.8 \times 10^{5} \left(e^{1.439\,\rho_r} - e^{-1.11\,\rho_r^{1.858}}\right) \qquad (2)$$

where $\xi = T_c^{1/6} / M^{1/2} P_c^{2/3}$ and $\rho_r = \rho/\rho_c$. Viscosities calculated with Equation (2) showed an average deviation of about 1% to 3% from the experimental values of argon, neon, and nitrogen[19], and of the light hydrocarbons[6,20,21].

Helfand and Rice[22] have provided a statistical mechanical proof of the principle of corresponding states for viscosity. It is required that the intermolecular potential be of the form

$u = \varepsilon u^*(r/\sigma)$, where ε and σ are characteristic energy and distance constants, u^* is a universal function of the one variable r/σ, and r is the distance between the molecules. They found that the reduced viscosity is a universal function of reduced temperature and pressure:

$$\eta_R = \eta^*(T_R, P_R) \tag{3}$$

where $\eta_R = \eta/(\sigma^{-2}\sqrt{m\varepsilon})$, $T_R = kT/\varepsilon$, $P_R = P\sigma^3/\varepsilon$, m is the mass of a molecule, and k is Boltzmann's constant. In applying Equation (3) to the viscosity of noble gases, Trappeniers et al[23] have replaced the reduced pressure P_R by the reduced density $\rho_R (= \sigma^3\rho/m)$ and obtained an empirical equation for the ratio $\eta_R/(\eta_o)_R$ in the form of a series expansion in T_R and ρ_R. This equation fits the viscosity data to within 3 to 5% over a wide range of temperatures and densities.

3. Concept of Acentric Factor

In applying the principle of corresponding states to the equation of state of real gases, Pitzer[24] suggested that the compressibility factor of a nonpolar gas with non-spherical molecules may be expressed as a function of one more parameter in addition to the reduced pressure and reduced temperature. The additional parameter is required because the intermolecular forces in less simple molecules are the sum of interactions between various parts of the molecules--not just their centers. Therefore, the compressibility factor is expressed[25] generally as a function of three variables:

$$\frac{PV}{RT} = Z(T_r, P_r, \omega_Z) \tag{4}$$

where $T_r = T/T_c$, $P_r = P/P_c$, and the additional variable ω_Z is the acentric factor. The compressibility factor can be expanded in a power series in the acentric factor:

$$Z(T_r, P_r, \omega_Z) = Z^{(0)}(T_r, P_r) + \omega_Z Z^{(1)}(T_r, P_r) + \cdots \tag{5}$$

It was found that over a wide range of temperatures and pressures, the first two terms were sufficient.

4. New Correlation of Dense Gas Viscosity

The concept of residual viscosity and the principle of corresponding states can be combined to form the following functional relationship:

$$(\eta - \eta_o)_R = F(\rho_R) \tag{6}$$

where $(\eta - \eta_o)_R = (\eta - \eta_o)/(\sigma^{-2}\sqrt{m\varepsilon})$ and $\rho_R = \sigma^3\rho/m$. In the plot of $(\eta - \eta_o)_R$ versus ρ_R , the separation of curves for different gases having nonspherical molecules is to be expected. By following the same technique used by Pitzer[24] for the compressibility factor, it is possible to reduce these separated curves to a single curve by introducing a third molecular parameter for each gas. The reduced residual viscosity can then be expressed as a function of reduced density and this third parameter, the acentric factor:

$$(\eta - \eta_o)_R = f(\rho_R, \omega_\eta) \tag{7}$$

$f(\rho_R,\omega_\eta)$ can be expanded into the following form, analogous to Equation (5)

$$f(\rho_R\ \omega_\eta) = f^{(0)}(\rho_R) + \omega_\eta\ f^{(1)}(\rho_R) \tag{8}$$

where $f^{(0)}(\rho_R)$ is the reduced residual viscosity for simple gases with spherical molecules and $f^{(1)}(\rho_R)$ is a viscosity correction function for gases with nonspherical molecules.

5. Experimental Data Used for the New Correlation

As discussed by Pitzer[24], the application of Equation (4), and consequently Equation (7), is limited to those gases which have no quantum effects. To test Equation (8), therefore, argon and nitrogen were selected to represent a simple gas and a diatomic linear molecule gas, respectively. To represent common nonpolar gases with nonspherical molecules, the light normal paraffin hydrocarbons were chosen for their systematic change in molecular structure.

Measurements of the viscosity of dense gases have been made by many investigators. To test the new correlation, it is advantageous to use a set of viscosity data which has been obtained from one instrument over a wide range of temperature and pressure.

The viscosity data used in this study were those of Flynn *et al*[19] for argon and nitrogen, and of Sage and co-workers[10-12] for methane, propane and n-butane. Auxiliary volumetric data were those of Sage and Lacey[26] and of Michels *et al*[27-31] as used by Flynn *et al*[19]. In Figure 1, a plot of residual viscosity versus density has been made from these data.

To calculate the reduced density and the reduced residual viscosity, the molecular force constants σ and ε/k based on the Lennard-Jones (6-12) intermolecular potential were used. Table I gives the values of σ and ε/k for argon, nitrogen, methane, ethane, propane, and n-butane, as reported by different investigators [2,32,33]. Different plots of reduced residual viscosity versus

reduced density have been prepared using the force constants of Hirschfelder et al[2], shown in Figure 2, and those of Milligan and Liley[32], shown in Figure 3. The curves of different gases are not systematically separated from each other. However, it should be noted that there is some doubt about the range and accuracy of the dilute viscosity data from which these force constants have been calculated. More recently, Galloway and Sage[33] recalculated these constants for the hydrocarbon series from methane to n-decane based on a wide range of experimental viscosity data of various sources. Using these new force constants for light hydrocarbons and those for argon and nitrogen in Reference (2), a new plot of reduced residual viscosity versus reduced density has been made and is shown in Figure 4. There is a systematic separation between the argon curve and other curves, which is found to be proportional to the value of reduced density. This suggested that the experimental viscosity data of these gases could be represented by the functional form of Equation (7).

6. Results

Equation (8) can be rearranged to evaluate $f^{(1)}$ from the experimental viscosity data:

$$\frac{f - f^{(0)}}{\omega_\eta} = f^{(1)}(\rho_R) \tag{9}$$

A plot of $\frac{f - f^{(0)}}{\omega_\eta}$ versus ρ_R should yield a single smooth curve for all gases studied. Taking the argon curve in Figure 4 as $f^{(0)}$, the actual plot using the acentric factor determined from the compressibility factor correlation by Pitzer *et al*[25] yields a family of curves as shown in Figure 5. This is to be expected, since the values of force constants σ and ε/k derived from PVT data differ from those based on dilute gas viscosity data[2]. Therefore, a new set of acentric factors for viscosity was chosen to adjust the $f^{(1)}$ versus ρ_R into a single reasonably smoothed curve which is plotted in Figure 6. The acentric factors for viscosity obtained from this study and those for compressibility factor by Pitzer *et al*[25] are tabulated and compared in Table II. The force constants used in the final correlation are also tabulated in Table II.

The final values of the functions $f^{(0)}$ and $f^{(1)}$ in Equation (8) were determined from the argon curve in Figure 4 and the smoothed curve in Figure 6, respectively. Large graphs were used to interpolate the values of $f^{(0)}$ and $f^{(1)}$, which are presented in Table III for the range of reduced density from 0.0 to 0.45.

7. Prediction of Dense Gas Viscosity Based on the New Correlation

To use Table III with Equation (8) for the prediction of dense gas viscosity, we must have the force constants of the gas and its dilute gas viscosity available. A single value of dense gas viscosity at a high pressure is also required in order to determine the acentric factor of the gas.

We take as an example the prediction of the dense gas viscosity of ethane which was not used in the correlation. The force constant data used are those of Galloway and Sage[33]. The atmospheric gas viscosity result of Carmichael and Sage[9] was used for the dilute gas viscosity, since the difference between the two is known to be less than a few tenths of 1%. The volumetric data used are those of Sage and Lacey[26]. To obtain the acentric factor for ethane, the viscosity at 2000 psia and 220°F was arbitrarily selected from the viscosity data of Carmichael and Sage[9]. The acentric factor fitted at this point, by using the values of $f^{(0)}$ and $f^{(1)}$ interpolated from Table III with Equation (8), is 0.083. Using this value, the viscosities at other pressures were calculated from Equation (8). The calculated and the experimental viscosities reported by Carmichael and Sage[9] are compared in Table IV and have an average deviation of 0.73%.

To further illustrate the generality of new correlation, the same comparison was made for the viscosity of carbon dioxide, as shown in Table V. The experimental viscosity data used for comparison were those of Michels *et al*[34]. The acentric factor was found to be 0.199 which was calculated from the experimental viscosity values at 107.2

atm and 50°C. For most data at other pressures the calculated values of viscosity are within ±1% of the experimental data.

8. Conclusion

From theoretical considerations, the correlation developed in this study is sounder than the one obtained by Thodos and co-workers, Equation (2). It should be noted that in the latter the molecular shape effects have been implicitly accounted for, as the critical constants were used as reducing parameters. This can be seen in the correlation of second virial coefficients through potential function parameters, recently developed by Kunz and Kapner[35]. They have obtained several empirical relationships between ε/k and T_c for different gases, depending on molecular structure. The correlation developed in this study treats the shape effect separately and yet at very little expense in terms of complexity. It can serve as a convenient and accurate method for predicting the dense gas viscosity of nonpolar gases.

NOMENCLATURE

$f^{(0)}$ - reduced residual viscosity for simple gases with spherical molecules

$f^{(1)}$ - viscosity correction function for gases with nonspherical molecules

k - Boltzmann's constant

m - mass of molecule

M - molecular weight

P - pressure

P_c - critical pressure

P_r - reduced pressure, P/P_c

P_R - reduced pressure, $P\sigma^3/\varepsilon$

r - distance between molecules

T - temperature

T_c - critical temperature

T_r - reduced temperature, T/T_c

T_R - reduced temperature, kT/ε

u - intermolecular potential function

Z - compressibility factor, PV/RT

$Z^{(0)}$ - compressibility factor function in Equation (5)

$Z^{(1)}$ - compressibility factor function in Equation (5)

Greek Letters

ε - depth of the intermolecular potential minimum

η - dense gas viscosity

η_o - dilute gas viscosity

η_R - reduced dense gas viscosity, $\eta/(\sigma^{-2}\sqrt{m\varepsilon})$

$(\eta_o)_R$ - reduced dilute gas viscosity, $\eta_o/(\sigma^{-2}\sqrt{m\varepsilon})$

ξ - reducing parameter for viscosity, $T_c^{1/6} / M^{1/2} P_c^{2/3}$

ρ - density

ρ_c - critical density

ρ_r - reduced density, ρ/ρ_c

ρ_R - reduced density $\sigma^3\rho/m$

σ - collision diameter of molecule

ω_z - acentric factor for compressibility factor

ω_η - acentric factor for viscosity

REFERENCES

1. S. Chapman and T. G. Cowling, The Mathematical Theory of Non-Uniform Gases (Cambridge University Press, Cambridge, England, 1964)

2. J. O. Hirschfelder, C. F. Curtiss, and R. B. Birds, Molecular Theory of Gases and Liquids (John Wiley & Sons, Inc., New York, 1954)

3. W. J. Brebach and G. Thodos, Ind. Eng. Chem. 50, 1095 (1958)

4. H. Shimotake and G. Thodos, A.I.Ch.E.J. 4, 257 (1958)

5. J. T. Kennedy and G. Thodos, A.I.Ch.E.J. 7, 625 (1961)

6. K. E. Starling, B. E. Eakin, and R. T. Ellington, A.I.Ch.E.J. 6, 438 (1960)

7. J. P. Dolan, K. E. Starling, A. L. Lee, B. E. Eakin, and R. T. Ellington, J. Chem. Eng. Data 8, 396 (1963)

8. A. L. Lee and R. T. Ellington, J. Chem. Eng. Data 10, 101 (1965)

9. L. T. Carmichael and B. H. Sage, J. Chem. Eng. Data 8, 94 (1963)

10. L. T. Carmichael and B. H. Sage, J. Chem. Eng. Data 8, 612 (1963)

11. L. T. Carmichael, V. Berry, and B. H. Sage, J. Chem. Eng. Data 9, 411 (1964)

12. L. T. Carmichael, V. Berry, and B. H. Sage, J. Chem. Eng. Data 10, 57 (1965)

13. O. A. Uyehara and K. M. Watson, Natl. Petrol. News 36, R764 (1944)

14. L. Grunberg and A. H. Nissan, Ind. Eng. Chem. 42, 885 (1950)

15. N. L. Carr, J. D. Parent, and R. E. Peck, Chem. Eng. Prog. Symposium Ser. 51, 91 (1955)

16. L. I. Stiel and G. Thodos, Progress in International Research on Thermodynamic and Transport Properties (Am. Soc. Mech. Engrs., New York, 1962), pp. 352-365

17. J. A. Jossi, L. I. Stiel, and G. Thodos, A.I.Ch.E.J. 8, 59 (1962)

18. D. E. Dean and L. I. Stiel, A.I.Ch.E.J. 11, 526 (1965)

19. G. P. Flynn, R. V. Hanks, N. A. Lemaire, and J. Ross, J. Chem. Phys. 38, 154 (1963)

20. B. E. Eakin, K. E. Starling, J. P. Dolan, and R. T. Ellington, J. Chem. Eng. Data 7, 33 (1962)

21. J. P. Dolan, M.S. Thesis, Illinois Inst. of Technology, Chicago, Illinois (1962)

22. E. Helfand and S. A. Rice, J. Chem. Phys. 32, 1642 (1960)

23. N. J. Trappeniers, A. Botzen, C. A. Ten Seldam, H. R. Van Den Berg, and J. Van Oosten, Physica 31, 1681 (1965)

24. K. S. Pitzer, J. Amer. Chem. Soc. 77, 3427 (1955)

25. K. S. Pitzer, D. Z. Lippmann, R. F. Curl, C. M. Huggins, and D. E. Petersen, J. Amer. Chem. Soc. 77, 3433 (1955)

26. B. H. Sage and W. N. Lacey, Thermodynamic Properties of the Light Paraffin Hydrocarbons and Nitrogen, API Research Project 37 (Amer. Petrol. Inst., New York, 1950)

27. A.Michels, H. Wouters, and J. de Boer, Physica 1, 587 (1934)

28. J. Otto, A. Michels, and H. Wouters, Physik. Z. 35, 97 (1934)

29. A. Michel, R. J. Lunbeck, and G. J. Wolkers, Physica 17, 801 (1951)

30. A Michels, Hub. Wijker, and Hk. Wijker, Physica 15, 627 (1949)

31. A. Michels, J. M. Levelt, and W. de Graaff, Physica 24, 659 (1958)

32. J. H. Milligan and P. E. Liley, ASME Preprint, 1964 (64-UT-20)

33. T. R. Galloway and B. H. Sage, Chem. Eng. Sci. 22, 979 (1967)

34. A. Michels, A. Botzen, and W. Schuurman, Physica 23, 95 (1957)

35. R. G. Kunz and R. S. Kapner, A.I.Ch.E.J. 17, 562 (1971)

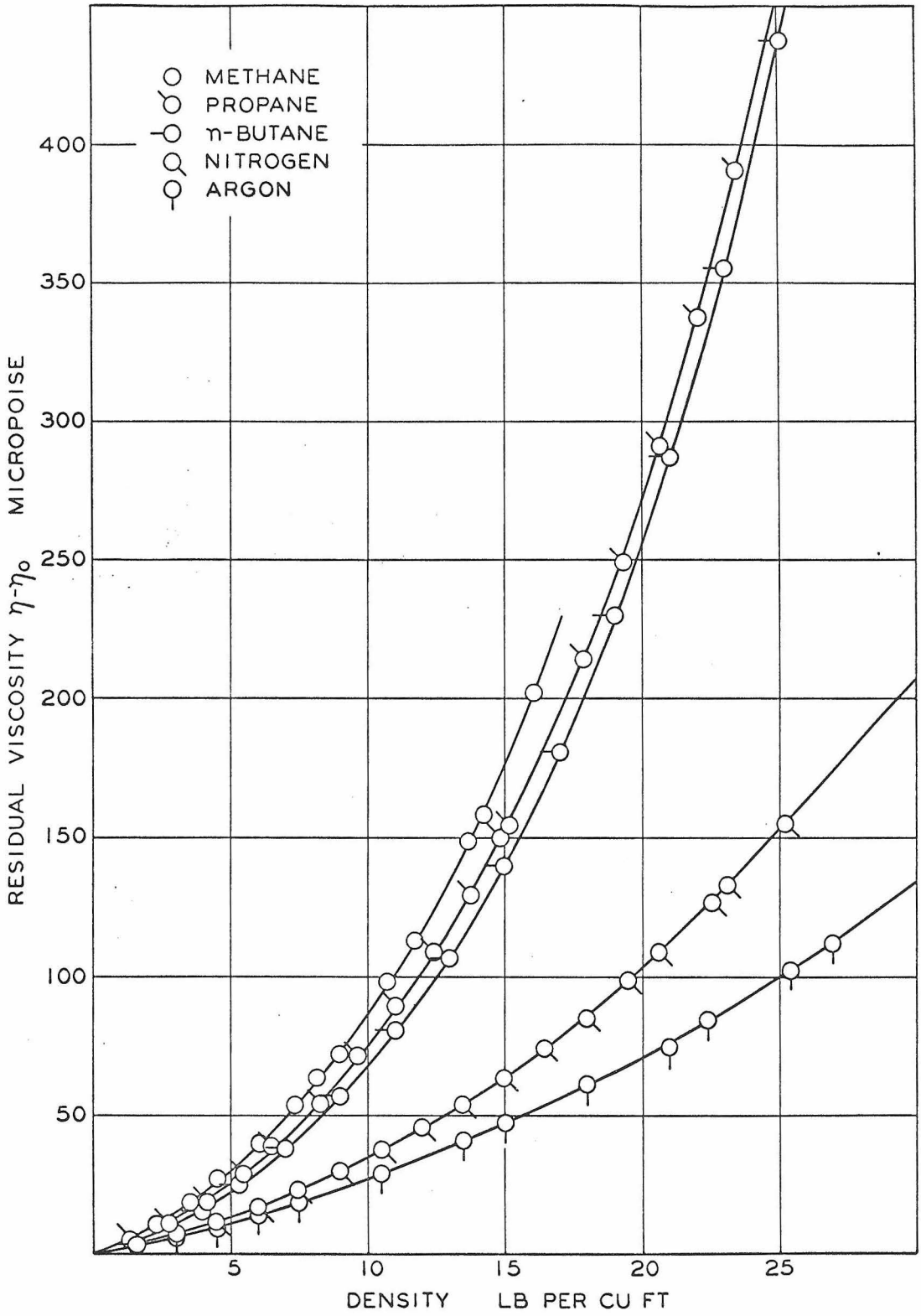

Figure 1. Residual Viscosity versus Density Plot

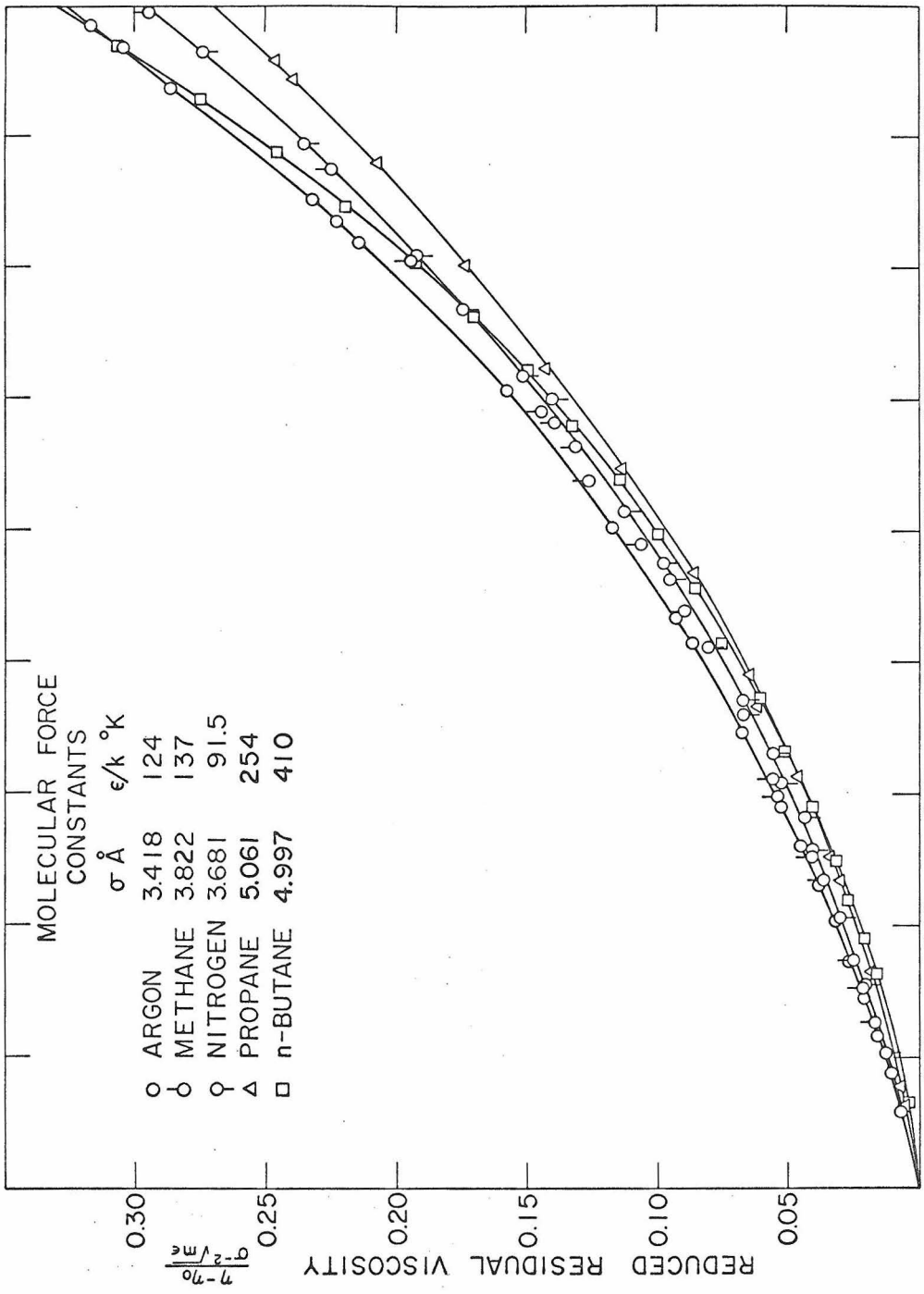

Figure 2. Reduced Residual Viscosity versus Reduced Density Plot Based on Force Constants by Hirschfelder et al(2)

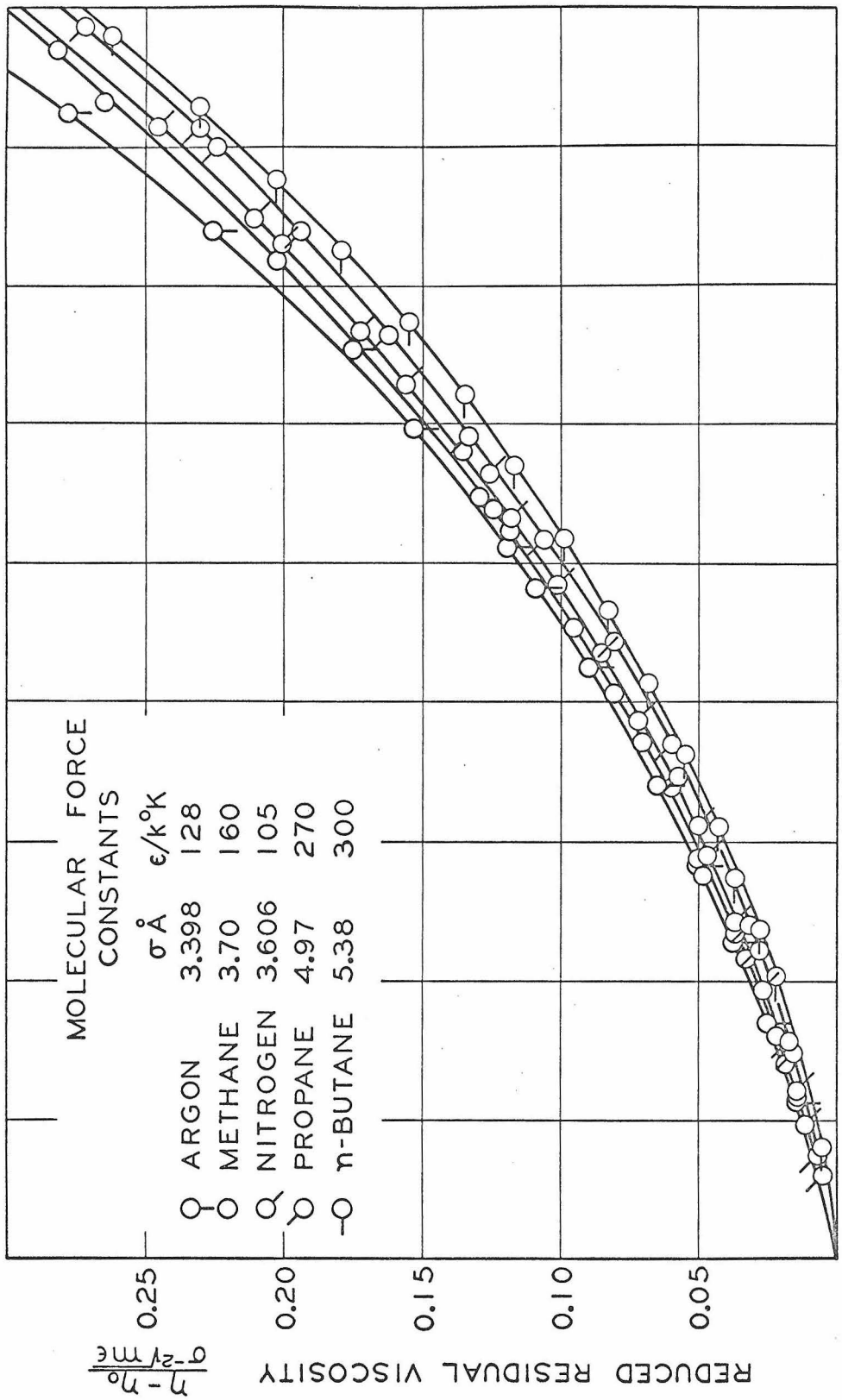

Figure 3. Reduced Residual Viscosity versus Reduced Density Plot Based on Force Constants by Milligan and Liley (32)

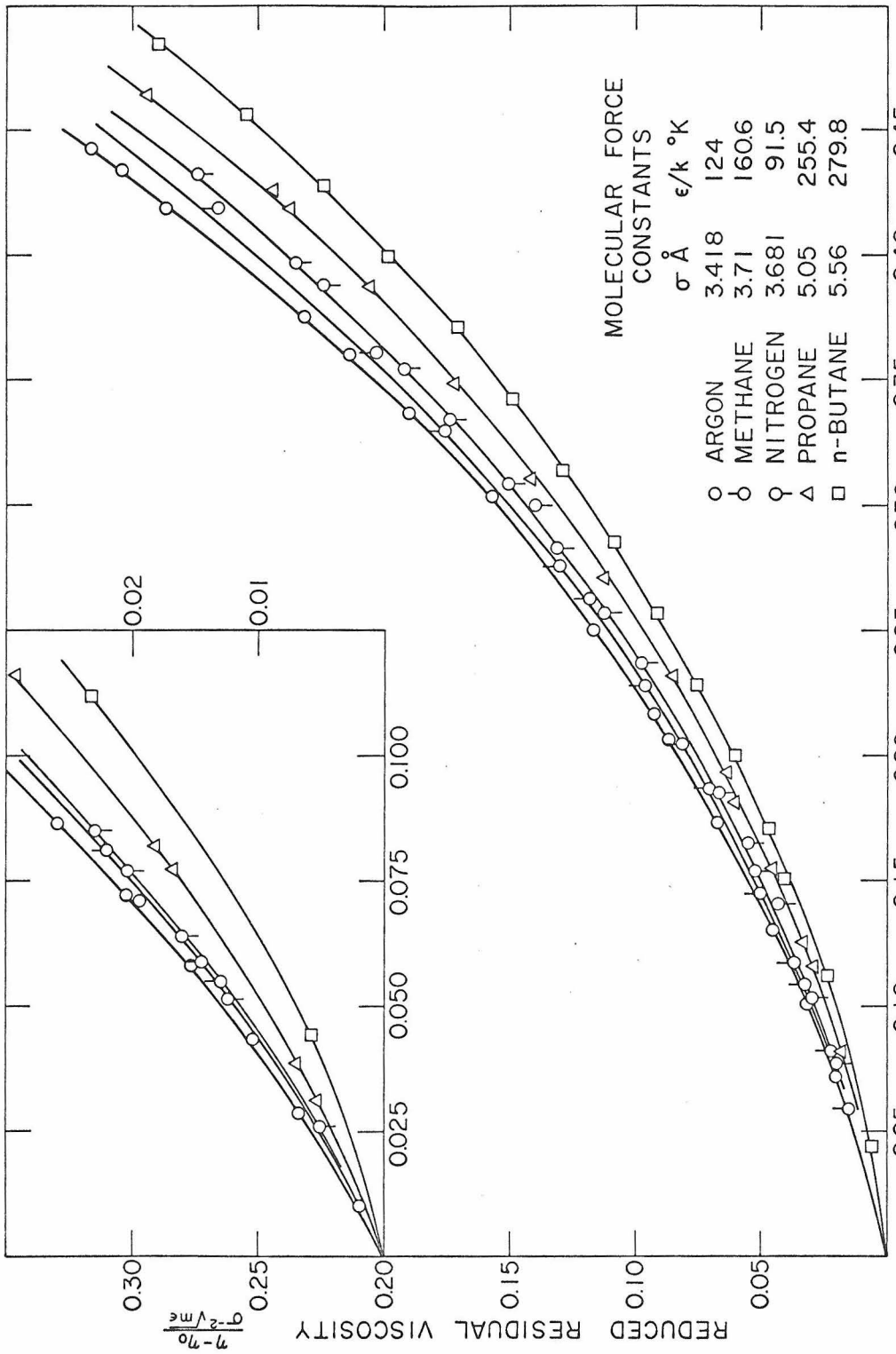

Figure 4. Reduced Residual Viscosity versus Reduced Density Plot Based on Force Constants by Galloway and Sage(33)

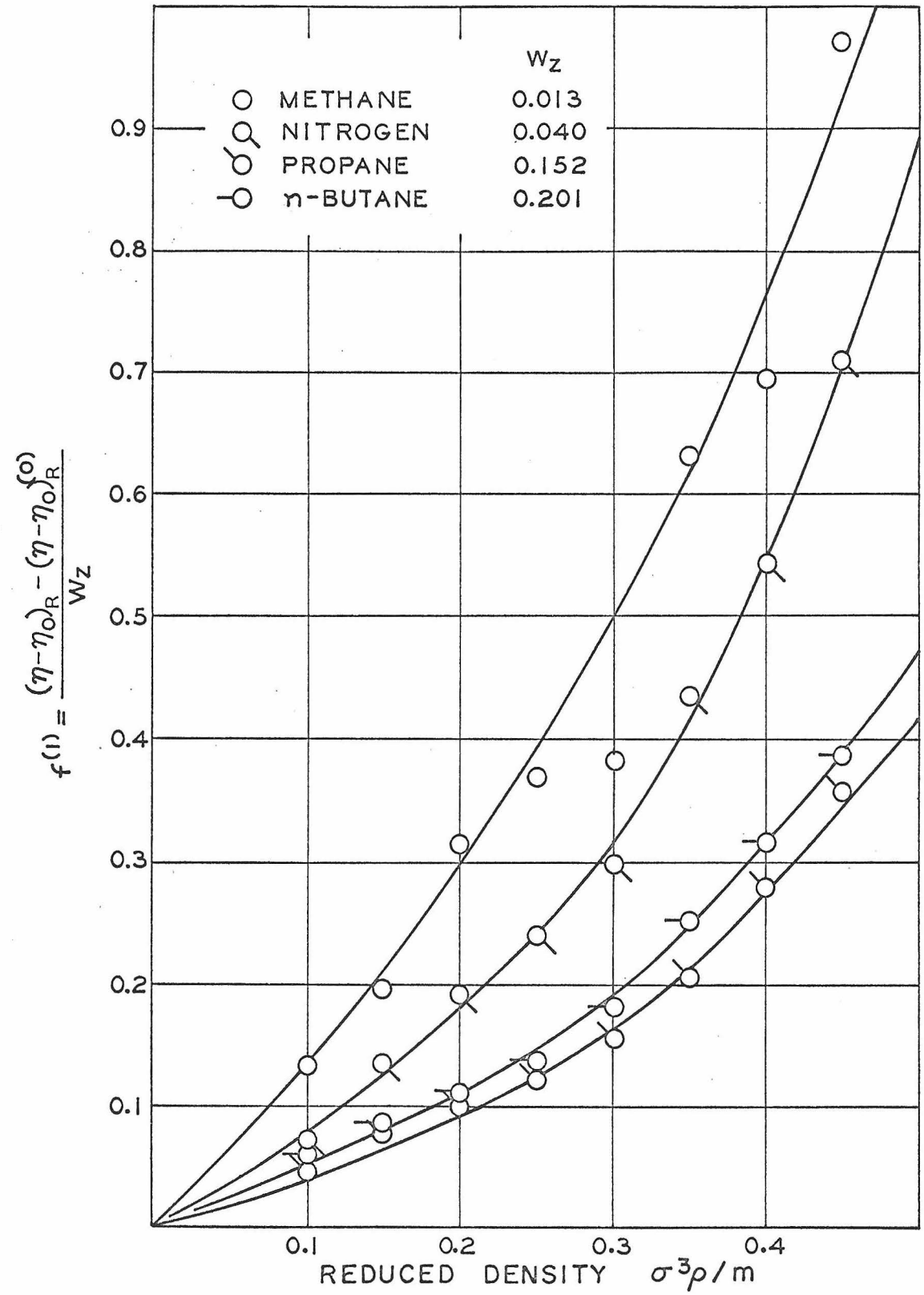

Figure 5. Functions $f^{(1)}$ versus Reduced Density Plot Based on Acentric Factors Obtained from Compressibility Factor Correlation[25]

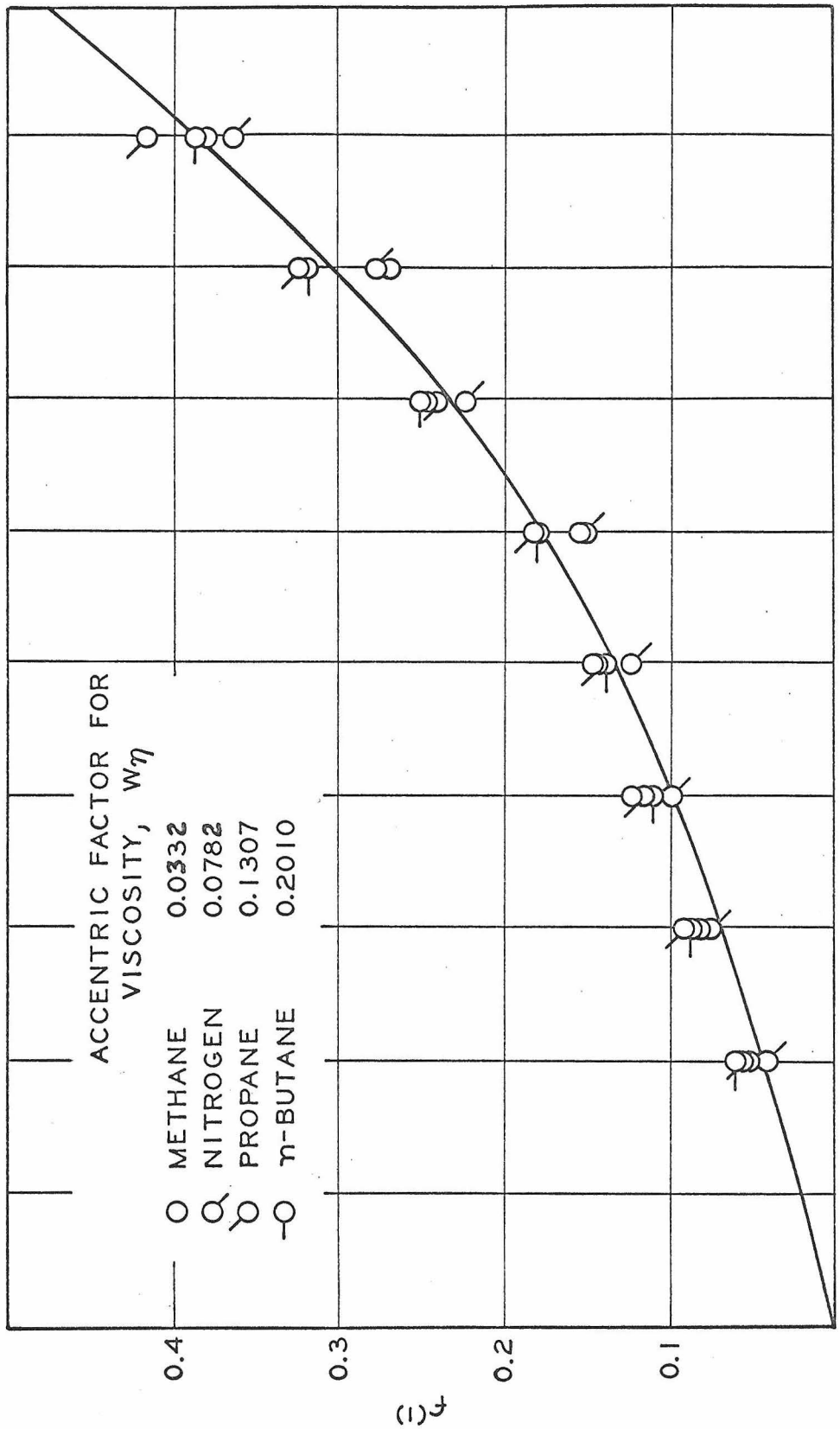

Figure 6. Viscosity Correction Function $f^{(1)}$ versus Reduced Density Plot

TABLE I

COMPARISON OF FORCE CONSTANTS FOR LENNARD-JONES (6-12) POTENTIAL

	σ(Å)			ε/k(°K)		
	Hirschfelder et al[2]	Milligan and Liley[32]	Galloway and Sage[33]	Hirschfelder et al[2]	Milligan and Liley[32]	Galloway and Sage[33]
Argon	3.418	3.398		124	128	
Nitrogen	3.681	3.606		91.5	105	
Methane	3.822	3.70	3.71	137	160	160.6
Ethane	4.418	4.45	4.45	230	220	212.6
Propane	5.061	4.97	5.05	254	270	255.4
n-Butane	4.997	5.38	5.56	410	300	279.8

TABLE II

COMPARISON OF ACENTRIC FACTORS FOR VISCOSITY

AND FOR COMPRESSIBILITY FACTOR

	σ(Å)	ε/k(°K)	ω_η*	$\omega_Z^{(25)}$
Argon	3.418	124	0.0	-0.002
Nitrogen	3.681	91.5	0.0782	0.040
Methane	3.71	160.6	0.0332	0.013
Propane	5.05	255.4	0.1307	0.152
n-Butane	5.56	279.8	0.2010	0.201
Ethane	4.45	212.6	0.083	0.105
Carbon Dioxide	4.0	190	0.199	0.225

*Determined in this study.

TABLE III

VALUES OF $f^{(0)}$ AND $f^{(1)}$

Reduced Density $\frac{\sigma^3 \rho}{m}$	Viscosity Function	
	$f^{(0)}$	$f^{(1)}$
0.01	0.0021	0.004
0.02	0.0045	0.008
0.03	0.0070	0.012
0.04	0.0098	0.017
0.05	0.0127	0.021
0.06	0.0160	0.026
0.07	0.0196	0.031
0.08	0.0234	0.036
0.09	0.0272	0.041
0.10	0.0310	0.046
0.12	0.0399	0.057
0.14	0.0497	0.068
0.16	0.0601	0.079
0.18	0.0712	0.092
0.20	0.0830	0.104
0.22	0.0954	0.118
0.24	0.1088	0.133
0.26	0.1230	0.149
0.28	0.1384	0.166
0.30	0.1550	0.185
0.32	0.1733	0.206
0.34	0.1933	0.229
0.36	0.2150	0.253
0.38	0.2375	0.280
0.40	0.2615	0.309
0.45	0.2760	0.387

TABLE IV

COMPARISON OF THE CALCULATED AND THE EXPERIMENTAL VISCOSITIES OF ETHANE AT 220°F

Pressure (psia)	Volume (ft^3/mole)	Reduced Density $\sigma^3\rho/m$*	$f^{(0)}$†	$f^{(1)}$†	Reduced Residual Viscosity $\frac{\eta-\eta_o}{\sigma^{-2}\sqrt{m\varepsilon}}$*	Residual Viscosity (micropoise)	Viscosity** (micropoise) Cal'd	Viscosity** (micropoise) Exp't[9]
200	34.70	0.0245	0.0050	0.0100	0.0042	2.58	119.07	118.64
400	16.41	0.0518	0.0133	0.0221	0.0115	7.01	123.50	123.05
600	10.30	0.0825	0.0243	0.0368	0.0213	13.02	129.51	128.03
800	7.24	0.1174	0.0386	0.0552	0.0340	20.79	137.28	136.93
1000	5.39	0.1577	0.0588	0.0784	0.0524	32.00	148.49	149.29
1500	3.04	0.2797	0.1384	0.1660	0.1247	76.22	192.71	194.58
2000	2.13	0.3988	0.2600	0.3072	0.2345	143.34	259.70	259.70

*The force constants[33]: σ = 4.45Å and ε/k = 212.6°K

†Interpolating from Table III

**Dilute gas viscosity of ethane at 220°F[9]: η_o = 116.49 micropoise

TABLE V

COMPARISON OF THE CALCULATED AND THE EXPERIMENTAL VISCOSITIES OF CARBON DIOXIDE AT 50°C

Pressure (atm)	Density (g/cm^3)	Reduced Density $\sigma^3\rho/m^*$	$f^{(0)}$ †	$f^{(1)}$ †	Reduced Residual Viscosity $\frac{\eta-\eta_o}{\sigma^{-2}\sqrt{m\varepsilon}}$ *	Residual Viscosity (micropoise)	Viscosity (micropoise) ** Cal'd	Viscosity (micropoise) ** Exp't[34]
11.22	0.0195	0.0171	0.0038	0.0070	0.0024	2.07	162.5	162.6
32.88	0.0634	0.0555	0.0145	0.0240	0.0097	8.42	168.8	167.9
42.96	0.0877	0.0768	0.0219	0.0340	0.0154	13.10	173.5	172.1
51.82	0.1121	0.0982	0.0305	0.0450	0.0216	18.64	179.0	176.7
65.16	0.1565	0.1371	0.0482	0.0665	0.0350	30.27	190.6	188.1
75.20	0.1999	0.1751	0.0685	0.0885	0.0509	44.03	204.4	201.7
79.07	0.2200	0.1927	0.0787	0.0995	0.0589	50.95	211.4	209.0
85.74	0.2620	0.2296	0.1017	0.1250	0.0768	66.46	226.8	225.4
90.98	0.3037	0.2661	0.1281	0.1540	0.0975	84.30	244.7	244.5
94.31	0.3359	0.2943	0.1500	0.1790	0.1144	98.96	259.4	259.1
97.42	0.3703	0.3244	0.1778	0.2105	0.1360	117.64	278.0	279.9
99.70	0.3974	0.3482	0.2020	0.2380	0.1546	133.78	294.2	294.7
103.3	0.4427	0.3879	0.2463	0.2910	0.1884	162.98	323.4	324.1
103.8	0.4484	0.3929	0.2521	0.2980	0.1928	166.79	327.2	329.2
107.2	0.4887	0.4282	0.2970	0.3530	0.2267	196.10	356.5	356.5

*The force constants[2]: $\sigma = 4.0\text{Å}$ and $\varepsilon/k = 190^\circ K$

†Interpolating from Table III

**Dilute gas viscosity of carbon dioxide at 50°C: $\eta_o = 160.9$ micropoise

PROPOSITION II

It is proposed that the unsteady-state diffusion and conduction problem in a porous catalytic spherical pellet can be solved numerically by using a simple model. Thus the effects of the different parameters on the maximum temperature in the pellet can be determined and compared.

---

1. Introduction

The problem of diffusion and conduction in a porous catalytic pellet under steady-state conditions has been studied by Wheeler[1], Prater[2], and Schilson and Amundson[3]. However, there appears to be little published information on the unsteady-state problem of this kind. Wei[4] has developed a method for solving the unsteady-state problem by using Green's function. He predicted a maximum transient temperature in the catalytic spherical pellet, which is independent of rate of reaction and has the following upper limit:

$$T_{max} \leq T_o[1 + \lambda + \lambda|L-1|(0.5+2.1\ \ell nN)] \quad , \quad \text{for} \quad L \geq 1$$

where T_o is the temperature at the external surface,

$$L = \frac{K}{\rho\ C_p D} \quad , \qquad \lambda = \frac{(-\Delta H_r)C_{A_o} D}{K\ T_o}$$

and N is the number of the molecules lying on the radius of pellet. The present method solves the same problem numerically by a finite difference method. The results obtained show the effect of different parameters on the maximum temperature which qualitatively confirms the results of Wei[4].

2. Nature and Model of the System

A single exothermic chemical reaction is carried out in a porous catalytic spherical pellet having randomly interconnected pores and uniform porosity. The surface available for reaction is assumed to be on the walls of pores in the pellet. It is also assumed that diffusion through the pore structure of the pellet is the only method operating in supplying the reactants to and removing the products from the reaction site within the pellet. It is further assumed that the heat produced by the reaction is transported by thermal conduction through the solid structure. By assuming a geometric configuration of the pores in the pellet, the effective diffusivity D_{eff} and thermal conductivity K_{eff} of the whole pellet can be roughly estimated[5,6].

Under the above assumptions, the equation of continuity for reactant A and the equation of energy in the pellet can be written as follows:

$$\frac{\partial C_A}{\partial t} = \frac{D_{eff}}{r^2} \frac{\partial}{\partial r} \left(r^2 \frac{\partial C_A}{\partial r}\right) - r_A \tag{1}$$

$$(\rho C_p)_{eff} \frac{\partial T}{\partial t} = \frac{K_{eff}}{r^2} \frac{\partial}{\partial r}\left(r^2 \frac{\partial T}{\partial r}\right) + (-\Delta H_r) \cdot r_A \tag{2}$$

The initial and boundary conditions are:

$$\text{at} \quad t = 0 \;,\; r \leq R \;; \quad T = T_o \;, \quad C_A = 0$$

$$t > 0 \;,\; r = R \;; \quad D_{eff} \frac{\partial C_A}{\partial r} = k_A(C_{A_o} - C_A) \;,$$

$$K_{eff} \frac{\partial T}{\partial r} = h(T_o - T)$$

$$t > 0 \;,\; r = 0 \;; \quad \frac{\partial C_A}{\partial r} = \frac{\partial T}{\partial r} = 0$$

For the simple case of an irreversible first order chemical reaction, the rate r_A in Equations (1) and (2) can be expressed in Arrhenius form:

$$r_A = k_o C_A \exp[\frac{E}{R}(\frac{1}{T_o} - \frac{1}{T})] \tag{3}$$

Introducing dimensionless groups and parameters, we have

$$U = T/T_o \;, \quad C = C_A/C_{A_o} \;, \quad Z = r/R$$

$$\tau = t\, D_{eff}/R \;, \quad \alpha = k_o R^2/D_{eff} \;, \quad \beta = E/RT_o$$

$$Nu = \frac{Rh}{K_{eff}} \;, \quad \lambda = \frac{(-\Delta H_r) C_{A_o} D_{eff}}{T_o K_{eff}} \;, \quad Sh = \frac{Rk_A}{D_{eff}}$$

$$L = \frac{K_{eff}}{(\rho C_p)_{eff} D_{eff}}$$

Equations (1) and (2) can be rearranged in the following dimensionless form:

$$\frac{1}{z^2} \frac{\partial}{\partial z}(z^2 \frac{\partial C}{\partial z}) - \alpha C \exp[\beta(1 - \frac{1}{U})] = \frac{\partial C}{\partial \tau} \tag{4}$$

$$\frac{1}{z^2}\frac{\partial}{\partial z}\left(z^2\frac{\partial U}{\partial z}\right) + \lambda\alpha C \exp\left[\beta\left(1 - \frac{1}{U}\right)\right] = \frac{1}{L}\frac{\partial U}{\partial \tau} \tag{5}$$

with the initial and boundary conditions:

$$\text{at } \tau = 0 \;,\; z \leq 1 \;;\quad U = 1 \;,\; C = 0$$

$$\tau > 0 \;,\; z = 1 \;;\quad \frac{\partial U}{\partial z} + Nu(U - 1) = 0$$

$$\frac{\partial C}{\partial z} + Sh(C - 1) = 0$$

$$\tau > 0 \;,\; z = 0 \;;\quad \frac{\partial U}{\partial z} = \frac{\partial C}{\partial z} = 0$$

3. Numerical Solution

Equations (4) and (5) can be solved numerically by the finite difference method to determine the effect of each dimensionless group on the temperature and concentration profiles. Using the implicit form of time derivatives, the difference equations obtained are

$$\left[\frac{1}{z^2}\frac{\partial}{\partial z}\left(z^2\frac{\partial C}{\partial z}\right) - \frac{C}{\Delta\tau}\right]_{j+1} = -\frac{C_j}{\Delta\tau} + \alpha C_{j+1} \exp\left[\beta\left(1 - \frac{1}{U'_{j+1}}\right)\right] \tag{6}$$

$$\left[\frac{1}{z^2}\frac{\partial}{\partial z}\left(z^2\frac{\partial U}{\partial z}\right) - \frac{1}{L}\frac{\partial U}{\Delta\tau}\right]_{j+1} = -\frac{1}{L}\frac{U_j}{\Delta\tau} - \lambda\alpha C_{j+1}\exp\left[\beta\left(1 - \frac{1}{U'_{j+1}}\right)\right] \tag{7}$$

It was found that a single iteration process is sufficient to solve the above coupled equations. The iteration scheme is as follows:

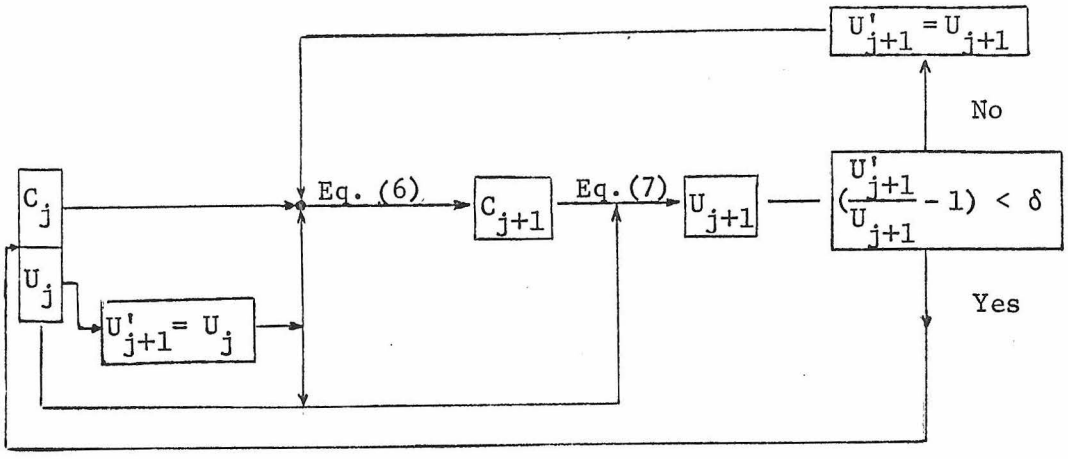

The numerical solution is obtained for Equations (6) and (7) based on the following values of six parameters:

$\alpha = 5$, $\beta = 20$, $Nu = 8$

$Sh = 15$, $\lambda = 0.5$, $L = 1$

The effect of a parameter on the solution can be found by varying its value and fixing the value of all other parameters.

The effect of the kinetics parameters λ and α on the temperature at the center of the pellet is shown in Figure 1. It is seen that the parameter λ has greater effect on the steady-state temperature than the parameter α.

Figure 2 shows the effect of parameter L on the temperature at the center of the pellet. When L is greater than unity, there exists a maximum transient temperature which is higher than the steady-state temperature and may damage the activity of the catalyst. This agrees qualitatively with Wei's results[4]. To avoid this temperature

peak, the physical properties of the solid catalyst and the pore structure of the pellet must be such that the resulting effective properties will make the parameter L less than unity.

NOMENCLATURE

C - dimensionless concentration, C_A/C_{A_o}

C_A - concentration of reactant A inside the pellet

C_{A_o} - concentration of reactant A on the surface of the pellet

$C_{P_{eff}}$ - effective heat capacity of the pellet

D_{eff} - effective diffusivity of the pellet

E - activation energy of reaction

h - heat transfer coefficient on the surface of the pellet

ΔH_r - heat of reaction

k_o - specific rate constant of reaction at T_o

k_A - mass transfer coefficient on the surface of the pellet

K_{eff} - effective thermal conductivity of the pellet

L - dimensionless parameter, $K_{eff}/(\rho_{eff} C_{P_{eff}} D_{eff})$

Nu - Nusselt number, Rh/K_{eff}

r - radial coordinate

r_A - rate of reaction

R - radius of the spherical pellet

Sh - Sherwood number, Rk_A/D_{eff}

t - time

T - temperature inside the pellet

T_o - temperature on the surface of the pellet

U - dimensionless temperature, T/T_o

Z - dimensionless radial coordinate, r/R

Greek Letters

α - dimensionless parameter, $k_o R^2/D_{eff}$

β - dimensionless parameter, E/RT_o

λ - dimensionless parameter, $(-\Delta H_r)C_{A_o} D_{eff}/(T_o K_{eff})$

ρ_{eff} - effective density of the pellet

τ - dimensionless time, tD_{eff}/R

REFERENCES

1. A. Wheeler, Advances in Catalysis 3, 249 (1951)

2. C. D. Prater, Chem. Eng. Sci. 8, 284 (1958)

3. R. E. Schilson and N. R. Amundson, Chem. Eng. Sci. 13, 226 (1961)

4. J. Wei, Chem. Eng. Seminar, California Institute of Technology, October 1965.

5. P. B. Weisz and C. D. Prater, Advances in Catalysis 6, 143 (1954)

6. R. L. Gorring and S. W. Churchill, Chem. Eng. Prog. 57(7), 53 (1961)

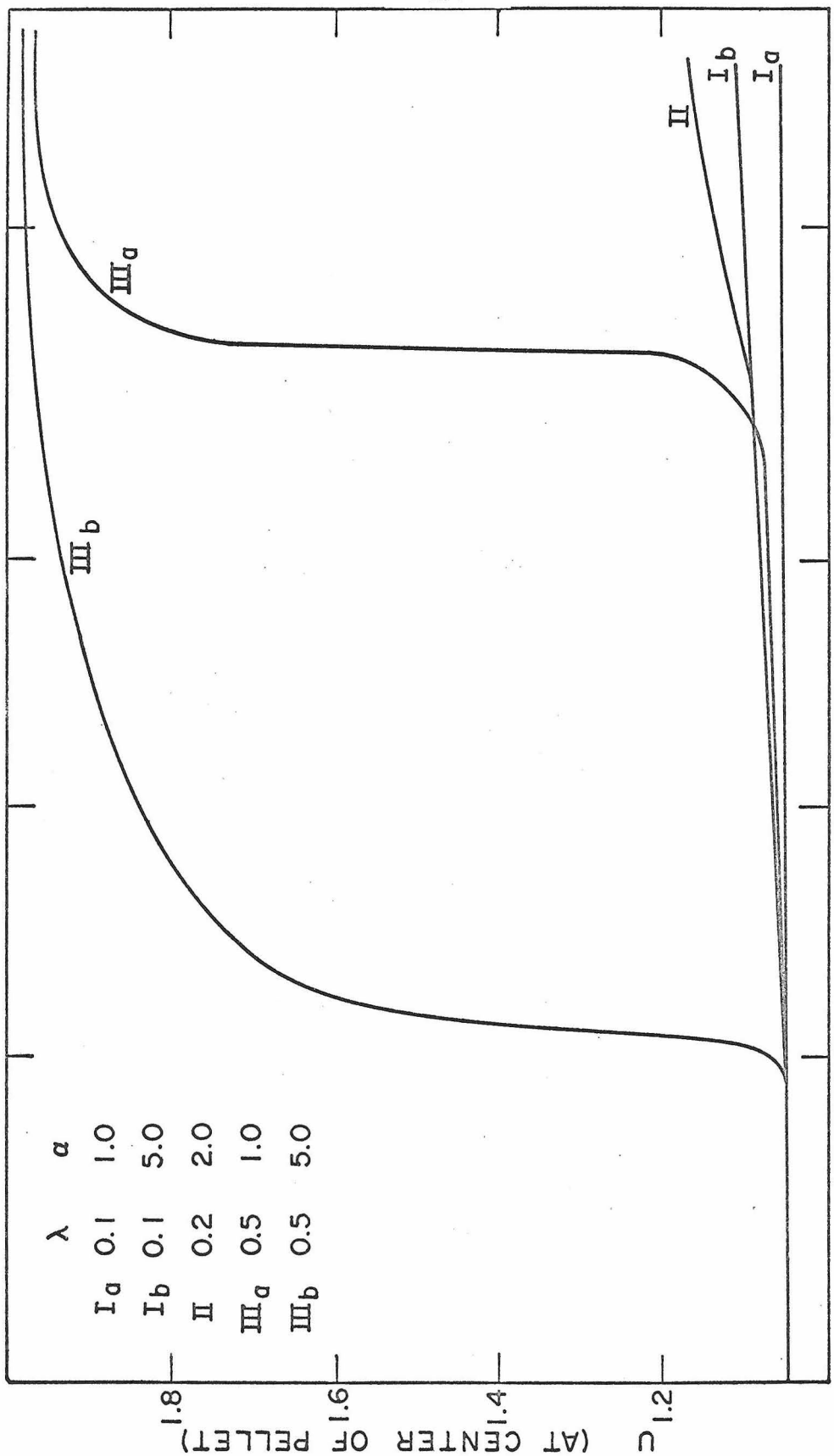

Figure 1. Effects of parameters α and λ on the temperature at the center of pellet

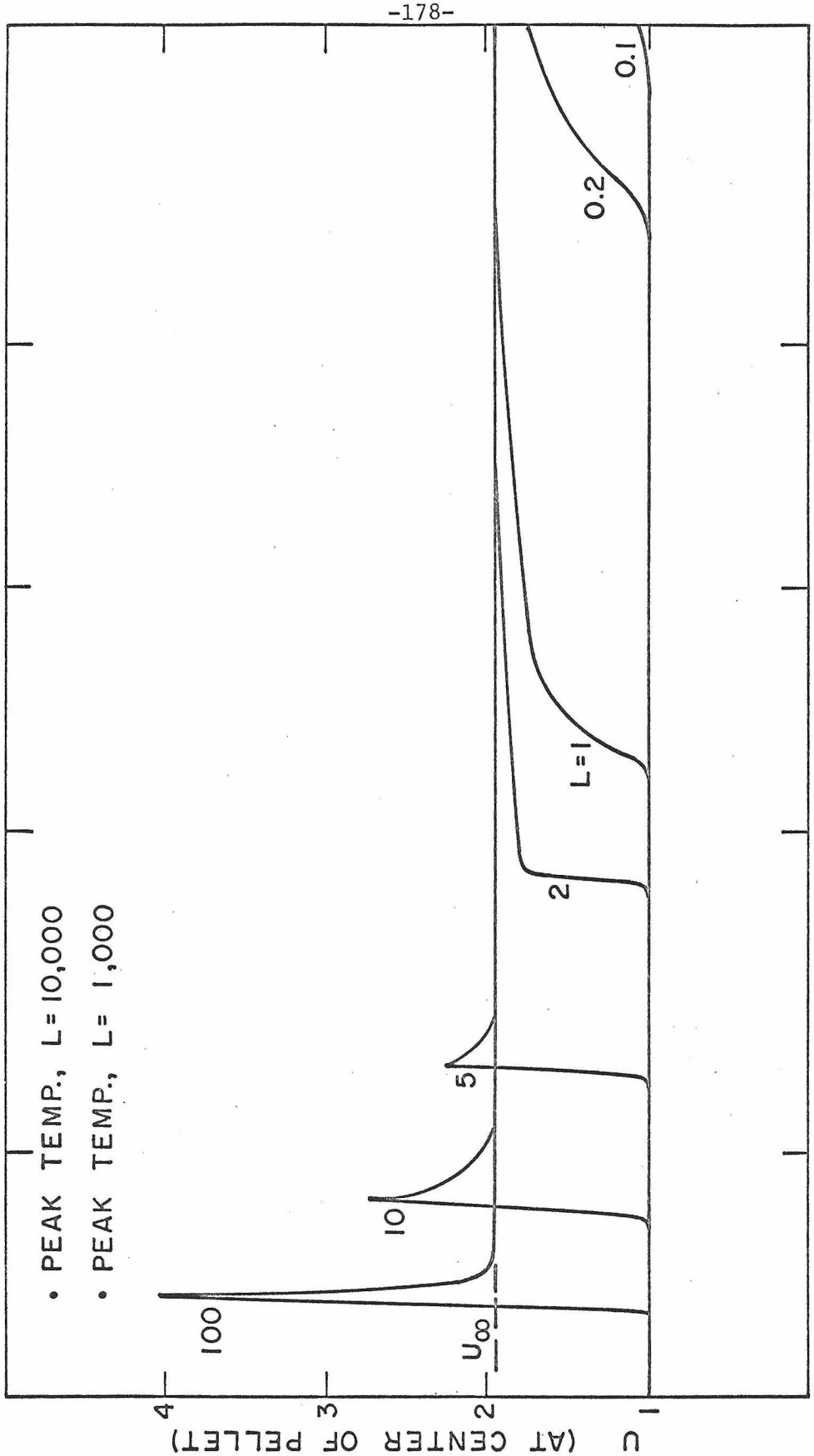

Figure 2. Effect of parameter L on the temperature at the center of pellet (U_∞ = steady-state temperature)

PROPOSITION III

A method similar in nature to gas chromatographic techniques has been developed by Giddings and Seager[1] for measuring gas phase diffusion coefficients. They suggested carrying out experiments with both a long and a short tube in order to subtract out the spreading due to the apparatus. Instead of this, it is proposed to carry out the experiments with two different flow velocities which can be easily changed through the use of tandem proportioning pumps. Thus, the experimental procedure is simplified.

1. Introduction

When a thin band of sample gas is injected into a laminar stream of carrier gas flowing in a tube, the injected sample will spread out due to the axial diffusion and the lateral nonequilibrium introduced by the viscous nature of the flow. Giddings and Seager[1] have applied their general theory of gas chromatography to this system and obtained the following relation:

$$H = \frac{2D_e}{\bar{u}} = \frac{2D}{\bar{u}} + \frac{r_o^2 \bar{u}}{24D}$$

where D_e = Effective diffusion coefficient

D = Molecular diffusion coefficient of sample gas in carrier gas

$\bar{u}$ = Mean flow velocity in tube

r_o = Radius of tube

H = Height equivalent to a theoretical plate (as defined in gas chromatographic analysis)

Levenspiel and Smith[2] have shown that the mean concentration of sample gas over the cross-section of the tube at length L becomes approximately a Gaussian error distribution function of time, if $D_e / \bar{u}L$ is very small. Then, the quantity H for a Gaussian curve can be determined by the formula

$$H = \frac{L \sigma_t^2}{t^2} \tag{2}$$

where L = Tube length

t = Passage time of the peak of the curve

σ_t = Standard deviation in passage time of the peak of sample which is injected as a δ function (thin band)

The standard deviation σ_t can be related to the width w at half height of the Gaussian curve by the following equation:

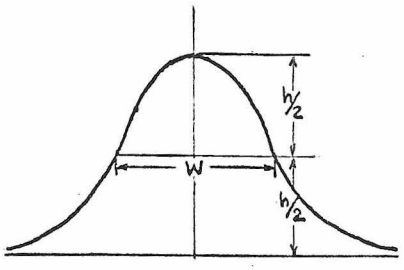

$$w = 2\sigma_t \sqrt{2 \ln 2} \tag{3}$$

Then Eq. (2) can be expressed by

$$H = \frac{Lw^2}{8 \ln 2t^2} = \frac{Lw^2}{5.545\ t^2} \tag{4}$$

Since the spreading due to a number of independent or consecutive

processes is given by $w^2 = w_1^2 + w_2^2 + w_3^2 + \cdots$ the spreading due to the tube alone may be obtained as follows:

$$w_{tube}^2 = w_{total}^2 - w_{apparatus}^2$$

Accordingly, the spreading due to the apparatus can be eliminated by subtracting the data of a short tube from those of a long tube with the same flow velocity. Thus, Equation (4) can be rewritten as follows:

$$H = \frac{(L_\ell - L_s)(w_\ell^2 - w_s^2)}{5.545\ (t_\ell - t_s)^2}$$

where the subscripts ℓ and s refer to the data for the long tube and the short tube, respectively. Substituting this equation into Equation (1), we obtain the relation between the width w at half height and the diffusion coefficient D as follows:

$$\frac{(L_\ell - L_s)(w_\ell^2 - w_s^2)}{5.545\ (t_\ell - t_s)^2} = \frac{2D}{\bar{u}} + \frac{r_o^2\,\bar{u}}{24D} \qquad (5)$$

However, this correction technique involves the replacement of tubes and dismantling part of the apparatus, which complicates the experimental procedure.

It is found that the relation between w and D, similar to Equation (5), can also be obtained from the analysis by Aris[3] on the dispersion of a solute in a flowing fluid. In this new relation, there is no term involving tube length and the diffusion coefficient D can be determined from two measurements of width w with different

flow velocities.

2. Analysis

By assuming laminar flow, a constant diffusion coefficient and cylindrical symmetry, the equation of continuity governing the concentration of sample gas in a stream of carrier gas flowing through a tube is

$$\frac{\partial C}{\partial t} + 2\bar{u}\left(1 - \frac{r^2}{r_o^2}\right)\frac{\partial C}{\partial x} = D\left(\frac{\partial^2 C}{\partial r^2} + \frac{1}{r}\frac{\partial C}{\partial r} + \frac{\partial^2 C}{\partial x^2}\right) \tag{6}$$

Taking the origin of the coordinates moving with the mean flow velocity $\bar{u}$ and using the dimensionless variables:

$$\xi = \frac{x - \bar{u}t}{r_o} \quad ; \quad R = \frac{r}{r_o}$$

$$\tau = \frac{Dt}{r_o^2} \quad ; \quad U = \frac{r_o\bar{u}}{D}$$

the above equation of continuity becomes

$$\frac{\partial C}{\partial \tau} + U(1 - 2R^2)\frac{\partial C}{\partial \xi} = \frac{\partial^2 C}{\partial R^2} + \frac{1}{R}\frac{\partial C}{\partial R} + \frac{\partial^2 C}{\partial \xi^2} \tag{7}$$

Initially, the sample gas is injected as a δ function at the origin, so the initial condition is

$$\text{at} \quad \tau = 0 \quad , \qquad C = \delta(\xi) \tag{8}$$

$$\text{and} \quad \int_{-\infty}^{\infty} C \, d\xi = 1 \tag{9}$$

The boundary conditions are

$$\text{at} \quad \xi = \pm\infty \quad , \quad C = 0 \tag{10}$$

$$\text{and} \quad \frac{\partial C}{\partial \xi} = 0 \tag{11}$$

$$\text{at} \quad R = 1 \quad , \quad \frac{\partial C}{\partial R} = 0 \tag{12}$$

Aris[3] defined a quantity $C_n(R,\tau)$, which is called the n^{th} moment of the distribution of sample gas in the cylindrical element through radius R at time τ, as follows:

$$C_n(R,\tau) = \int_{-\infty}^{\infty} \xi^n \, C(\xi,R,\tau) \, d\xi \tag{13}$$

The average of $C_n(R,\tau)$ over the cross-section of the tube is

$$\overline{C_n(\tau)} = \frac{1}{A} \int\int_A C_n(R,\tau) \, RdRd\theta$$

$$= 2 \int_0^1 C_n(R,\tau) \, RdR \tag{14}$$

Integrating Equation (7) with respect to ξ from $-\infty$ to $+\infty$ and using conditions (10) and (11), we have

$$\frac{\partial C_o}{\partial \tau} = \frac{\partial^2 C_o}{\partial R^2} + \frac{1}{R} \frac{\partial C_o}{\partial R} \tag{15}$$

The solution of Equation (15) can be expressed in terms of Bessel functions as follows:

$$C_o = \sum_{i=0}^{\infty} A_i J_o(\lambda_i R)\, e^{-\lambda_i^2 \tau} \tag{16}$$

Applying the conditions (8) and (12) to this, we find $J_1(\lambda_i) = 0$ and

$$A_i = \begin{cases} 1 & \text{if } i = 0 \\ 0 & \text{if } i \neq 0 \end{cases}$$

Therefore,

$$C_o = 1 \tag{17}$$

Similarly, if Equation (7) is first multiplied by ξ and then integrated, we obtain the solution for C_1 as follows:

$$C_1 = \frac{U}{4}\left[\frac{1}{3} - R^2\left(1 - \frac{R^2}{2}\right)\right] + \sum_{i=1}^{\infty} \frac{8U}{\lambda_i^4} \frac{J_o(\lambda_i R)}{J_o(\lambda_i)} e^{-\lambda_i^2 \tau} \tag{18}$$

where

$$J_1(\lambda_i) = 0$$

Now multiplying Equation (7) by ξ^2 and integrating with respect to ξ from $-\infty$ to $+\infty$, we have

$$\frac{\partial C_2}{\partial \tau} = \frac{\partial^2 C_2}{\partial R^2} + \frac{1}{R}\frac{\partial C_2}{\partial R} + 2C_1 U(1 - 2R^2) + 2C_o \tag{19}$$

If this equation is averaged over the cross-section of the tube, the use of Green's theorem and the condition (12) reduces it to

$$\frac{d\overline{C_2}}{d\tau} = 2U\,\overline{C_1(1 - 2R^2)} + 2\,\overline{C_o} \tag{20}$$

Substituting Equations (17) and (18) into this, we find the solution

as follows:

$$\overline{C_2(\tau)} = \overline{C_2(0)} + (2 + \frac{U^2}{24})\tau - 128U^2 \sum_{i=1}^{\infty} \frac{1 - e^{-\lambda_i^2 \tau}}{\lambda_i^8} \qquad (21)$$

where $J_1(\lambda_i) = 0$.

By definition, the square of the standard deviation in passage time of the peak of the concentration profile $C(x,r,t)$ is

$$\sigma_t^2 = \frac{\int_A dA \int_{-\infty}^{\infty} C(x,r,t)\, x^2 dx}{\int_A dA \int_{-\infty}^{\infty} C(x,r,t)\, dx}$$

$$= \frac{\frac{2r_o^5}{u^3} \int_0^1 RdR \int_{-\infty}^{\infty} C(\xi,R,\tau)\xi^2\, d\xi}{\frac{2r_o^3}{u} \int_0^1 RdR \int_{-\infty}^{\infty} C(\xi,R,\tau)\, d\xi}$$

$$= \frac{r_o^2}{u^2} 2 \int_0^1 RdR \int_{-\infty}^{\infty} C(\xi,R,\tau)\xi^2\, d\xi$$

$$= \frac{r_o^2}{u^2} \overline{C_2(\tau)} \qquad (22)$$

Experimentally, a thin band of sample gas is injected at the origin and the initial concentration profile can be expressed as follows:

at $t = 0$

$$C(x,r,p) = \begin{cases} 0 & \text{for } x < -h \\ \frac{1}{2h} & -h \le x \le h \\ 0 & x > h \end{cases}$$

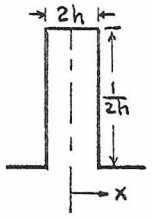

Then, we find

$$\overline{C_2(0)} = \frac{h^2}{3r_o^2} \tag{23}$$

By combining Equations (21), (22), and (23), we obtain the following relation

$$\sigma_t^2 = \frac{h^2}{3\bar{u}^2} + (2+\frac{U^2}{24})\frac{r_o^2}{\bar{u}^2}\tau - \frac{128U^2r_o^2}{\bar{u}^2}\sum_{i=1}^{\infty}\frac{1-e^{-\lambda_i^2\tau}}{\lambda_i^8}$$

$$= \frac{h^2}{3\bar{u}^2} + (2D+\frac{\bar{u}^2r_o^2}{24D})\frac{t}{\bar{u}^2} - \frac{128r_o^4}{D^2}\sum_{i=1}^{\infty}\frac{1-e^{-\lambda_i^2Dt/r_o^2}}{\lambda_i^8} \tag{24}$$

Then

$$\Delta\sigma_t^2 = 2D\,\Delta(\frac{t}{\bar{u}^2}) + \frac{r_o^2}{24D}\Delta t + \frac{h^2}{3}\Delta(\frac{1}{\bar{u}^2})$$

$$- \frac{128r_o^4}{D^2}\sum_{i=1}^{\infty}\frac{e^{-\lambda_i^2D/r_o^2}}{\lambda_i^8}(e^{t_2}-e^{t_1}) \tag{25}$$

Now in the same way as before, we use Equation (3) to relate the standard deviation σ_t with the width w at half height. Then Equation (25) can be rewritten as follows:

$$\frac{\Delta w^2}{5.545} = 2D\,\Delta(\frac{t}{\bar{u}^2}) + \frac{r_o^2}{24D}\Delta t + \frac{h^2}{3}\Delta(\frac{1}{\bar{u}^2})$$

$$- \frac{128r_o^4}{D^2}\sum_{i=1}^{\infty}\frac{e^{-\lambda_i^2D/r_o^2}}{\lambda_i^8}(e^{t_2}-e^{t_1}) \tag{26}$$

When the last two terms are very small as compared to the first two, we obtain

$$\frac{\Delta w^2}{5.545} = 2D\ \Delta\left(\frac{t}{\bar{u}^2}\right) + \frac{r_o^2}{24D}\ \Delta t \qquad (27)$$

3. Conclusion

Equation (26) or (27) can serve as a basis for determining the diffusion coefficient D from two measurements of the width w with different flow velocities, instead of different tube lengths. Through the use of tandem proportioning pumps, the flow velocity can be easily changed without any dismantling of the apparatus. Thus, the experimental procedure is simplified.

NOMENCLATURE

A_i - coefficient in Equation (16)

C - concentration of sample gas in a stream of carrier gas

C_n - n^{th} moment of the distribution of sample gas in the cylindrical element through radius R at time τ

D - molecular diffusion coefficient of sample gas in carrier gas

D_e - effective diffusion coefficient

h - maximum height of a Gaussian curve

H - height equivalent to a theoretical plate

J_o - Bessel function of the first kind of zero order

J_1 - Bessel function of the first kind of order 1

L - tube length

r - radial coordinate

r_o - radius of tube

R - dimensionless variable, r/r_o

t - passage time

$\bar{u}$ - mean flow velocity in the tube

U - dimensionless variable, $r_o\bar{u}/D$

w - width at half height of a Gaussian curve

Greek Letters

δ - delta function

ξ - dimensionless variable, $(x - \bar{u}t)/r_o$

σ_t - standard deviation in passage time of the peak of the concentration C

τ - dimensionless variable, Dt/r_o^2

Superscript

$\overline{}$ - average over the cross-section of the tube

REFERENCES

1. Giddings, J. C. and Seager, S. L., I. E. C. Fundamentals 1, 277 (1962).

2. Levenspiel, O. and Smith, W. K., Chem. Eng. Sci. 6, 227 (1957).

3. Aris, R., Proc. Roy. Soc. (London) A235, 67 (1956).